A STUDY OF THE DISPERSION OF A MODULATED ELECTRON BEAM IN A FIELD-FREE SPACE.

by

RICHARD DEANE PROSSER

Thesis submitted for the degree of
Ph.D. in the University of London

Physics Department
Imperial College
London S. W. 7.

January 1970

ABSTRACT

The time dispersion and frequency dispersion associated with a modulated electron beam in a field-free space are examined. Experiments with a 60 cm beam are described and the results are compared with theoretical predictions. Also described is a practical instrument in which time dispersion on an electron beam is used to generate, from a single transient signal, a similar signal which is lengthened in time. This facilitates the display of transient signals which occur too rapidly to be accurately detected by conventional oscilloscopes. The performance of this instrument is investigated and suggestions for improvements and further development are made.

CONTENTS

1. Introduction. 6

- 1.1 Limitations of conventional oscilloscopes
- 1.2 The sampling technique
- 1.3 The principle of time dispersion
- 1.4 Electron dynamics
- 1.4.1 The ballistic theory
- 1.4.2 The theory of electron flow under space-charge conditions
- 1.4.3 Space-charge wave theory

2. The electron tube. 18

- 2.1 Design considerations
- 2.2 Tube construction

3. The electrical circuitry. 30

- 3.1 Bias network
- 3.2 Pulse generating network

4. Steady-state operation. 37

- 4.1 Current flow between planes
- 4.2 Current flow through a conducting cylinder
- 4.3 Energy spread of the electrons
- 4.4 Secondary electron emission

4.5 Model for equilibrium flow
4.6 Experimental results
4.6.1 Cathode-grid space
4.6.2 Maximum current through drift section
4.6.3 Anode characteristic
4.6.4 Overall transfer characteristic
4.7 The confining magnetic field

5. Modulated operation. 54

5.1 Current modulation
5.1.1 The elastic rod model
5.1.2 Space charge waves
5.1.3 Pulse distortion
5.1.4 Transit time measurements
5.2 Velocity modulation
5.2.1 Experimental results

6. Dispersive operation. 75

6.1 Ballistic theory of dispersive operation
6.1.1 Pulse separation in dispersive mode
6.2 First attempts at pulse stretching
6.3 Designing for linearity

7. A practical device. 87

7.1 The tube design, construction and processing.
7.2 Electrical circuitry

7.3 Experimental results

7.3.1 Steady-state operation

7.3.2 Modulated operation

7.3.3 Dispersive operation

7.3.4 Operation with a real-time oscilloscope

8. Conclusionsand suggestions for further development. 108

9. Appendix. 111

9.1 Derivation of the space-charge wave equation

9.2 Application to a cylindrical system

9.3 Higher order modes

9.4 Convectional impedance for space-charge limited diode

10. Acknowledgements. 119

11. References. 120

1. INTRODUCTION

The work to be described in this thesis was undertaken with a view to developing an improved method of recording electrical signals. Conventional oscilloscopes will respond satisfactorily to pulses which have risetimes longer than a few nanoseconds, but there is a limit to the speed with which an oscilloscope may respond while maintaining an acceptable sensitivity. In this chapter we shall indicate briefly how this limitation arises and then consider the techniques which have been devised to overcome it, showing in particular how the use of a modulated electron beam and a field-free space leads to a simple and convenient solution. Finally the theoretical approach used in the subsequent chapters will be introduced.

1.1. Limitations of conventional oscilloscopes.

In a conventional oscilloscope electrons from a gun are accelerated and focused by two anodes and swept across a phosphor screen by means of a voltage applied to two sets of mutually perpendicular deflecting plates. The spot deflection on the screen is approximately proportional to the deflecting field and to the time for which it acts on the electrons. It follows that if there is a change in the deflection voltage during the time an electron is passing between the plates then the spot deflection will not be simply proportional to the deflection voltage. For a sinusoidal deflection waveform of given amplitude the spot deflection amplitude is reduced as the period of the waveform becomes comparable with the electron transit time through the deflection plates. The deflection diminishes to zero with further shortening of the period.

A further complication which arises with high frequency deflection is due to the reactances of the deflecting plates and their connection leads. Precautions must be taken to minimize these as far as possible so that the deflection system does not act as a resonant circuit. These reactances and the transit

time effects associated with the deflection plates are limiting factors in the high frequency performance of a conventional oscilloscope.

Transit time distortion can be reduced by using short deflection plates but this also reduces the deflection sensitivity (measured in cm/volt) at the screen. Some amplification of the deflection signal would be necessary if a reasonable deflection were to be obtained with small amplitude signals and this complicates the total design. The deflection sensitivity can be increased by using several pairs of short plates situated in tandem along the beam axis. The capacitances between the plates together with small connecting inductances form a low pass filter network, the constants of the network being so chosen that the velocity of a pulse through it is equal to the velocity of the electron beam. An extension of this travelling wave idea leads to a deflection system in the form of a transmission line such as two flat metal strips. The speed at which a pulse travels along this line will be much greater than the electron velocity and the line must be coiled up so that the path traversed by the pulse is longer than that for the electrons, and both pulse and electrons can travel synchronously towards the screen. Tubes of this kind can display nanosecond pulses but the size of the display is small.

The deflection sensitivity has so far been considered in terms of the voltage required to deflect the spot through 1 cm. The screen display may however be magnified by optical means so that a more fundamental measure of sensitivity is defined by the voltage required to shift the spot by one spot width. It is then important that the electron optical system in the cathode ray tube should be designed to give as small a spot as possible. For a given deflection the deflection sensitivity in terms of spot widths per volt may be increased by reducing the spot size. This may be accomplished by lowering the beam current but this entails a loss of spot brightness. The brightness can be restored by using a beam at a higher potential; however as the electrons are then travelling faster through the deflection region they are more difficult to deflect and the deflection sensitivity is again reduced. This conflict between the requirements of sensitivity and adequate brightness can be

minimized by delaying the acceleration of the beam towards the screen until after it has been deflected at a relatively low voltage. An electric field derived from a spiral of high resistance material on the tube walls is sometimes used for this purpose.

Summarizing the situation, it may be said that because the electron has mass, the requirements of rapid deflection and high sensitivity are not compatible. The conflict may be minimized by specially constructed deflection systems. By using a small spot, high frequency performance may still be obtained although the display is small and may have to be observed through a low power microscope. Larger displays can be obtained with the help of post deflection acceleration techniques. Table 1 shows the performance which has been obtained with some of the fastest experimental and commercial oscilloscopes; the decrease in sensitivity as the risetime is reduced is clearly evident. A quantitative discussion of oscilloscope limitations and a fuller account of some of the experimental systems is given by Lewis and Wells (1).

Table 1

	1	2	3	4	5
Risetime (nsec)	3.5	2.4	.35	.17	.035
Sensitivity (cm/volt)	100	62	0.1	7.5	.0006
Spot width (cm)	-	-	.01	.004	.02
Display height (cm)	8.6	4.8	2	0.8	-

1 Tektronix 647 A.
2 Tektronix 454
3 Tektronix 519. Travelling wave deflection.
4 Tube with travelling wave deflection by Edgerton (12).
5 Ferranti 06/20P as used by Jackson et al. (13). The deflection plates are straight wires sealed through the glass and matched to a transmission line system.

1.2. The sampling technique.

It is frequently the case that an electronic signal can be made to repeat itself when suitably triggered. For such repetitive waveforms the sampling technique can give performance greatly superior to that obtainable from conventional real-time oscilloscopes. In this technique the waveform is sampled at a particular time and the result displayed in the form of a dot on the screen. The coordinates of the dot correspond respectively with the instantaneous magnitude of the waveform and the time at which the sample was taken. On the subsequent cycle the sample is taken at a slightly later time relative to the initiating trigger so that eventually the complete waveform is built up in the form of a pattern of dots. The frequency of sampling can be quite low, of the order of 10 kHz, so that deflection problems are obviated. A recent instrument of this type (Hewlett Packard, Model 1411) has a risetime of 28 psec at 1 mV/cm sensitivity. A review of sampling techniques applied to high speed oscillography is given by Gilbert (2).

1.3. The principle of time dispersion.

In Section 1.1 it was shown that the main problems of high speed oscillography are connected with the rapid deflection of the electron beam. If there were some way of slowing down the signal of interest systematically, i.e. to expand the time axis of the waveform before it was applied to the deflection system, then these problems would be resolved. This is the principle of time dispersion.

There have been a number of suggestions (3,4, 5) as to how this systematic time expansion might be achieved using electrical networks, but a working device does not appear to have been forthcoming. Caputi (6) has constructed a time dispersion system in which the original waveform is used to [illegible] modulate a microwave carrier which is then fed to a frequency dispersive device and demodulated with a swept frequency oscillator. A second dispersive device restores the dispersed frequency components to a form corresponding to

the original waveform but with its time axis expanded. The dispersive device used by Caputi was a waveguide operated near its cut-off frequency. It is doubtful whether this technique could be conveniently used in conjunction with an oscilloscope unless a compact dispersive device can be found. A system of the form proposed would require a waveguide of at least 30 metres in length to provide signals suitable for feeding to an oscilloscope having a rise-time of 10 nsec.

The fundamental idea upon which this work is based is another example of time dispersion. An input voltage signal is used to current modulate an electron beam. This may be achieved by feeding the signal to a grid placed close to a thermionic cathode, as in a triode. The modulated beam is then physically stretched out by passing it through a hollow metal drift tube to which a decreasing voltage waveform, called the dispersión pulse, is applied. In this way electrons are made to enter the tube at progressively lower energies and so to travel at progressively slower velocities through it. As the electrons pass down the tube the modulation pattern will thus become increasingly extended, because once an electron has entered the tube it is shielded from all external electric fields and continues to move with the same velocity no matter what potential the drift tube may subsequently assume relative to the cathode. The electrons are prevented from reaching the walls of the tube by an axial magnetic field.

As the electrons emerge from the drift tube they are collected at an anode plate. This is connected to a positive potential via a suitable load resistor across which the modulation may be observed with a conventional oscilloscope. As a result of the stretching of the beam the modulation pattern detected will be similar to the input signal waveform but will now have its time axis expanded.

A practical device which makes use of this dispersion principle is shown schematically in Fig. 1.1. The cathode, modulation grid and the drift section have already been mentioned. Between the modulation mesh and the drift tube is a shorter similar tube which screens the modulation mesh from the dispersion pulse. Also shown in the Figure is a metal cylinder

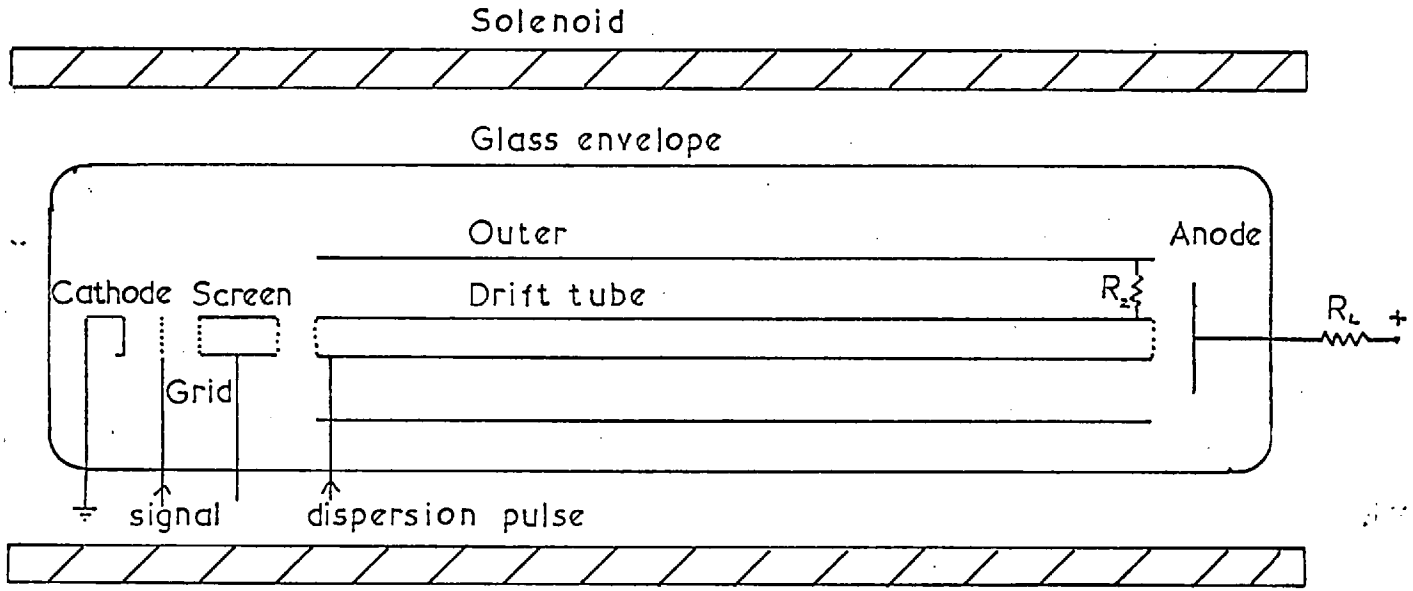


Fig. 1.1 Time dispersion tube (schematic)

enclosing the drift tube. These two coaxial tubes may be considered to form the inner and outer conductors of a transmission line. The dispersion pulse travels down this line and is absorbed in the resistance R_z which matches the characteristic impedance of the line. This arrangement ensures that the dispersion pulse has been adequately damped by the time the modulation arrives at the anode. Otherwise there would be some feed-through via the anode-drift capacitance. The electrode structure is enclosed in an evacuated glass envelope and this is placed in a solenoid which produces the necessary axial magnetic field.

1.4. Electron dynamics.

If a device just described is to be used as an instrument the output waveform must be related in a simple way to the input waveform, and this relationship must not depend on the shape of the input waveform. In order to understand exactly how this relationship is determined we have to consider the forces acting on the electrons as they pass through the device. A theory is required which will predict the number and energy of electrons at any point in the tube at any time. The complete solution of this problem can in principle be derived from a combination of Maxwell's equations and the electron secondary emission characteristics, but would be so cumbersome as to be of little help for design purposes. The most useful practical approach is to make use of three theoretical models. These are not independent; they are simply the form to which the complete solution would reduce under suitably idealized circumstances. The three models and their realms of application are as follows.

1.4.1. The ballistic theory.

When the density of electrons is sufficiently low, their mutual repulsion can be neglected. The potential distribution may then be considered to be that which would exist in the total

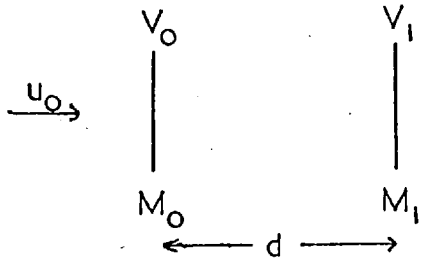
absence of electrons. Radial motion of the electrons is prevented by the magnetic field and the electrons move only under the influence of the axial electric field, E. The equation of motion is

$$du/dt = (e/m)E \qquad (1.1)$$

Also

$$\int(dx/u) = t \qquad (1.2)$$

These two equations enable the velocity and position of an electron at time t after leaving the cathode to be determined provided E is known. Consider an electron travelling between two planes M_o , M_1 which are d metres apart and having potentials V_o , V_1 , respectively relative to the cathode.



These planes could be those defining the ends of the screen and drift sections for example. There are two cases of interest: (i) in which V_o and V_1 are both fixed, and (ii) in which V_o is fixed and V_1 is variable.

Case 1: Fixed potentials.

Eqn. 1.1 can be written in the form

$$\int u\,du = (e/m)\int E\,dx \qquad (1.3)$$

$\int E\,dx$ is the potential V_x at the point x. V_x is defined to be zero at the cathode, which has abscissa x_c , so that we can write

$$V_x = \int_{x_c}^{x} E\,dx \qquad (1.4)$$

Substituting in eqn. 1.3 we obtain

$$u = \sqrt{(2eV/m)} \qquad (1.5)$$

(We neglect here the spread of electron velocities; u is assumed zero at the cathode).

The potential of a point between the planes at a distance x from M_o is given by

$$V_x = V_o + (V_1 - V_o)(x/d) \qquad (1.6)$$

Substituting eqns. 1.5 and 1.6 in eqn. 1.2 shows that the time taken for an electron to travel from M_o to x is

$$t = \sqrt{(m/2e)}\int_o^x dx/\sqrt{V_x}$$

$$= \sqrt{\frac{2m}{e}}\left|\frac{\sqrt{V_x} - \sqrt{V_o}}{V_1 - V_o}\right|d \qquad (V_1 \neq V_o) \qquad (1.7)$$

If $V_1 \longrightarrow V_o$ we obtain simply

$$t = \sqrt{(m/2e)}x/\sqrt{V_o} \qquad (1.8)$$

Case 2: V_1 varies.

If E is a function of t, $\int Edx$ will have a defined value at any instant and the concept of potential is still meaningful. However in eqn. 1.1 E refers to the field experienced by the electron as it travels between the planes and the integration of the equation must be considered over this path. The velocity of the electron after it has taken time t to travel to x is therefore

$$\dot{u} = (e/m)\int_o^t E(t)dt + u_o \qquad (1.9)$$

Suppose that the potential on M_1 changes from V_1 to $V_1 + v$ during the time τ which an electron takes to travel between the planes. The potential change will be assumed linearly proportional to t so that E is given by

$$E = \{(V_1 - V_o) + vt/\tau\}/d \qquad (1.10)$$

Substituting in eqn. 1.9 and integrating gives

$$u = u_0 + (e/m)\{(V_1 - V_0)t + vt^2/2\tau\}(1/d) \quad (1.11)$$

where u_0 is the velocity at M_0. Since V_0 is fixed we may assume

$$u_0 = \sqrt{(2eV_0/m)} \quad (1.12)$$

From eqn. 1.2,

$$x = \sqrt{(2eV_0/m)}t + (e/m)\{(V_1 - V_0)t^2/2 + vt^3/6\tau\}(1/d) \quad (1.13)$$

We obtain the transit time by putting $x = d$, $t = \tau$ in eqn. 1.13. For the case when $v \ll (V_1 - V_0)$ this gives

$$\tau = \sqrt{\frac{2m}{e}} \frac{\sqrt{V_1 + v/3} - \sqrt{V_0}}{V_1 + v/3 - V_0} d \quad (1.14)$$

and substituting in eqn. 1.11 the velocity at M_1 is

$$u_\tau = \sqrt{(2e/m)(V_1 + v/3)} \quad (1.15)$$

Thus although M_1 is at a potential of $V_1 + v$ at the time the electrons reach it, the electrons are travelling with a velocity corresponding to a potential of $V_1 + v/3$.

1.4.2. Theory of equilibrium flow under space-charge conditions.

With increasing electron density it can no longer be assumed that the potential distribution in the tube will be the same as in the absence of electrons. The calculation of potential distributions involving free charge requires the solution to Poisson's equation and this is available in the literature for a number of cases. A study of electron flow between planes

has been made by Fay, Samuel and Shockley (7) and the case of flow through a hollow conducting cylinder has been treated by Smith and Hartman (8). A detailed discussion of these analyses is given in Chapter 4; we now note only some salient points.

It is a known but perhaps a surprising fact that there is a maximum current which can be passed through a hollow metal tube no matter what radius the tube may have (9). There is also a maximum current which can be passed between two planes of unit area. These maximum currents are given by eqns. 4.4 and 4.5. As a rough guide, the theory of the preceeding section may be considered valid when the actual currents are less than 10% of the maximum, provided we are dealing with equilibrium conditions (see next Section). An important region of the tube where the ballistic theory is not valid is in front of the cathode. Here the current is space-charge limited. It can be shown (9) that the transit time in these conditions is 50% greater than in the absence of space charge, and is given by

$$\tau = 3\sqrt{(m/2eV)}d \qquad (1.16)$$

1.4.3. Space-charge wave theory.

The theory of the last section describes the conditons prevailing when a state of equilibrium has been attained. However, if the transit time of an electron through a given region is long compared with the period of density modulation which may have been previously imposed on the beam, then it is possible to introduce non-equilibrium conditions into the region concerned. This situation occurs in the drift section, where the transit time is about 100 nsec whereas the modulation may have a risetime of less than 1 nsec.

A theoretical study of such time dependent phenomena involves the use of the complete set of Maxwell's equations. Such an approach is provided by the theory of space-charge waves which shows how the original electron modulation separates into two pulses which are transmitted with different

velocities. The existence of these two pulses may be clearly seen in Fig. 5.1.

A full account of space charge wave theory is given by Beck (10) and a review of the original papers by Trotman (11). A condensed account of the theory as it applies to the device is given in Section 9. The theory is similar to that for waveguides with the difference that as the waveguide now contains free charge Poisson's equation must be used in place of Laplace's.

2. THE ELECTRON TUBE

2.1 Design considerations.

The tube first used to examine the theories outlined in the last chapter is shown in Fig. 2.1. Certain of the dimensions are critical and we now consider how these affect the operation of the tube.

2.1.1 Cathode-grid spacing and cathode emission.

It was intended to modulate the beam with signals having a risetime as short as 0.35 nsec, corresponding to a bandwidth of 1000 Mhz*. For such fast signals, where the electron transit time between cathode and grid may be an appreciable fraction of the modulation period, theoretical analysis requires a more comprehensive concept of electric current than that represented by the rate of arrival of electrons at an electrode surface. In general the displacement current arising from time-changing fields due to the moving charges must be included, and the total current may be written

$$J = \rho v + \varepsilon_0 dE/dt \qquad (2.1)$$

This equation was originally due to Maxwell. The first term on the R.H.S. represents the electron convection current, and the second term the displacement current. The higher the frequency the greater is the relative magnitude of the displacement current

The application of eqn.. 2.1 to electrode systems has been studied by various workers of whom Llewellyn (14) is best known. A review of the topic is given by Birdsall and

---

* Throughout this thesis the following relation between bandwidth B(Hz) and risetime t_r (sec) is assumed :

$$Bt_r = 0.35$$

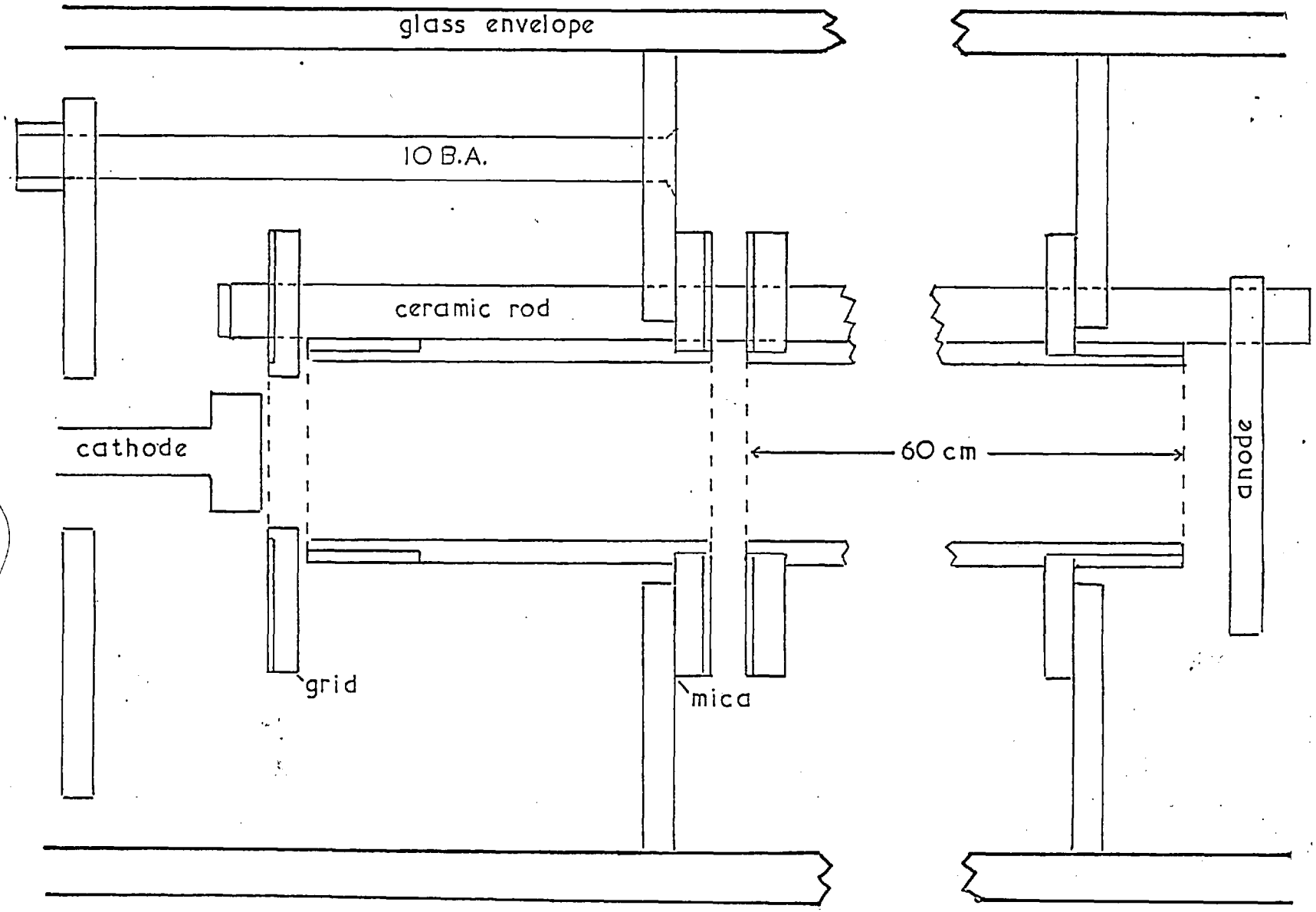


Fig. 2.1 Experimental tube (x4).

Bridges (15). Llewellyn's work leads to a method of representing vacuum tubes by active networks when the frequency is so high that the ordinary representation in terms of constant dynamic impedances is inadequate. The results for a plane parallel diode are plotted in Fig. 2.2 which shows the variation of plate impedance, Z_p, with transit angle. If τ represents transit time then the transit angle for a signal of frequency w is defined as $w\tau$. To obtain these results Llewellyn assumed (i) that the a.c. signal magnitude was small compared with the standing current and (ii) that the electrons travel in one direction with a single velocity so that no overtaking occurs. Thus the existence of the potential minimum in front of the cathode and the spread in energy of the emitted electrons are neglected.

The grid-cathode region of the tube may be treated as a diode for the purpose of investigating current flow. We are primarily interested in the variation of the convection current I_v with grid voltage, since it is only this current which flows on into the rest of the tube. An expression for the convection current can be obtained from the Llewellyn analysis (see Appendix 2) and written in the form of a convectional impedance $Z_v = r_v + jx_v$ viz :

$$I_v = V_g/Z_v \qquad (2.2)$$

I_v is taken to refer to the convection current leaving the cathode surface at any instant.

The real and imaginary parts of Z_v are also plotted in Fig. 2.2. As with the plate impedance the convectional impedance becomes significantly complex at high frequencies which implies that I_v will not be in phase with V_g. It can be seen from Fig. 2.2 that distortion will not be serious provided the transit angle is less than 1 radian. For modulation at a frequency of 1000 MHz the transit time must thus be less than 0.16 nsec.

The cathode-grid transit time for the ideal case of

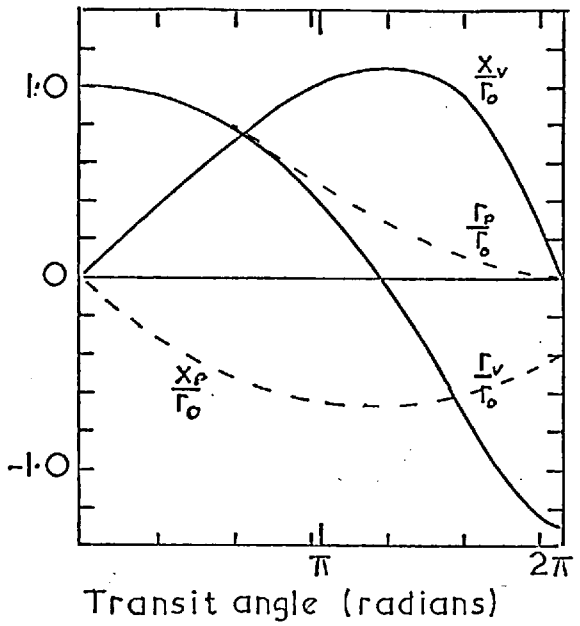


Fig. 2.2 Variation of convection impedance, Z_v, with transit angle. $Z_v = r + jx$, r_o = d.c. impedance (Z_p shown by broken line)

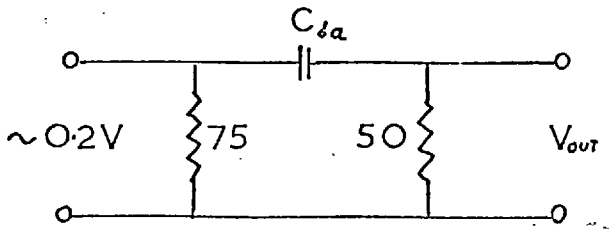


Fig. 2.3 Equivalent circuit of anode region (omitting beam)

zero electron emission velocity as given by Beck (9) is :

$$\tau_{cg} = 6.71 \times 10^{-8} (d_{cg}/J_{sat})^{\frac{1}{2}} \text{ sec} \qquad (2.3)$$

J_{sat} represents the maximum cathode current density which for ordinary oxide coated cathodes is about 10^4 A metre^{-2}. Thus if τ_{cg} is to be less than 0.16 nsec the cathode-grid separation d_{cg} must be less than 0.136 mm. If J_{sat} is reduced from its maximum value, by lowering the cathode temperature for example, eqn. 2.3 shows that τ_{cg} will be increased and consequently the high frequency modulation performance will be reduced. Table 2.1 column 1 shows transit times calculated from eqn. 2.3 for d_{cg} of 0.1 mm and various values of J_{sat} .

In practice modulation is achieved by biasing the grid so that less than the saturation current flows, and applying small changes in voltage about the bias value. Under these conditions there will be a potential minimum in front of the cathode at which some electrons will be reflected. The Llewellyn analysis is not strictly applicable to this case, but the requirement that the transit angle should be less than 1 radian is probably adequate as a design criterion.

The potential distribution between cathode and grid in the case of steady current flow can be determined using a method due to Langmuir (16), which takes into account the spread of electron emission energies, and the presence of the minimum. From this potential distribution the transit time can be determined and is shown in column 4 of Table 2.1 for the slowest electron, i.e. an electron which is just able to pass the minimum. It can be seen that the transit

J_{sat} (Am^{-2})	τ_{cg} (nsec)	J (Am^{-2})	τ (nsec)
10^4	.14	10^4	.15
10^3	.31	10^3	.64
10^2	.67	10^2	1.18

Table 2.1. Current density and Transit Time $d_{cg} = 0.1$ mm. Column 4 calculated assuming $J_{sat} = 10^4 A m^{-2}$ and cathode temperature = 800°C.

time is increased at low current densities. This is because the grid must be set at a low potential for low current and the electrons will travel relatively slowly towards it.

Thus far we have considered the beam alone. However the cathode and grid will possess a capacitance which is effectively in parallel with the beam impedance. It can be shown (9) that this capacitance is effectively equal to 0.6 of that which the electrodes would have in the absence of space charge. The magnitude of this capacitance is normally much greater than that due to the reactive component of Z_p and will limit the speed with which the grid may respond. If the grid is to respond properly to signals of 0.3 nsec risetime fed to it via a 50 ohm cable the CR constant of the circuit must be of the order of 0.1 nsec; i.e. the effective capacitance of the grid, C, to earth must be less than about 2 pf. Since d_{cg} is determined by transit time considerations the only way of reducing C is by reducing the cathode area.

To sum up, for good high frequency performance a small value of grid-cathode spacing and a cathode with high emission are required. It is also necessary that the grid should not bias off a large fraction of the emitted current and that the grid capacitance to earth should be small.

The value of d_{cg} used was 0.1 mm this being the smallest distance consistent with practical convenience. The oxide coated cathode of 5 mm diameter was supplied by E.M.I. Ltd. The effect of stray capacitance was underestimated in the design of the modulation structure and when it was assembled it was found to have a cold grid-earth capacitance of 7 pf. Much of the stray capacitance was eliminated by a grounded grid design in a later tube.

2.1.2. Grid-screen spacing.

This distance (d_{gs}), is governed by the need for a small capacitance between grid and screen, which requires a large spacing, and the need to avoid forming a potential minimum in this region which requires a short spacing. (See eqn. (4.4)). A value of 2 mm was chosen as a suitable compromise.

2.1.3. Length of screen section.

The dispersion pulse applied to the drift section is of the order of some tens of volts in amplitude. In spite of the decoupling of the screen it was difficult to prevent some of this signal reaching the grid and so producing some beam modulation. However the screen section introduces a delay which allows modulation by the modulation pulse to be completed before the dispersion pulse is applied. A screen length, d_s , of 2 cm was chosen. At 10 volts this results in a delay of about 10 nsec.

2.1.4. Screen-drift spacing.

The principal consideration in this space, d_{sd} , is that an electron should enter the drift section with a velocity corresponding to the drift section potential. This will always be the case when the drift potential is fixed but is not necessarily so when this potential is pulsed, as we have seen in Chapter 1. It can be seen from eqn. 1.15 that the necessary condition is that v should be small compared to V_1 , i.e. the change in potential of the drift section as the electron crosses the gap must be small. If the screen and drift sections are each initially at 25 volts and a spacing of 1 mm is chosen, then the transit time between them will be about 0.3 nsec. The rate of change of voltage imposed on the drift section will be about 10V/nsec; it then follows from eqn. 1.15 that the electron will enter the drift section with a velocity about 2% less than that which it would have possessed in the absence of the dispersion pulse. A spacing of 1.5 mm was actually used to avoid the possibility of contact between the mesh clamping annuli.

2.1.5. Length of drift section.

The maximum duration of the magnified modulation pulse is of the order of the drift section transit time. To

obtain a magnification of 30 on a pulse originally of 3 nsec duration a drift transit time of 90 nsec is required. Accordingly a drift length, d_d , of 60 cm was chosen; this gives a transit time of about 100 nsec at 100 volts.

2.1.6. Drift-anode spacing.

The most critical feature of this section, d_{da}, is the drift-anode capacitance C_{da} which must be very small so as to prevent feed-through of the dispersion pulse from the drift section. As the dispersion pulse may be several tens of volts and the output signal only a few millivolts this is a serious problem. Fortunately the output pulse does not appear until some 100 nsec after the dispersion pulse has ended. Even so it was found that, using a carbon resistor to terminate the drift section and a 30 volt dispersion pulse, about 0.2 volts of spurious reflections persisted at the termination after this period.

The output signal was fed to an oscilloscope via a 50 ohm cable, so that the equivalent circuit of the anode region can be represented as in Fig. 2.3. The period of the spurious oscillations was about 100 MHz ; this corresponds with the fall time of about 3 nsec of the dispersion pulse. If V_{out} is to be less than 2mV then it can easily be shown that C_{da} in Fig. 2.3 must be less than 0.3 pF. If the anode plate and the mesh defining the end of the drift section are considered as a parallel plate condenser, this capacitance should correspond with a spacing of 2 mm. This distance was used, although in the assembled tube the measured capacitance was 0.7pF again indicating the importance of stray capacitances due to pin clips etc.

As in cathode-grid region, it is necessary that the drift-anode transit time should be small compared with the period of modulation of the beam, if the anode voltage is to be linearly related to the instantaneous beam current. This is not a very critical requirement because the electrons travel much faster near the anode than in the cathode grid region. Moreover, if any stretching of the modulation pulse has been

obtained the modulation period at the anode will be increased. With 25 volt electrons emerging from the drift section and the anode at the same potential, a spacing of 2 mm corresponds to a transit time of 0.6 nsec. This can be reduced if necessary by increasing the anode voltage.

2.1.7. Diameters of beam, drift tube and glass envelope.

The beam diameter is a parameter which influences the steady state conditions and the propagation of space-charge waves as described in Chapters 4 and 5. At the design stage of the tube these influences were not fully understood and a beam diameter of 5 mm was chosen arbitrarily.

The drift tube diameter should be fairly close to the beam diameter, but not so close that the alignment of the magnetic field becomes critical. A tube with 0.375" o.d. and 0.036" wall was used.

The impedance of the transmission line formed by the platinum coating on the inside of the glass envelope and the drift tube is given by the relation

$$Z = 60 \ln(d_1/d_2) \qquad (2.4)$$

where d_1 , d_2 , are respectively the i.d. of the envelope and the o.d. of the drift tube. Pyrex tube of 36 mm o.d. and 1.5 mm wall was used to provide a nominal impedance of 75 ohms.

2.1.8. Lead inductance.

Strictly speaking inductance can be defined only for a closed circuit. However it is possible to calculate the contribution to the total flux arising from a length of conductor forming the circuit. In this sense it is possible to talk about the inductance of a wire, but the inductance is not defined

unless the circuit of which the wire forms a part is also defined.

In tube design it is not practicable to calculate the exact value of inductance corresponding to all the tube elements. Nevertheless it is desirable to have some idea of the order of magnitude of inductance introduced by the various screws, leads etc.

The computation of the inductance for short single loop circuits is complicated but has been carried out by Snow (17) for certain simple configurations. For the case of a rectangular circuit formed by a total length l cm of wire of diameter d cm Snow's results may be represented by the approximate formula

$$L \simeq 2\times10^{-9} l\{\ln(21/d) - 1.21\} \text{ henry} \quad (2.5)$$

Using this formula we give in the table below the inductance of lengths of 10 BA studding and 22 gauge wire.

l	L (nH)	
(cm)	10 BA	22 SWG
1	2.7	4.2
5	29	37

Table 2.2. Inductance of leads.

The reactance of 5 cm of 10 BA studding is thus about 180 ohms at 1000 MHz. For this reason the outer sheath of the cable carrying the dispersion pulse was not earthed at the cathode but was connected to the screen, thus minimizing inductive elements between the cable and the screen-drift space across which the pulse was to be applied.

2.2. Tube construction.

The cylindrical and annular sections of the tube were all made of a nonmagnetic grade of stainless steel. The grid mesh was of nickel and had 500 t.p.i. and a 50% transmission factor. The other meshes were of tungsten with 100 t.p.i. and a 90% transmission factor.

The annuli supporting the meshes were clamped together by 12 B.A. stainless screws which were tapped into the thicker annulus and this was fixed to the cylindrical section by spot welding. At one end of the drift and screen sections the meshes were secured by a close fitting collar.

The drift and screen sections were joined using 0.092" diameter ceramic rods and inconel clips. A similar arrangement supported the anode plate. The screen flange was separated from the earth plate by 3 layers of mica sheet each about 0.001" thick. This provided a non inductive capacitance to earth of approximately 30 pF so that the screen was effectively decoupled at high frequencies. The earth plate was attached to the screen by 10 B.A. stainless steel screws having insulating pyrophilite sleeves which had previously been fired at 1200°C for one hour.

The tube envelope was made of 1.5 mm wall pyrex glass. 1 mm diameter tungsten pins were used to make contact through this envelope but before these were inserted the section of the glass surrounding the drift tube was painted with platinum and fired in a gas-air flame. Contact between the pins and electrodes was made by inconel clips and 22 gauge Eureka wire. These were so attached that the whole structure could be inserted into the glass envelope and that on rotation of the structure all the clips gripped their corresponding tungsten pins.

The cathode supporting legs were designed with care. The construction has to be rigid since d_{cg} is only 0.1 mm, but on the other hand too massive a support will result in too much heat loss by conduction and the heater will not be able to maintain the cathode at the correct temperature. In the structure used the cathode was clamped in a collar and this was supported by two legs about 5 mm long which were secured by tapped screws to the cathode plate. The inconel strip used to

form these legs was of 3 x 0.4 mm section. The legs are not shown in Fig. 2.1.

The resistive termination of the coaxial line formed by the drift tube and plantinum coated envelope was obtained by two carbon film resistors each of 150 ohms; it was found that this arrangement provided a better termination than a single 75 ohms resistor. The paint coating on the resistors was removed with dichloromethane and their brass end contacts replaced by inconel strip, so that they could be used in vacuum.

The preparation of all glass and metal parts for vacuum use followed a standard routine (18). When this had been carefully carried out the tube was assembled and placed on the pump. After baking at 350°C for two days the pressure was 10^{-7} torr, and this fell to less than 2 x 10^{-8} torr on cooling to room temperature. The cathode was then activated following a routine recommended by Rosebury (18). Finally the getters were fired and the tube sealed off.

3. THE ELECTRICAL CIRCUITRY

The electrical networks required for the operation of the tube consist primarily of bias supplies and pulse generators. These networks were designed to operate in conjunction with fixed voltage sources of -12V, + 12V, and +150V which were obtained from commercial stabilized power supplies.

3.1 Bias network.

The bias supply network is shown in Fig. 3.1. The most important requirements in this design are that each bias supply line should be well screened and decoupled to prevent pick-up from the dispersion pulse, and that the network should be compatible with proper termination of the pulse cables.

At the bottom left of Fig. 3.1 is the grid bias network. This was designed to provide a variable bias of from 0 to -2 volts and an output impedance of approximately 50 ohms. The grid bias cable and modulation pulse cable were both of 50 ohms characteristic impedance so that the modulation pulse travelled down the bias cable and was absorbed by the bias network without appreciable reflections. The impedance to earth presented by the grid itself is much higher than that of the cables and so has a negligible loading effect. The 1nF capacitor at the grid end of the modulation pulse cable served to isolate the pulse generator from the grid bias voltage. The capacitors used were all of the non-inductive disc variety and their connecting leads were kept very short. The coaxial cables terminated on a contact strip adjacent to the tube and connections from this to the appropriate pins were made via lightweight coaxial cable to avoid straining the glass-metal seals.

On the lower right of Fig. 3.1 the screen and drift bias networks are shown. The screen voltage was variable from 0 - 75 volts and the drift voltage from 0 - 150 volts.

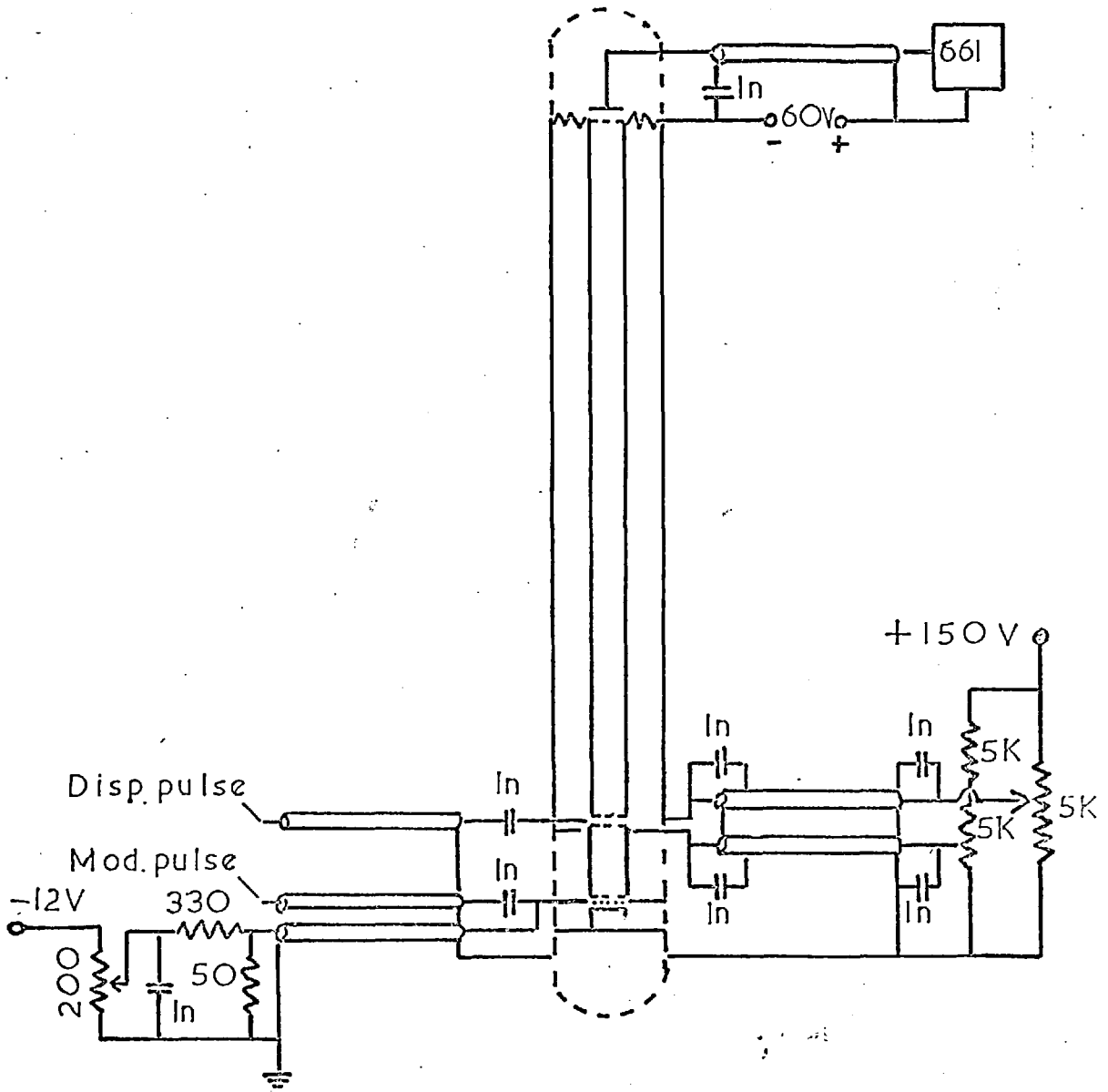


Fig. 3.1 Bias network.

The 50 ohm supply cables were decoupled at each end. There is no problem of matching impedances in this case; no pulse is applied to the screen and the bias to the drift section is applied to the outer conductor so that its transmission line properties are not altered.

At the top right of Fig. 3.1 a cable is shown connecting the anode to the Tektronix 661 oscilloscope. This cable matched the 50 ohm input impedance of the oscilloscope. Complete screening of the cable is very important on account of the small output signal. A special shielded pin clip was designed so that the coaxial sheath braiding could be continued right up to the tube envelope. It was found that some pick-up from the dispersion pulse arose from field penetration of the cable outer sheath. To obviate this the whole tube was screened in copper foil and it then proved possible to reduce the pick-up to about 2 mV.

To ensure that the link between the anode and the oscilloscope was perfectly matched and screened the output cable was connected directly to the oscilloscope without an isolating capacitor. Consequently the oscilloscope was at anode potential.

3.2 Pulse-generating network.

The circuit shown in Fig. 3.2 provides modulation and dispersion pulses, and a trigger pulse for synchronizing the oscilloscope.

The circuit is based on the Mullard range of integrated circuits. It is driven by the negative step from an OMY 121 multivibrator. Two appropriately connected 1nF capacitors provide a clock rate of approximately 100 KHz.

The FJH 131 units each comprise 4 NAND gates each of which has two inputs and one output. When either input is in a "high" state the gate is "on" and the output voltage is "low". If both inputs are in the "low" state the gate is "off" and the output voltage is "high". The minimum "high" voltage for the FJH 131 is 2 volts and the maximum "low" voltage is 0.4 volts. If an input is unconnected the effect on the gate operation is the same as if the input was earthed

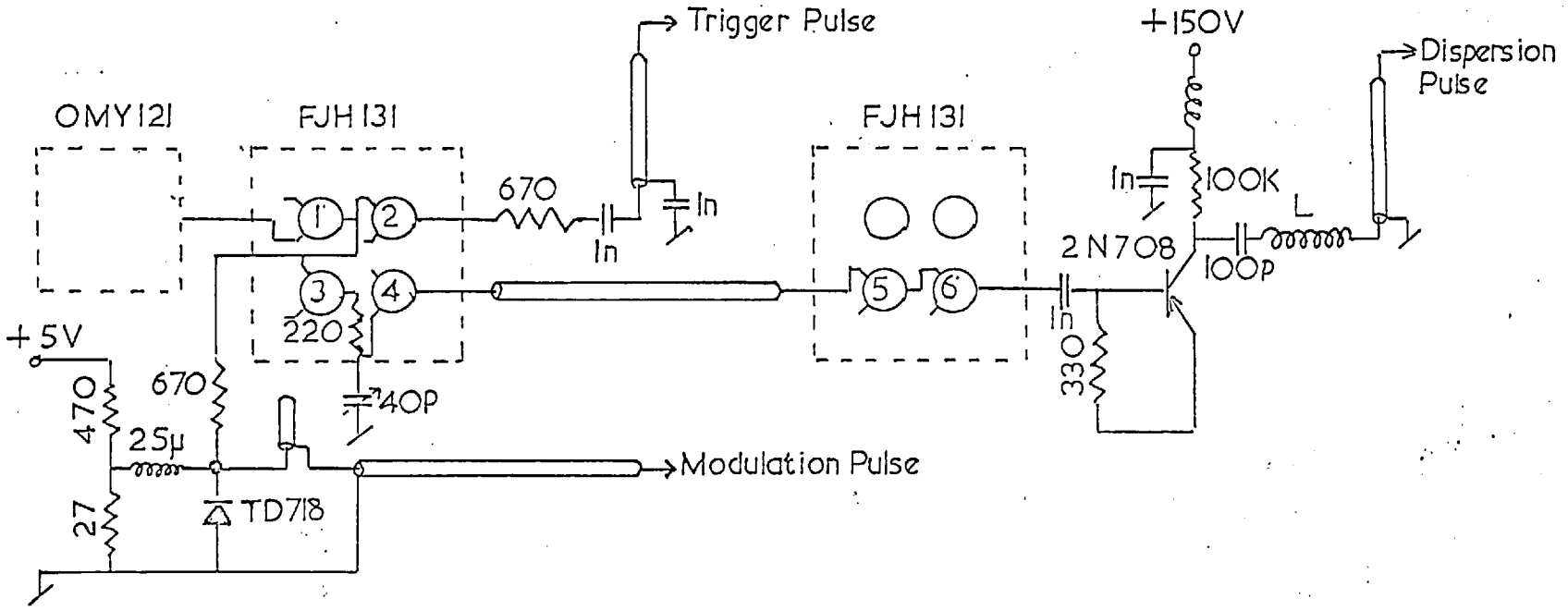


Fig. 3·2 Pulse Generator

or in the"low" state. The supply voltage is + 5 volts and was derived from the + 12 volts supply via a potential divider. (The supply leads are not shown in Fig. 3.1). Switching rise and fall times are typically 10 nsec and 4 nsec respectively.

Gate 1 is a buffer stage which drives gates 2, 3 and the tunnel diode. Gate 2 provides a 250 mV pulse for triggering the Tektronix 661 oscilloscope. The trigger cable is isolated by two 1 nF capacitors so that the oscilloscope is not earthed via the trigger cable.

The modulation pulse was normally derived from a tunnel diode. The diode is switched on by a positive current pulse from gate 1; it is switched off again some 10 μsec later by a negative pulse corresponding with the positive clock pulse. Bias is provided from a resistive network via a 25 μH inductor formed from two turns of 30 gauge enamelled copper wire on a ferrite core. A description of the switching mechanisms involved is given by Millman and Taub (19).

To obtain pulses of short duration a piece of coaxial cable was connected to the diode as shown. The resulting pulse length is then twice the signal transit time for the length of cable. The pulse obtained with this circuit is shown in Fig. 3.3. The rise and fall times are about 2 nsec and are mainly determined by the quality of the tunnel diode. For investigations where a synchronized dispersion pulse was not required the modulation pulse was derived from the Tektronix 661 oscilloscope which is able to provide a pulse from a tunnel diode circuit with a rise time of less than 350 psec.

The maximum voltage step which can be obtained from a tunnel diode is about 0.4 volts and the effect of the clipping cable is to halve this so that a modulation signal of only 0.2 volt is available. When a larger amplitude was required the pulse was derived from an avalanche transistor using a circuit similar to that described below for the dispersion pulse. A clean pulse cannot generally be obtained by this means, however, on account of the transient processes which occur as the transistor is recovering from the avalanche.

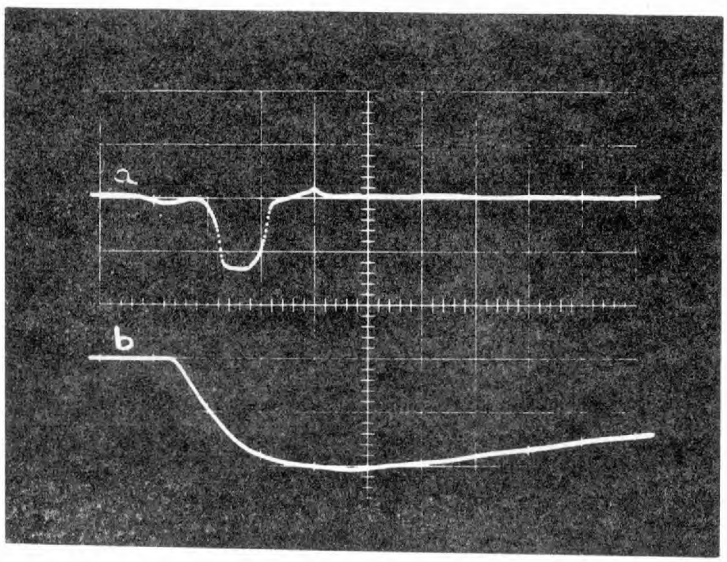


Fig. 3.3 Pulse generator output
(a) modulation pulse, 10ns/cm, 100 mV/cm.
(b) dispersion pulse, 10ns/cm, 10 V/cm.

The dispersion pulse was derived from a 2N708 transistor operating in the avalanche mode (20). This transistor can produce a 30 volt pulse into 75 ohms with a fall time less than 1 nsec. For the dispersion pulse an exponential waveform with a fall time of about 8 nsec was required. A suitable waveform was obtained from the avalanche pulse with the help of the inductance L. This consisted of 10 turns, 5 mm in diameter of 22 gauge enamelled copper wire. To reduce radiation the avalanche transistor and associated components were enclosed in a metal box mounted close to the tube and remote from the modulation pulse circuit. All power supply lines to this box were carefully decoupled. Two buffer gates 5, 6, were used to prevent feedback to the modulation circuit and reduce radiation from the trigger cable. A variable delay for the avalanche trigger pulse was made available by the preset capacitor at the output of gate 3. This provides an exponentially falling pulse and the time taken for the voltage to reach the "low" threshold for gate 4 is determined by the RC time constant of the capacitor and the 220 ohms resistor. Using the component values shown the time at which the avalanche began could be varied over a range of 12 nsec, thus facilitating synchronization of the dispersion pulse with the arrival of the modulated electron beam at the drift section.

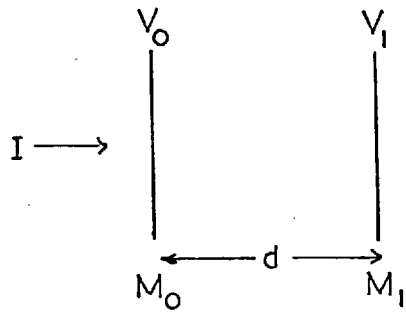
4. STEADY-STATE OPERATION.

In this chapter we consider the flow of current in the tube when an equilibrium state has been attained.

The tube may be considered to consist of a series of elemental regions which are of two kinds. These are (i) the space between two planes each plane corresponding either with the cathode, or with a mesh, or with the anode, and (ii) a conducting cylinder with a mesh across each end. We shall first examine the flow of current through an idealized representation of each of these elemental regions. Subsequently it will be shown that by also considering the energy spread of the electrons and the emission of secondary electrons the experimentally observed currents may be accounted for.

4.1. Current flow between planes.

Consider the current flow between two infinite plane electrodes at potentials V_0 , V_1 respectively and separated by a distance d, as shown below:



If we assume that the electrons are emitted with zero velocity from a plane cathode then the subsequent flow will be uniform in a plane parallel to the electrodes and may therefore be described by Poisson's equation in one dimension.

$$\frac{d^2V}{dx^2} = -\frac{\rho}{\epsilon_0} \quad ; \qquad (4.1)$$

Expressing the charge density ρ in terms of the potential V and current density J one obtains

$$(dV/dx)^2 = (4J/\varepsilon_0)\sqrt{(m/2e)}\sqrt{V} + K_1 \qquad (4.2)$$

where K_1 is a constant. The solutions to this equation which give V as a function of x for any given value of J have been investigated in detail by Fay, Samuel and Shockley (7) and we give here a summary of the relevant conclusions.

In the particular case when $V_0 = o$, plane M_0 can be identified with the cathode. Integration of eqn. 4.2 then yields Child's law, or the diode eqn.

$$J = (4\varepsilon_0/9)\sqrt{(2e/m)}(V^{3/2}/x^2)$$

$$= 2.34\times10^{-6}V^{3/2}/x^2 \text{ Amp metre}^{-2} \qquad (4.3)$$

In general V_0 will not equal zero as for example when M_0 represents the grid.

The results of integrating eqn. 4.2 in this case are illustrated schematically in Fig. 4.1. The electrons are emitted from a cathode in plane c so that, in the region between c and M_0, V is described by eqn. 4.3. When V_1 is large the potential between M_0 and M_1 approximates to the charge free case where V is a linear function of x (curve a). As V_1 is reduced space charge depresses the potential between the planes so that it is no longer linear (curve b). When V_1 is close to V_0 a potential minimum exists (curve c). As V_1 is further reduced the minimum moves towards the anode (curve d). Finally at sufficiently low values of V_1 a virtual cathode is formed and the potential distribution changes suddenly (curve e). When this occurs some electrons are reflected and do not reach M_1.

If V_0 and V_1 are fixed and J is gradually increased the potential distribution will pass through ~~the~~ curves similar to (a) - (e). The condition of maximum current flow is obtained just before a virtual cathode forms. Increasing the injected current to greater values results in the formation of the virtual cathode and a decrease in the current transmitted to M_1.

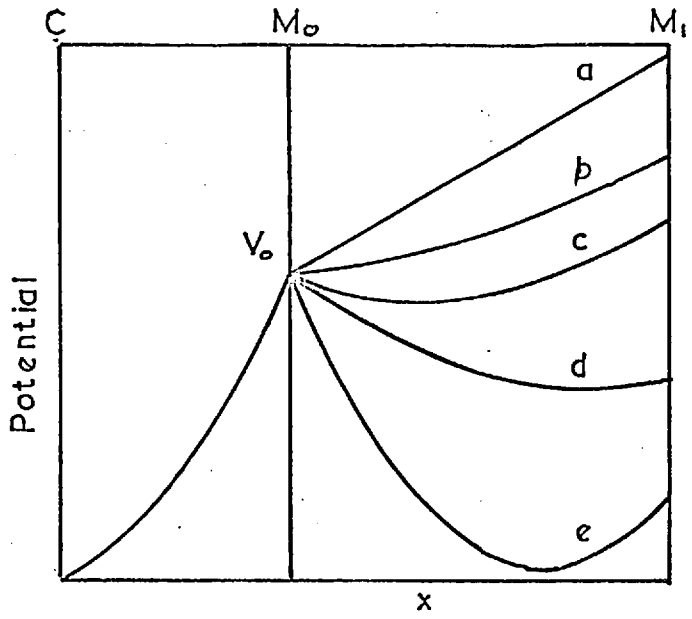


Fig. 4.1 Potential distribution between planes.

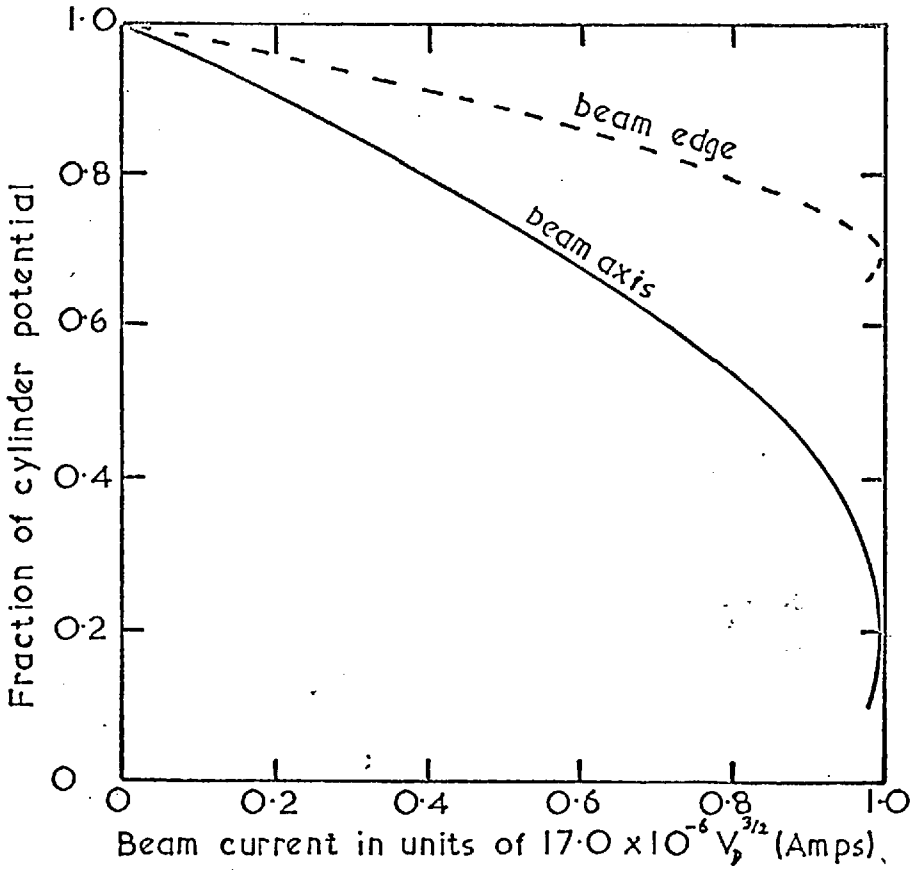


Fig. 4.2 Potential distribution in cylinder (a/b=1·5)

From a practical point of view it is important that a virtual cathode should not be formed in the tube. This produces a reduction in the output signal on the one hand and on the other the reflected electrons can produce parasitic oscillations or they may return to the anode at a later time so causing signal distortion.

The sufficient condition that a virtual cathode should not be formed is that the injected current J_i should be less than a critical current J_c where

$$J_c = \frac{2.34\times10^{-6}V_0^{3/2}}{d^2}\left[1 + \left(\frac{V_0}{V_1}\right)^{3/4}\right]^2 \qquad (V_1 > V_0)$$

$$J_c = \frac{2.34\times10^{-6}V_0^{3/2}}{d^2}\left[\frac{(V_0/V_1)^{\frac{1}{4}}}{1 + (V_0/V_1)}\right]^{\frac{1}{2}} \qquad (V_1 \leq V_0) \qquad (4.4)$$

It is interesting that the R.H.S. of the above equations do not represent the maximum current densities which can occur. For values of J_i greater than J_c the potential distribution is not uniquely determined by the boundary conditions but depends also on the way in which these are established. If J_i is increased from a very low value, the virtual cathode is not formed until J_i reaches a value ($> J_c$) given by

$$J' = \frac{2.34\times10^{-6}V_0^{3/2}}{d^2}\left[1 + \left(\frac{V_0}{V_1}\right)^{1/2}\right]^3 \qquad (4.5)$$

However if the injected current is reduced from a high value the virtual cathode persists until the boundary represented by eqns. 4.4 is reached. These equations therefore represent the boundary on the lower current side of which a virtual cathode is never formed. The phenomenon is analogous to the hysterisis of magnetic materials.

The variation in potential between the planes will affect the transit time for an electron passing between them. When $V_0 = V_1$ the transit time when a virtual cathode is present is three times as great as in the case for which space charge

effects are negligible. The electrode planes in the tube are generally too closely spaced to allow a significant depression of potential between them and the effect of space charge on transit time is very slight except, as mentioned in chapter 2, in the region between cathode and grid.

4.2. Current flow through a conducting cylinder.

As an ideal representation of the screen and drift sections we consider the flow of current in a beam of radius b within a conducting cylinder of radius a at a fixed potential V_a. The beam is confined by an infinitely strong magnetic field. Moreover we assume that the length of the cylinder is much greater than its radius so that end effects may be neglected and the potential within the cylinder may be considered to be a function only of the distance r from the beam axis. Under these conditions Poisson's equation in cylindrical coordinates reduces to

$$\frac{1}{r}\frac{d}{dr}\left(r\frac{dV}{dr}\right) = \frac{J}{\epsilon_0}\left(\frac{m}{2eV}\right)^{1/2} \qquad (4.6)$$

We require a solution in which $V = V_a$ at the cylinder wall and which satisfies the standard boundary conditions at the periphery of the beam. Fig. 4.2 shows solutions obtained using the methods of Smith and Hartman (8) for the case in which a/b = 1.5.

The maximum total current which can be passed through the cylinder is given by

$$I_{max} = kV_a^{3/2} \qquad (4.7)$$

when a/b = 1.5, $k = 17 \times 10^{-6}$, k is surprisingly, independent of the cylinder diameter. If the beam completely fills the cylinder $k = 32.5 \times 10^{-6}$.

Fig. 4.2 shows that the potential inside the beam may be considerably less than the potential on the cylinder wall.

Moreover the potential on the beam edge is not the same as on the axis. This implies that for a fixed cylinder potential, electrons on the edge of the beam travel faster than those on the axis. In order to avoid pulse distortion, therefore, the operating current should be considerably less than I_{max}. In Fig. 4.2 it can be seen that if the operating current is about 10% of I_{max} then the potential on the beam axis will be about 3% less than that on the edge. For operating currents less than 1% of I_{max}, the beam edge and axis potentials may be considered equal to the cylinder potential for practical purposes.

4.3. Energy spread of the electrons.

In the preceeding sections it has been assumed that all the electrons have zero velocity at the cathode surface, although it is well known that these electrons in fact have a Maxwellian velocity distribution. For such a distribution 99% of the electrons will have axial velocities which fall within a range corresponding to an energy of 3 kT. For an oxide cathode operating at 800°C this range is thus about 0.3V. There may be depression of potential due to space charge but this should not affect the spread in the energies of the electrons at a particular point in the system, at least so long as a virtual cathode is not formed.

Nevertheless it has been established by Boersch (21) and others that in any electron beam system the spread in energy is generally much greater than the Maxwellian value of 3kT which is only approached at very low current densities. The observed spread in energy is too great to be accounted for by the modification of the distribution caused by a virtual cathode or by variations in work function over the surfaces of the real cathode.

An interesting explanation of the additional broadening of the energy distribution has been given by Hartwig and Ulmer (22) based on the idea that the equilibrium distribution of electrons in phase space is symmetrical (Liouville's Theorem). Thus if the momentum and position of the electrons emerging from the cathode are plotted in phase space the resulting distribution should

be symmetrical with respect to the three spatial axes of this space. However, because the electrons are then accelerated in one particular direction away from the cathode a new distribution will be formed which is no longer symmetrical. Consequently the electrons rearrange their momentum on account of mutual collisions until the distribution becomes again symmetrical in phase space. This involves an increase in the longitudinal velocity spread at the expense of the transverse components, which are reduced. The rearrangement is naturally not instantaneous and a relaxation time can be defined which depends upon the degree of interaction of the electrons. If, in a given region, the transit time is short compared with the relaxation time the relaxation will not be complete. It is for this reason that the Maxwellian distribution is only observed at very small current densities, where the electron interaction is very slight. If the relaxation is complete the longitudinal spread in energy ΔE_x of electrons with mean energy E_1 is given by

$$\Delta E_x = \left(\frac{8}{3} E_1 \, \Delta E_{x_0}\right)^{\frac{1}{2}} \qquad (4.8)$$

where ΔE_{x_0} is the longitudinal energy spread at the cathode. $\Delta E_x, \Delta E_{x_0}$ are here defined as the smallest increments of energy which can include 63% ($\simeq 1 - 1/e$) of the total number of electrons.

4.4. Secondary electron emission.

Studies of secondary electron emission (23, 24) have shown that when a metal is bombarded with electrons having an energy, E_p , greater than about 100 eV the electrons which are subsequently emitted may be separated into three groups:

Group 1 consists of elastically reflected primary electrons having an energy E_p .

Group 2 consists of electrons with energies mainly between E_p and about 50 eV. These are rediffused primary electrons which have penetrated the bulk material and been subsequently emitted. They are relatively few in number.

Group 3 consists of electrons with energies less than 50 eV. The majority of electrons fall into this group and are called true secondaries.

The value of 50 eV is somewhat arbitrarily taken as the division between groups 2 and 3 since there is no way of discriminating between the processes involved in the emission. For primary energies less than 100 eV the distinction between all the groups is less marked.

The presence of secondary electrons in the tube is generally undesirable since they tend to increase space-charge effects and to obscure the main output signal. Since most secondaries are produced at the anode we shall first consider their effect there.

Suppose that a primary current I_p is incident at the anode surface and that a fraction r of this current is reflected, then the fraction (1 - r) will penetrate the anode surface. A number of secondaries of groups 2 and 3 will subsequently be emitted giving rise to a secondary current of magnitude $I_p (1 - r)\delta_t$, where δ_t is the secondary yield coefficient for these groups. If the drift section potential is higher than that of the anode these secondaries will re-enter the drift section and the current flowing from the anode will be $I_p (1 - r)(1 - \delta_t)$. However if the anode is maintained at a potential of more than 50 V relative to the drift section the secondary current will be recollected by the anode and the anode current will be $I_p (1 - r)$ which is independent of δ_t.

δ_t is not equal to the total secondary yield δ which as usually defined includes also the group 1 electrons. δ_t is related to δ by the relation

$$\delta_t = \frac{\delta - r}{1 - r} \qquad (4.10)$$

(See Bruining (24)).

Secondary emission also occurs at the various meshes in the tube. Here some secondaries may be reflected and others transmitted through the mesh in the direction of the primary beam so that a current gain results, as in an electron multiplier. Reflection of the electrons especially at the anode results in a current flowing in the direction opposite to the primary beam so

that electrons are incident on the mesh from both sides. If we were to allow for all possible currents which could flow any analysis would become very complicated.

However the shadow ratio of the meshes in the drift and screen sections is small and the electrons travel so slowly to the grid that few secondaries result, so that we can afford to neglect entirely the secondary emission at meshes and consider that they simply absorb a certain fraction of the current incident upon them. With this assumption a simple model of the currents flowing can be developed which accounts adequately for the currents observed. This model is explained in the next Section.

4.5. Model for equilibrium flow.

Consider the schematic representation of the tube in Fig. 4.3. Suppose a forward current I_1 is initially incident at the cathode end of the drift section. At the first drift section mesh some of this current will be absorbed and a fraction $I\alpha$ will pass into the drift section, α being the transmission factor for the mesh. Similarly at the anode end of the drift section more current will be absorbed and the fraction $I\alpha^2$ will pass on towards the anode. At the anode surface a fraction r of the incident current will be reflected and the measured anode current will be $(1 - r)I\alpha^2$, provided that the anode is maintained at a potential more than 50 V higher than that of the drift section so that we can neglect the effect of inelastically scattered primary electrons and true secondaries as discussed in Section 4.4.

The reflected electrons will return to the drift section where they form a reverse current of magnitude $I\ r\alpha^3$. Thus in the drift section we have a forward current of $I\alpha$ and a reverse current of $I\ r\alpha^3$ while the current flowing the anode circuit is $I\alpha^2(1 - r)$. These relations are of importance in the next section. For clarity we have assumed that both meshes have the same α and consider only the drift and anode regions of the tube, but there is no difficulty in extending the scheme to include all the tube regions if necessary.

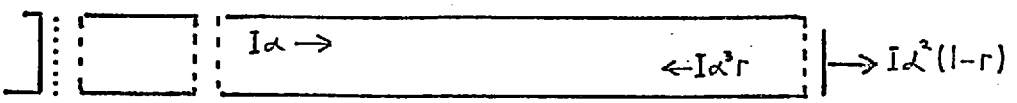


Fig. 4-3 Model for equilibrium flow

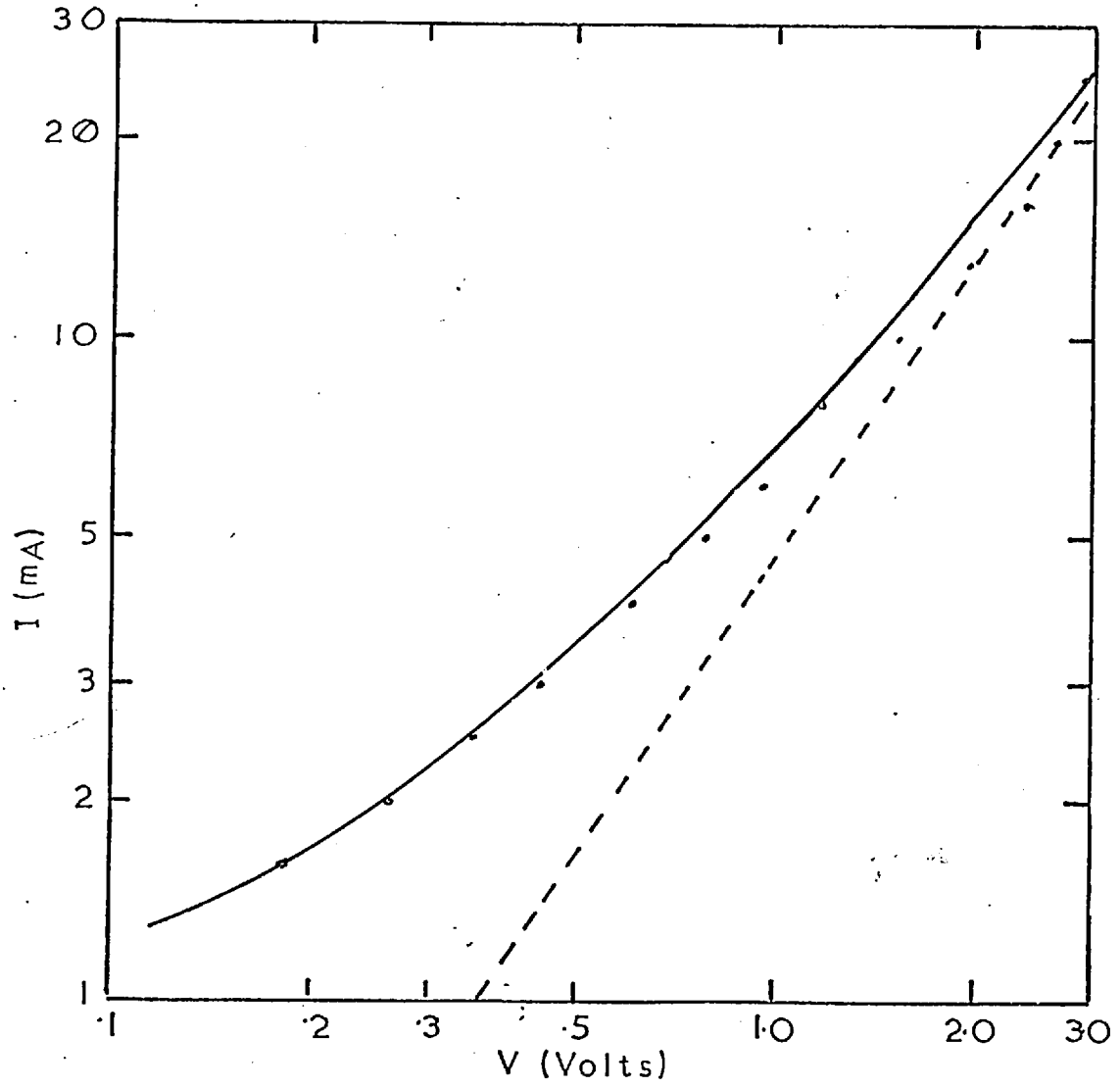


Fig. 4-4 Diode characteristic

The mesh transmission factor α is largely determined by the geometrical shadow ratio of the mesh but it is also affected to some extent by the local electric and magnetic fields which may increase or reduce the number of electrons intercepted by the mesh wires.

4.6. Experimental results.

The tube has five electrodes and the current flowing to each is a function of the relative potentials of all the other electrodes. From the numerous set of possible characteristic which could be drawn for this arrangement four have been selected which are important from a practical point of view and which illustrate the ideas discussed earlier in this chapter.

4.6.1. Cathode-grid space.

The effect of the grid in modulating the electron stream leaving the cathode can be examined by connecting the grid to the screen, drift and anode sections and observing the current flow to this composite electrode as a function of its potential relative to the cathode. This composite electrode is practically equivalent to an anode plate in the plane of the grid and the characteristic obtained is called the diode characteristic.

The simple theory of diode behaviour leads to the relation between current density, J, and applied voltage, V, expressed by eqn. 4.3. In a practical diode we should not expect the relation to hold at low values of V. This is for two reasons. First, the contact potential will be of the order of 0.5. volts so that the potential difference between cathode and anode will differ from the applied voltage by this amount. Secondly the electrons are emitted from the cathode with a spread in energy of the order of 0.3 volt whereas eqn. 4.3 is derived assuming all electrons have zero energy at the cathode. Both these effects would be expected to increase

the number of electrons emitted in comparison with the idealized case. This can be seen in Fig. 4.4.in which the broken line represents eqn. 4.3 with d = 0.1 mm. The experimental results indicated by dots are quite well represented by this equation when V is greater than 2 volts.

The spread in energy of the electrons leaving the cathode can be taken into account with the help of an analysis due to Langmuir (16). The result is shown by the full line curve in Fig. 4.4 where we have assumed that the contact potential of the anode is 0.5 volts relative to the cathode, that d = 0.12 mm and that the saturated cathode current density is $1 A/cm^2$. We thus obtain good agreement with the experimental points over the whole of the measured range.

4.6.2. Maximum current through drift section.

Fig. 4.5 is a log. plot showing the maximum anode current I_a (max) which can be obtained with various values of the drift section potential. The line has a slope of 1.5 and is well described by eqn. 4.7 with $k = 10.9 \times 10^{-6}$.

In section 4.2 it was shown that k should equal 17.0×10^{-6} considering the ratio of the beam and drift tube diameters. However, from the point of view of space charge effects it does not matter whether the space charge is due to a forward or a reverse current. The current expressed in eqn. 4.7 refers to the sum of these currents which we designate $\bar{I}_d$.

Using the model of Section 4.5 we obtain

$$\bar{I}_d = \frac{1 + r\alpha^2}{\alpha(1 - r)} I_a \qquad (4.11)$$

The mesh transmission factor α was determined by measuring the fraction of current transmitted by the mesh under various conditions. For the tungsten meshes an average value of 0.87 was obtained. The value of the reflection coefficient r was determined by deriving the current incident on and collected by the anode again using the model to interpret the

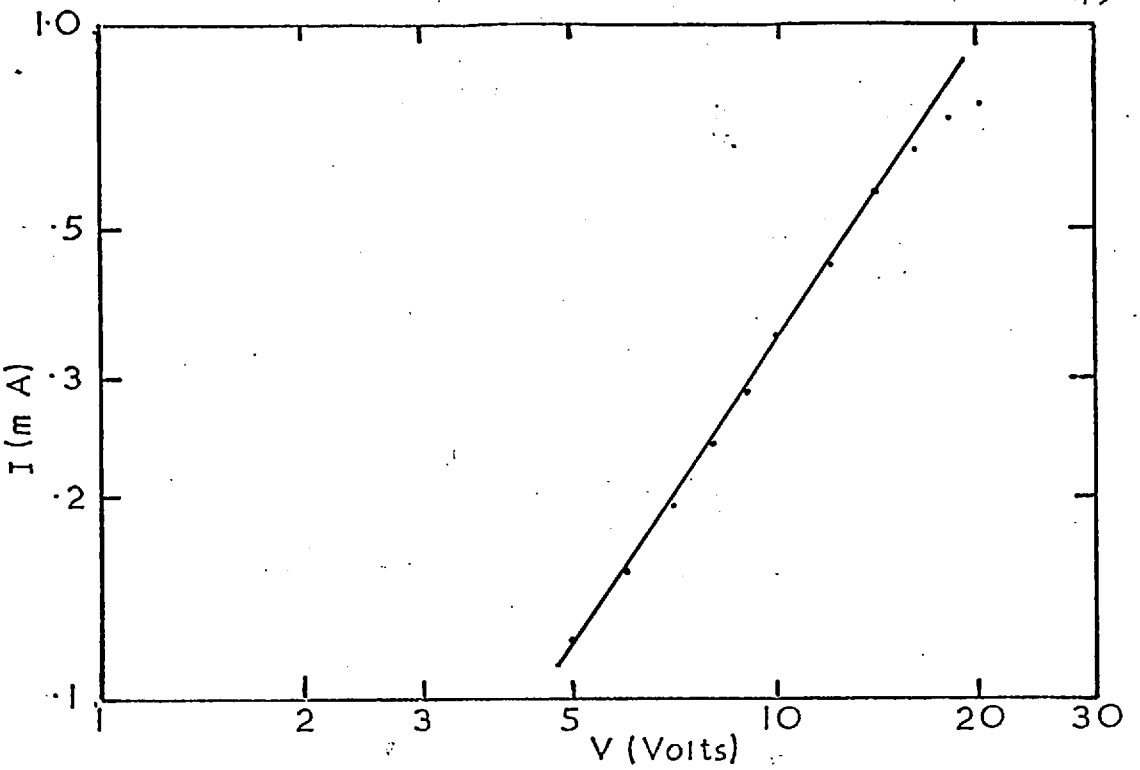


Fig. 4.5 Anode current/drift voltage characteristic

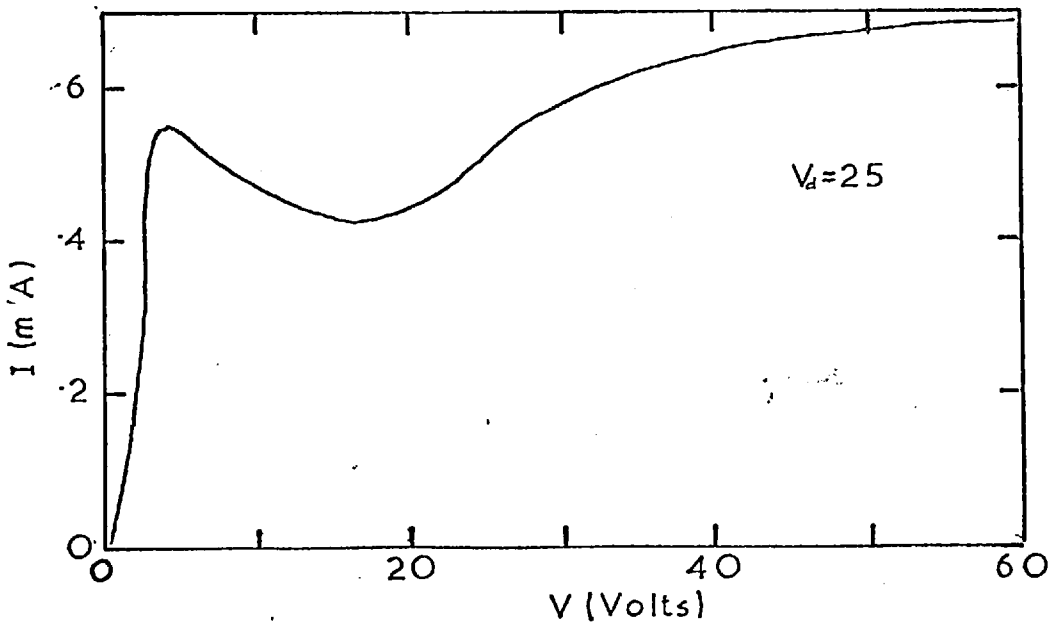


Fig. 4.6 Anode current/anode voltage characteristic

experimental measurements. A value of 0.15 was obtained which compares with a figure of 0.22 given by Sternglass (26) for iron.

Substituting these values of r and α in eqn. 4.11 gives

$$\bar{I}_d = 1.51 I_a \qquad (4.12)$$

If we now substitute for $\bar{I}_d$ in eqn. 4.7 we obtain a new value of k equal to 11.2×10^{-6} which agrees well with the observed value.

4.6.3. Anode characteristic.

In Fig. 4.6 the anode current/voltage characteristic is plotted. The dip in the curve at 17 volts is due to secondary emission from the anode surface and is analogous to the well known effect found in the corresponding characteristic for a tetrode valve.

A notable feature of Fig. 4.6 concerns the initial rise of current which occurs over about 3 volts. This is evidence of the velocity broadening discussed in Section 4.3. The value of ΔE_x determined from the graph is 1.4 eV whereas the maximum value calculated from eqn. 4.8, assuming that the velocity distribution at the cathode is Maxwellian, is 2.5 eV. Evidently the relaxation is not complete.

An additional contribution to the broadening could be a variation in the number of secondaries returned by the anode. These electrons will consist of all groups in this case since the anode is not generally at a higher potential than the drift section. Thus the fraction of returned electrons will be greater than r, which applies only to Group 1 electrons, and is likely to vary markedly with the anode potential. Consequently it would be difficult to use the tube to provide reliable measurements of the relaxation time although such measurements would be of interest because they could form a basis for the understanding of the detailed mechanism of the relaxation process - so far not understood.

4.6.4. Overall transfer characteristic.

On account of the absorbtion and reflection of electrons at the tube electrodes only about a quarter of the electrons which leave the cathode can be detected at the anode. We need to know how this useful current varies with the grid voltage so that the output current from the anode can be related to the input signal; in practice it will be desirable to confine the input signal to a linear portion of this characteristic which is shown by the full line in Fig. 4.7. The potentials of the screen and drift sections were set sufficiently high for this measurement so that only one virtual cathode was formed, very close to the front of the real cathode. Under these conditions the anode current is a monotonically increasing function of the grid voltage.

The fraction Ia/Ic of the total current which reaches the anode is shown by the dotted line in Fig. 4.7 and varies between 0.24 and 0.31. Since the transmission factor for the tungsten meshes is 0.87, four such meshes have a combined transmission factor of $(0.87)^4 = 0.58$. The control grid was found to have a transmission factor of 0.51 under the conditions of measurement. Assuming that the anode reflection coefficient is again 0.15 it would be expected that the overall transmission factor would be .58 x .51 x .85 = 0.25 which is included within the observed range. However the fact that the observed overall transmission factor varies slightly indicates that the actual processes occurring in the tube are more complicated than those represented by the simple model of Section 4.5.

4.7. The confining magnetic field.

The electrons leaving the cathode have transverse as well as longitudinal velocity components. Furthermore any space charge depression of potential at the beam axis will produce a transverse field also tending to accelerate electrons towards the tube wall. The effect of the magnetic field is to cause the electrons to move in helical paths, the

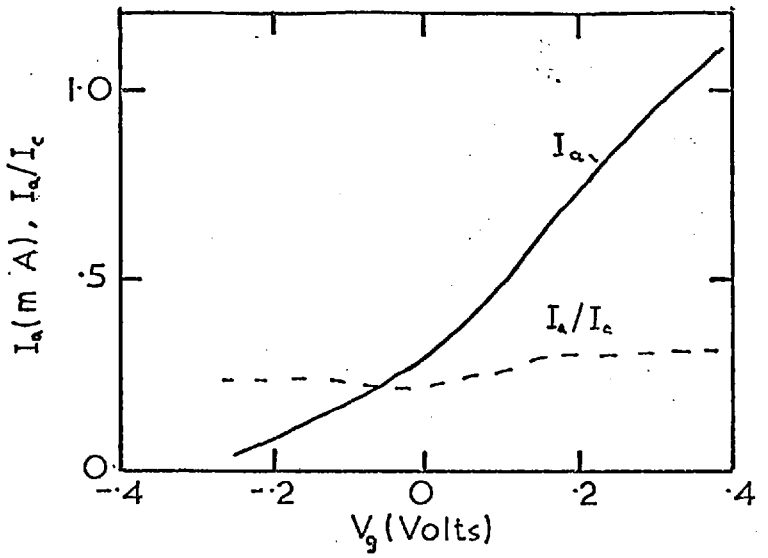


Fig. 4.7 Overall transfer characteristic

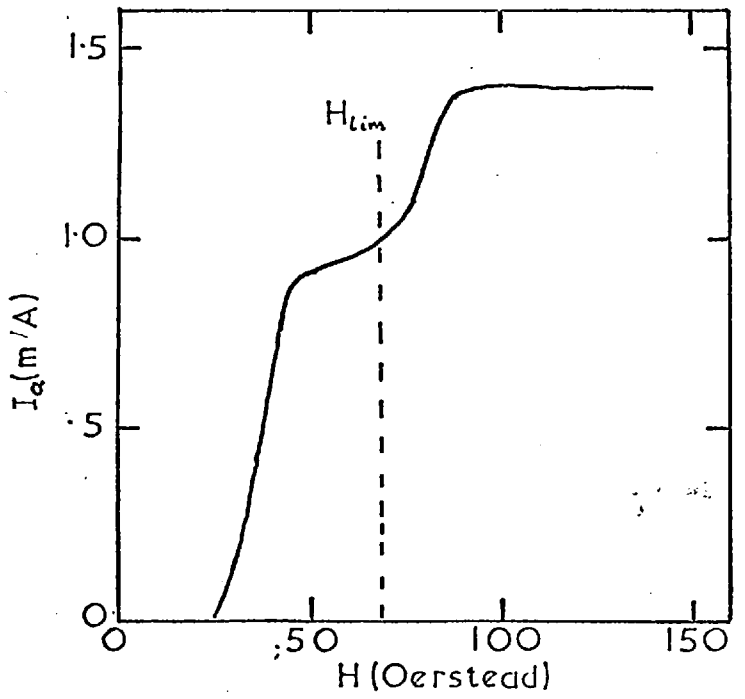


Fig. 4.8 Anode current and axial field

radius of the helix being determined by the relative strength of the field and the transverse forces.

For maximum current transmission the helical radius must be sufficiently small to ensure that the electrons at the beam edge do not touch the walls of the cylindrical electrodes. This condition has been calculated by Beck (9) for a beam initially of radius b enclosed by a cylinder of radius a:

$$H_{lim} = \left(\frac{2m}{e}\right)^{\frac{1}{2}} \frac{(V_a - V_b)^{\frac{1}{2}}}{\mu_o (a - b)}$$

$$= \frac{2.68 (V - V)^{\frac{1}{2}}}{(a - b)} \quad \text{Amp/metre} \qquad (4.13)$$

Here V_b , b, refer to the case of an infinite confining field. From Fig. 4.2 it can be seen that for maximum current flow $V_b = 0.69\ V_a$. Since $(a-b) = 1.35 \times 10^{-3}$ m we obtain

$$H_{lim} = 1.11 \times 10^{3} V_a^{\frac{1}{2}} \quad \text{Amp/metre}$$

$$= 13.9 V_a^{\frac{1}{2}} \quad \text{Oerstead} \qquad (4.14)$$

The variation with magnetic field of current transmitted through the drift section is shown in Fig. 4.8, together with the value of H_{lim} calculated from eqn. 4.14. The beam was not centred exactly on the drift section axis so that a field strength slightly greater than H_{lim} was required to prevent all of the electrons from reaching the wall.

All experiments were normally carried out using a field of approximately 3.8 Amp/metre (300 Oerstead).

5. MODULATED OPERATION

In this chapter we consider the effects arising from current and velocity modulation of the beam when the period of these modulations is short compared with the cathode-anode electron transit time and consequently the steady state theory of the preceeding chapter is not valid.

5.1. Current modulation.

Voltage modulation applied to the grid will produce current modulation of the beam. It will also produce a very small degree of velocity modulation owing to the change in potential of the minimum in front of the cathode as the electrons cross the cathode-grid space, but for practical purposes this can be neglected.

Fig. 5.1 shows the inverted traces obtained at the anode with (A) a 10 nsec 200 mV square pulse and (B) a 400 mV negative step applied at the grid. (The trace inversion facility of the Tektronix 661 oscilloscope was normally used so that input and output signals would appear in the same sense, i.e. so that a positive pulse at the grid would appear as a positive pulse at the anode). The most striking feature of Fig. 5.1 is that there are two pulses, not one as might have been expected, although the pulses merge together as Vd is increased. Moreover the pulses are distorted. For an understanding of these phenomena which are due to space-charge forces we must refer to the theory of space-charge waves but before introducing this it is useful to demonstrate how the pulses arise by means of a simple model.

5.1.1. The elastic rod model.

We can consider the electron beam to be represented by an elastic rod which is travelling in the direction of the

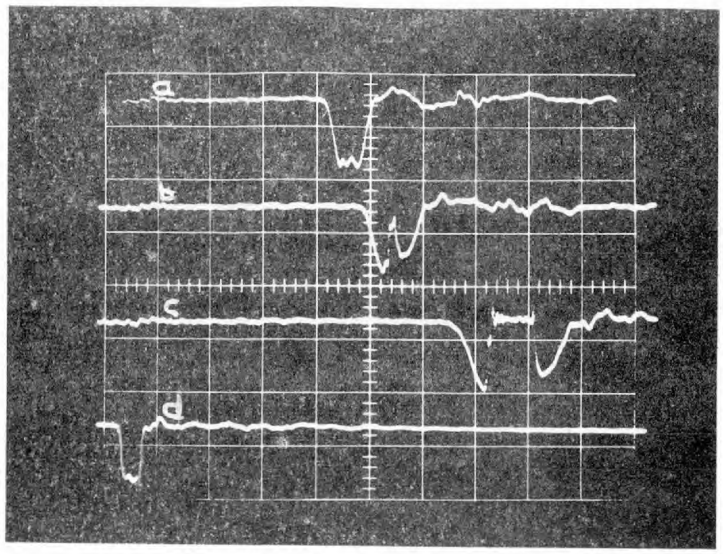


Fig. 5.1A Response to 10ns 200mV square pulse
20ns/cm, 5mV/cm, I_a=0.4mA.
(a) V_d=140V, (b) V_d=100V, (c) V_d=50V,
(d) pulse seen at grid (200mV/cm)

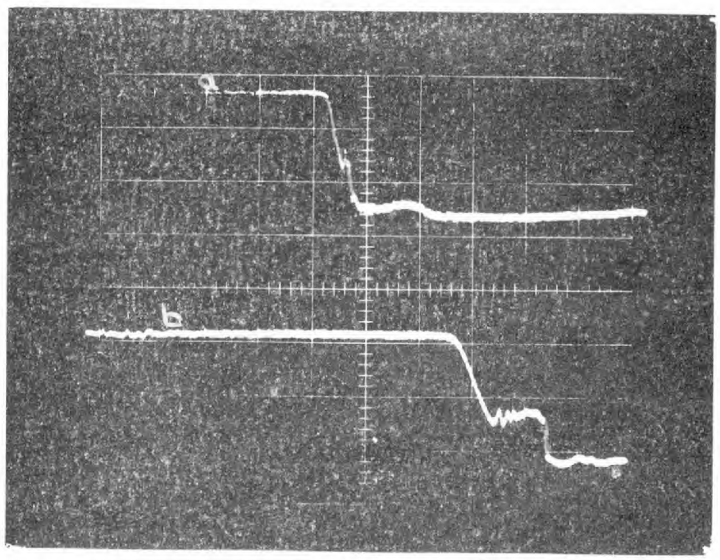


Fig. 5.1B Response to 400mV step.
20 ns/cm, 5mV/cm, I_a=0.4mA.
(a) V_d=140V, (b) V_d=50V.
(see also Fig. 5.11)

anode. Initially we consider the rod to be at rest and suppose that the elastic material is compressed over a section of the rod (Fig. 5.2 a). This corresponds to an increase in beam current or electron density caused by a positive grid pulse. As soon as the compressing forces are released pressure waves will travel along the rod in both directions from the site of the compression with a velocity u' , say. (Fig. 5.2 b). Now consider what happens if the rod travels towards the anode A with the electron velocity u_o . (Fig. 5.2 c). If u_o is greater than u' an obsever at the anode will see two compression waves with velocities $u_o + u'$, $u_o - u'$ respectively. If the compression is formed initially at the grid G, then the times taken for the fast and slow wavefronts to reach the anode will be $s/(u_o + u')$, and $s/(u_o - u')$ respectively, s being the grid-anode distance.

If u' is small in comparison with u_o , or if s is very short, then the compression waves will not have time to spread out before A is reached, and only one pulse will be observed. This is the case in a conventional valve where s is of the order of a few millimetres only.

5.1.2. Space-charge waves.

For a proper analysis of the motions of electrons forming the beam it is necessary to obtain solutions to Maxwell's equations which are appropriate to the tube design. The principles of such analyses have been described by several authors (10, 11, 30) and an abbreviated account of the application of these principles to the case of a uniform cylindrical beam enclosed in a conducting cylinder is given in Section 9.2. The analysis shows that in this system two waves having different velocities can be propagated. The transit times for the corresponding fast and slow pulses

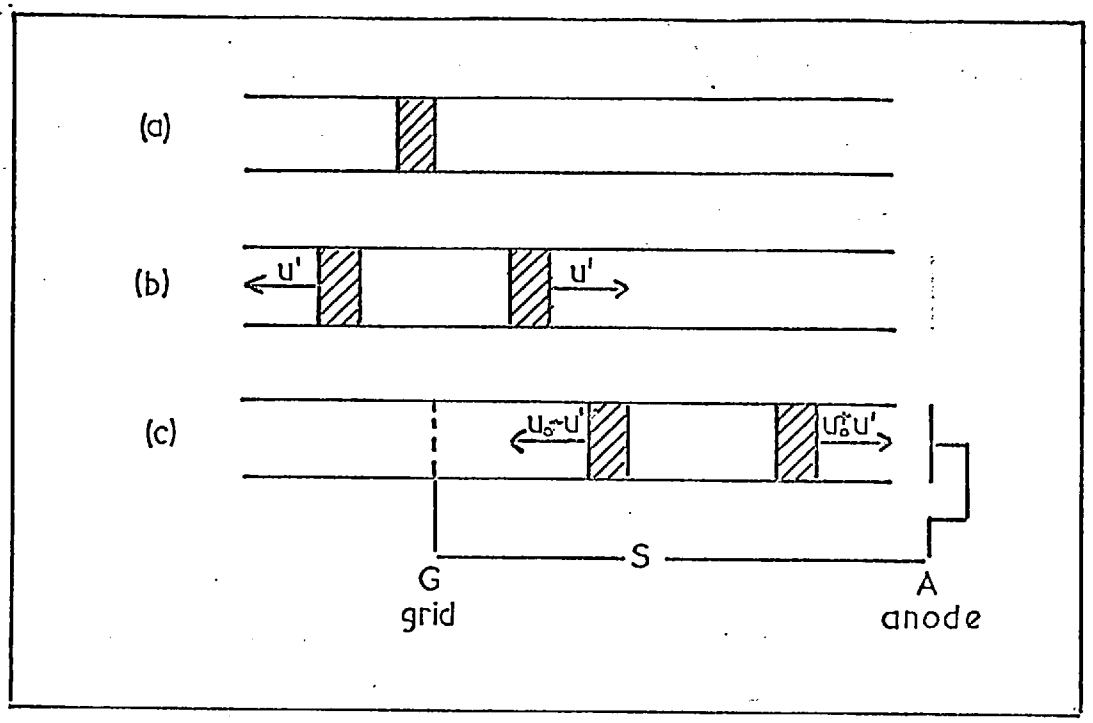


Fig. 5·2 Elastic rod model

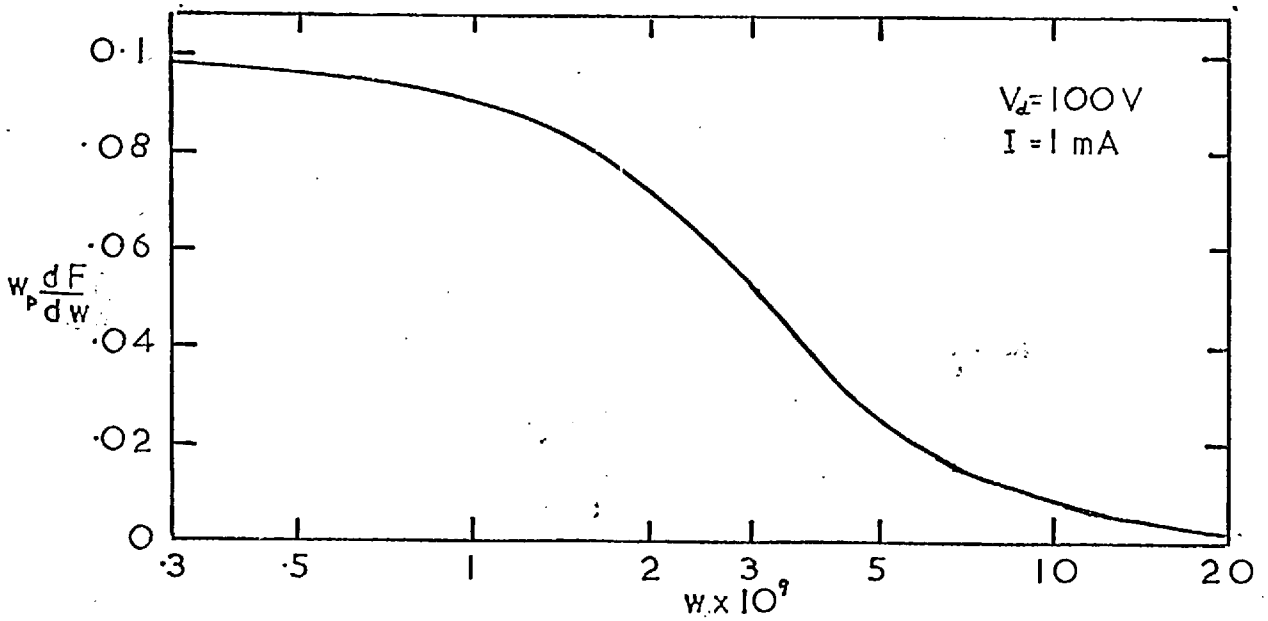


Fig. 5·3 $w_p(dF/dw)$ as a function of w

are given by

$$T_f = T_o\{1 - w_p(dF/dw)\} \tag{5.1}$$

$$T_s = T_o\{1 + w_p(dF/dw)\} \tag{5.2}$$

$$T_o = (m/2eV_d)^{\frac{1}{2}} s \tag{5.3}$$

$$w_p^2 = I_o(e/2mV_d)^{\frac{1}{2}}/(\varepsilon_o \pi b^2) \tag{5.4}$$

T_o is the transit time according to the ballistic model, i.e. neglecting space charge forces, s is the length of the conducting cylinder (0.6 m) and I_o is the beam standing current. F is the space-charge reduction factor, so called because the effect of confining the electrons in a conducting cylinder is to reduce their natural frequency of oscillation from the electron plasma frequency w_p to Fw_p. In Section 9.2 it is shown that F is defined by the equation

$$\{(1/F)^2 - 1\}^{\frac{1}{2}}(w \pm Fw_p) = 712u_o \tag{5.5}$$

where u_o is the beam velocity, according to the ballistic model, and the + and - signs refer to the slow and fast waves respectively.

Eqn. 5.5 shows that in general F is a rather complicated function of w, w_p and u_o. However if we take typical operating conditions with I_a = 1mA, V_d = 100V and use eqn. 5.5 to determine F it turns out that Fw_p is never greater than 0.1w. (If I_a = 1mA, V_d = 50 V, then $Fw_p \not> 0.16w$). By neglecting Fw_p in comparision with w in eqn. 5.5 we can obtain an explicit expression for F which greatly simplifies the subsequent mathematics. We write therefore

$$(1/F)^2 - 1 \simeq (712u_o/w)^2 \tag{5.6}$$

whence

$$(dF/dw)^{-1} \simeq 712u_o\{1 + (w/712u_o)^2\}^{3/2} \tag{5.7}$$

Eqns. 5.6, 5.7 give values for F and dF/dw which are correct to about 10%. If greater accuracy is required or if the operating conditions are such that Fw_p is not small in comparison with w we must revert to eqn. 5.5 and also take into account that the F for the fast and slow waves will not then be the same. Having obtained dF/dw, substitution in eqns. 5.1, 5.2 gives T_f and T_s .

In Fig. 5.3 w_p dF/dw, obtained from eqn. 5.7 is plotted as a function of w. For w greater than 10^{10}, corresponding to a pulse risetime of less than 0.2 nsec the function has a value less than 0.01 and accordingly we may expect $T_f - T_s$ to be less than 1% of T_o . For w less than 5×10^8, corresponding to a risetime of 4 nsec or more, the function tends to a constant value of $w_p / 712 u_o$, i.e. about 0.1 for I_o = 1mA, V_d = 100V, and the pulse separation will then be about 10% of T_o . However if we are dealing with pulses having risetimes bf between 4 and 0.2 nsec, as is usually the case, then it can be seen that $w_p dF/dw$ is a function of w. This implies that T_f, T_s, will be frequency dependent; different frequency components of the original pulse will not arrive at the anode in the same phase relation as that in which they left the grid. It is this frequency dispersion which is the principal cause of the observed pulse distortions, as is made clear in the following Section.

5.1.3. Pulse distortion.

When space-charge effects are negligible all frequency components of a pulse are transmitted with the same phase velocity u_o. Relative to these waves, space-charge waves of angular frequency w and phase velocity u_p will, at the anode, have acquired a phase difference given by

$$\phi = ws\{(1/u_p) - (1/u_o)\} \qquad (5.8)$$

The resulting distortion in a transient pulse f(t) can be analysed

by considering it as a superposition of an infinite number of continuous sinusoidal waves as expressed by the Fourier Integral Theorem:

$$f(t) = (1/2\pi)\int_{-\infty}^{+\infty} F(w)\exp(jwt)dw \qquad (5.9)$$

where

$$F(w) = \int_{-\infty}^{+\infty} f(t)\exp(-jwt)dt \qquad (5.10)$$

Now because the effect of transmitting these waves along an electron beam is to introduce a relative phase change at the anode the resultant pulse is no longer f(t) but is given by

$$f'(t) = (1/2\pi)\int_{-\infty}^{+\infty} F(w)\exp(jwt + \phi)dw \qquad (5.11)$$

Since ϕ is not in general a simple function of w eqn. 5.11 is not amenable to integration by standard analytical methods. Nonetheless we can obtain a good idea of the manner in which distortion occurs by returning to the continuous wave train case and considering a simple example.

In Fig. 5.4a the fundamental and first harmonic of a square wave are shown dotted, and their resultant by the full line. The wave can be thought of as a series of alternate positive and negative pulses. Consider that this waveform is transmitted along a beam and that as a result the phase of the first harmonic is retarded by 30° with respect to the fundamental, as could occur in the fast wave. The resultant waveform is shown in Fig. 5.4b. It can be seen that considering either the positive or the negative pulses the effect of the phase change is to produce a more sharp falling edge and a more gradual rising edge. In the case of the slow wave the harmonic would be advanced with respect to the fundamental so producing a faster rise and a slower fall.

We cannot represent a single pulse by a train of waves having only two frequencies. Nevertheless it is to be

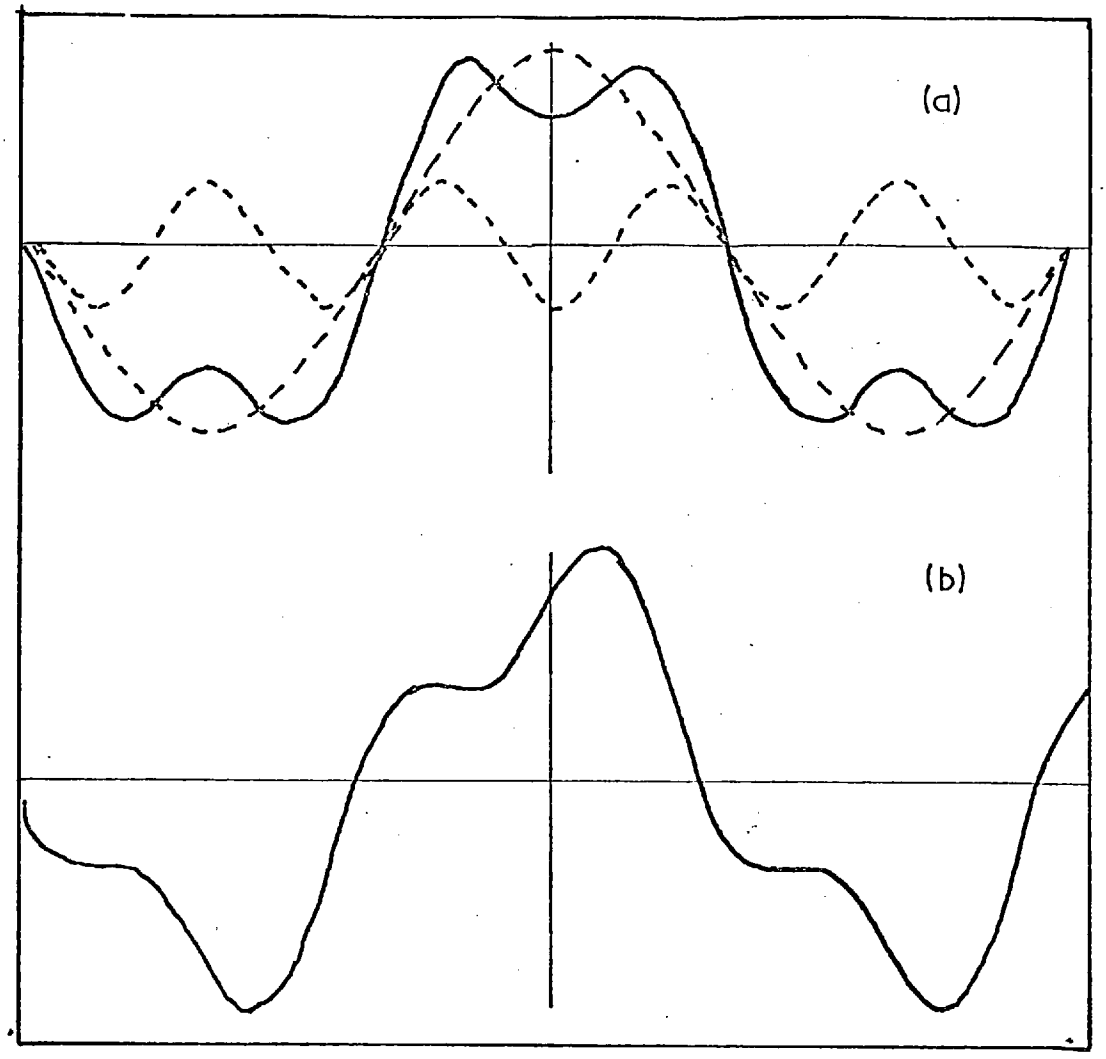


Fig. 5.4 Harmonics of a square wave

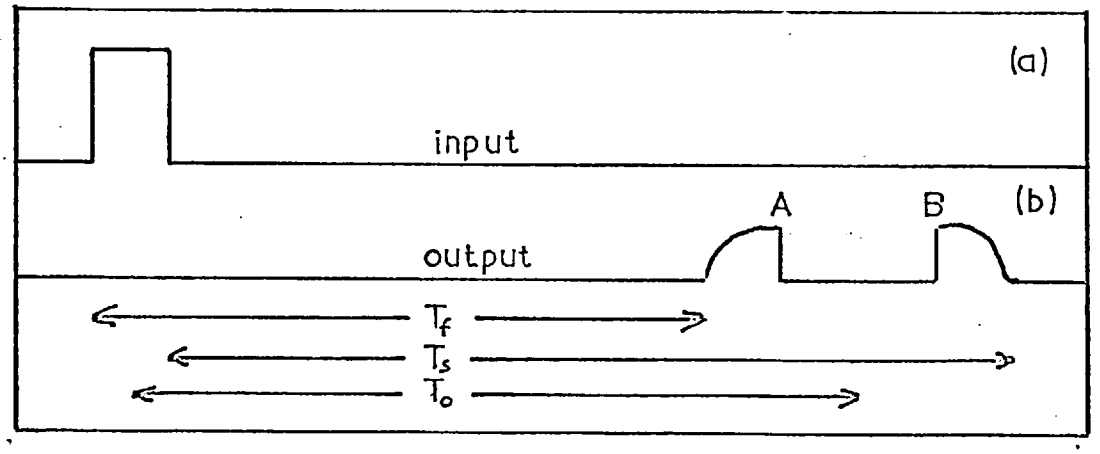


Fig. 5.5 Transit time measurements

expected that the distortion of a single pulse will retain qualitatively the same features of the distortion which arises in a train of such pulses. Experimentally this is found to be so. In Fig. 5.1A it can be seen that the fast pulse exhibits a gradual rise and a sharp fall, while the opposite is true for the slow pulse. Fig.5.1B shows the response at the anode to a single 400 mV negative step at the grid. Here again there are two pulses; the fast pulse has a slow rise and the slow pulse has a fast rise. This is because $w_p dF/dw$ is small for the high frequencies which are transmitted with velocities close to the beam velocity u_o while the lower frequencies undergo greater dispersion. Hence for the fast pulse the low frequency components associated with the slow rise arrive before the high frequency components. Conversely, for the slow pulse the high frequency components corresponding with a fast rise arrive before the low frequency components.

5.1.4. Transit time measurements.

Having obtained expressions for the transit times of the fast and slow pulses it is of interest to examine how these compare with the experimentally determined values.

Fig. 5.5 is a diagram of a typical pulse trace at (a) the input and (b) the output of the tube. We have seen already that it is only frequency components corresponding to pulse risetimes between 2 and 0.2 nsec which are subject to frequency dispersion. In the case of a 10 nsec square pulse these components are responsible for the sharp edges of the pulse and if they were removed by a low pass filter both edges of the pulse would become rounded. After transmission along an electron beam these high frequencies will not be removed but they will suffer some phase distortion and will be reproduced in some form between A and B in Fig. 5.5, since the group velocity for these waves tends to u_o with increasing w. The gradual edges at A and B can be identified with undispersed and undistorted components

of the original pulse, since for these low frequencies we can assume that dF/dw has reached its asymptotic value of $(712u_o)^{-1}$. Substitution in eqns. 5.1, 5.2 then gives T_f, T_s. In measuring T_f we note the time at which the beginning of the leading edge of the fast pulse appears at the anode; for T_s we note the time at which the end of the trailing edge of the slow pulse appears. (See Fig. 5.5). By restricting the measurement of T_f and T_s to low frequencies one can thus avoid the problem which arises when dF/dw is frequency dependent as in measurements pertaining to the fast edges.

Measurements of T_f and T_s were made as described using a 10 nsec square modulation pulse. These results can be most clearly presented in terms of the mean transit time $(T_f + T_s)/2$ and the transit time difference $T_f - T_s$. Eqns. 5.1, 5.2 show that the mean transit time is T_o which should be simply related to V_d by eqn. 5.3. Fig. 5.6 shows the measured results and the line representing this equation. At low V_d the measured transit time diverges from the predicted value because the space charge depression of potential described in Chapter 4 becomes important and this is not allowed for in the analysis given in Section 9.

Eqns. 5.1, 5.2 show that the transit time difference is given by

$$T_f - T_s = 2w_p(dF/dw)T_o \qquad (5.12)$$

Substituting for w_p and the asymptotic value of (dF/dw) leads to

$$T_f - T_s = 1.92\times10^{11} I_o^{\frac{1}{2}} T_o^{5/2} \qquad (5.13)$$

The analysis also disregards the effects of reverse current flow in the tube due to reflected electrons. I_o in eqn. 5.13 was taken to refer to the forward current alone, the reverse current which was generally about 10% of the forward current being neglected. Making the same assumptions as in Section 4.6.2 it follows that the forward current I_f is related to the anode current by the expression

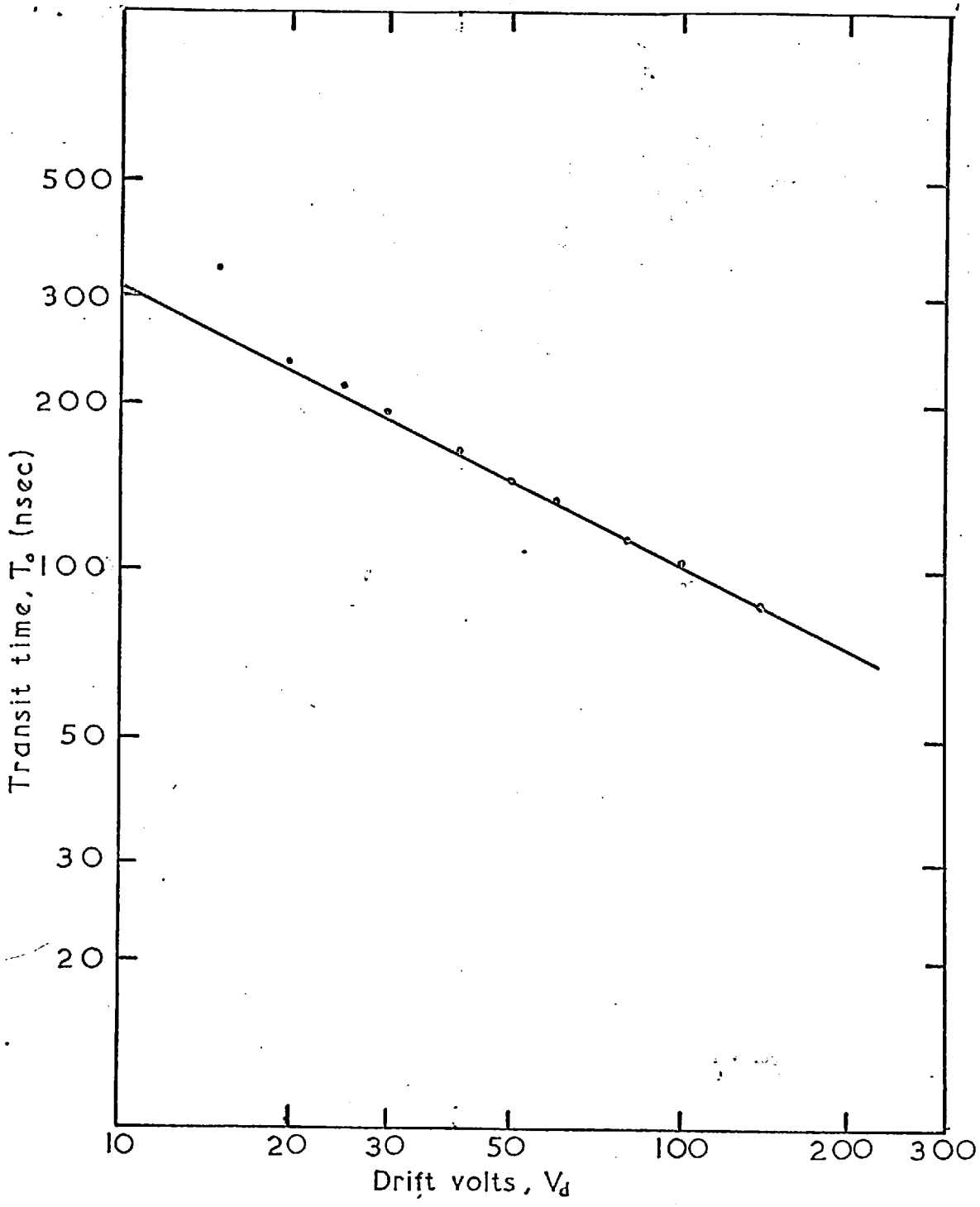


Fig.5.6 Transit time and drift potential.

$$I_f = 1.37 I_a \qquad (5.14)$$

$T_f - T_s$ is plotted as a function of I_f in Fig. 5.7 and as a function of T_o in Fig. 5.8. The plotted points have been corrected for the effect of the screen section. The line corresponding to eqn. 5.13 is shown in each case. The experimental results fall generally within about 5% of the theoretical prediction which is as much as can be expected in view of the assumptions involved.

5.2. Velocity modulation.

If a voltage pulse is applied to the drift section a current pulse results at the anode even though the current entering the drift section remains constant. In considering how this happens we assume to begin with that we are dealing with currents which are small enough for the pulse separation effects discussed in Section 5.1 to be neglected.

In this case the transit time T_o is dependent only on the potential of the drift section at the time the electrons enter it and is given by eqn. 5.3. The change dT in the transit time due to a small change dV in drift potential is thus given by

$$dT/T_o = -\tfrac{1}{2}(dV/V_d) \qquad (5.15)$$

Consider the electrons in a small sectional element of the beam which enters the drift section during a time dt. Suppose that during this time V_d changes to $V_d + dV$ and that the corresponding transit time changes to $T_o + dT$. Then if zero time corresponds to the entry of the leading edge of the bunch into the drift section, this leading edge will emerge at time T_o and the trailing edge at time $T_o + dT + dt$, so that the time taken for the whole element to emerge will be $dT + dt$. The element has thus been

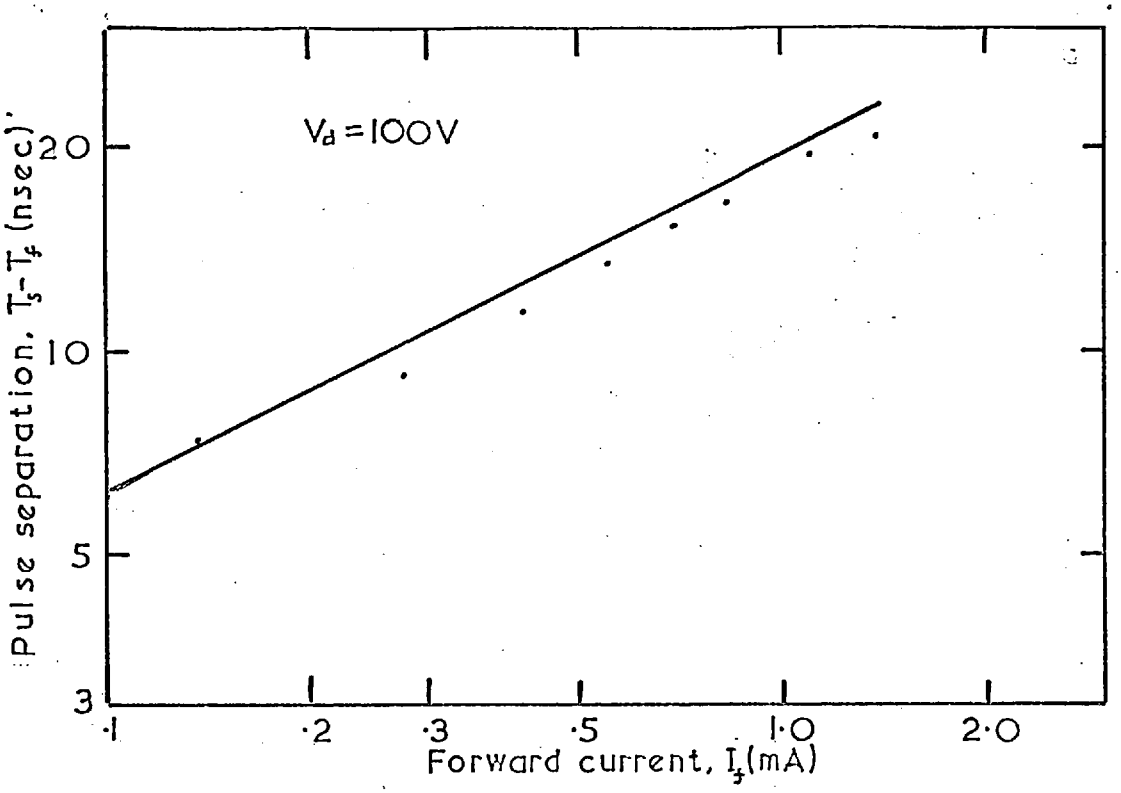


Fig. 5·7 Pulse separation and forward current

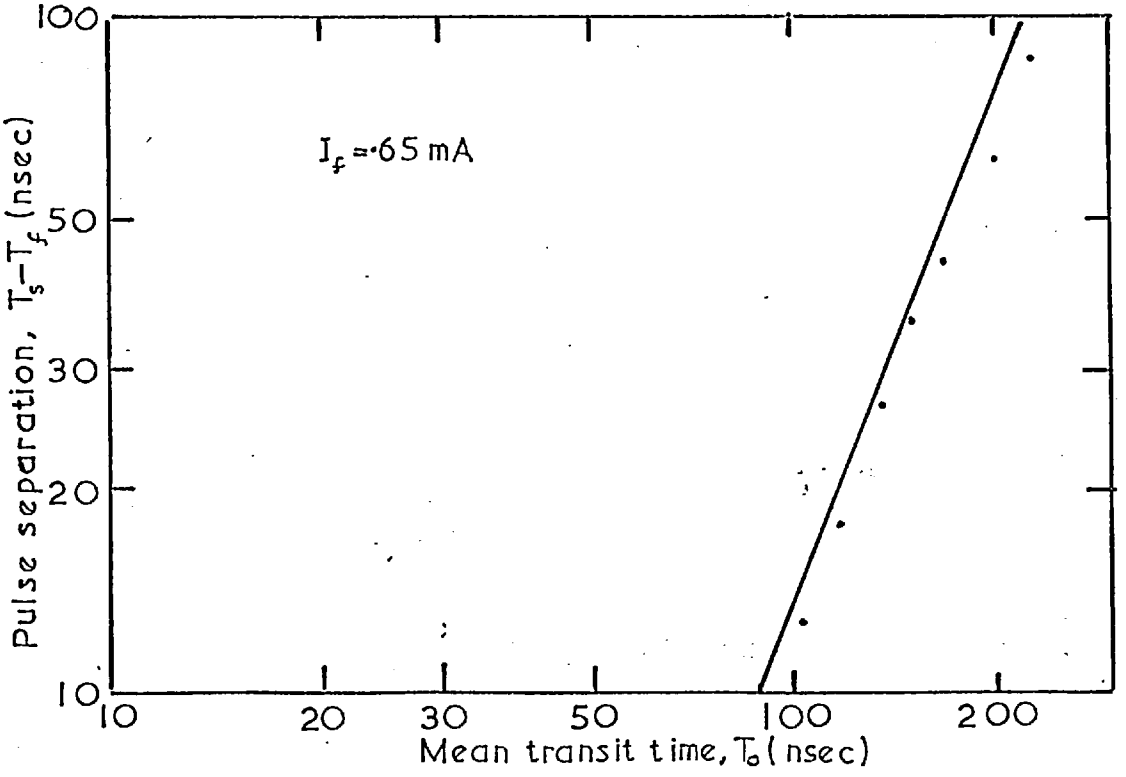


Fig. 5·8 Pulse separation and mean transit time

stretched in a time sense by a factor M, where

$$M = 1 + (dT/dt) \qquad (5.15a)$$

The total number of electrons composing the bunch must remain the same so that the current I_m which flows as a result of the stretched pulse arriving at the anode must be less than the standing current I_o which would have been observed if stretching had not occurred. I_m is given by

$$I_m = I_o/(1 + dT/dt) = I_o/M \qquad (5.16)$$

Substituting in eqn. 5.15 we obtain

$$\frac{I_m}{I_o} = \frac{1}{1 + (T_o/2V_d)(dV/dt)_t} \qquad (5.17)$$

This equation allows the calculation of the output current-time profile arising from a voltage pulse on the drift section. Note that I_m refers to the output current at time $T_o + t$ whereas $(dV/dt)_t$ refers to time t.

If I_o is not small, eqn. 5.3 is not valid and as we have seen the transit times T_f, T_s for the fast and slow pulses are dependent on I_o as well as on V. As a first approach to this situation we again consider only frequencies for which dF/dw is not frequency dependent but is equal to the low frequency value $(712\ u_o)^{-1}$. This assumption is quite reasonable in this case since the dispersion pulse is relatively slow in comparison with the modulation pulse, and substitution in eqn. 5.1 gives the transit time for the fast pulse when I_o is constant, i.e.

$$T_f = T_o(1 - w_p/712u_o) \qquad (5.18)$$

Further substitution of eqns. 1.5, 5.4 in the above yields

$$T_f = T_o(1 - 97.8I_o^{\frac{1}{2}}/V_d^{\frac{3}{4}}) \qquad (5.19)$$

Similarly for the slow pulse

$$T_s = T_o(1 + 97.8I_o^{\frac{1}{2}}/V_d^{\frac{3}{4}}) \qquad (5.20)$$

However when velocity modulation occurs I_o is not constant but decreases as the pulse travels down the tube. Suppose the time taken for an electron in the fast pulse to travel a distance x is T_{fx} then the time taken to travel a further distance dx is

$$dT_{fx} = (m/2eV_d)^{\frac{1}{2}}(1 - 97.8I_x^{\frac{1}{2}}/V_d^{\frac{3}{4}})dx \qquad (5.21)$$

where I_x is the total forward current at the point x. This is composed of currents due to both slow and fast waves so we may write

$$I_x = I_{fx} + I_{sx} \qquad (5.22)$$

At x = 0 the fast and slow currents I_{fo} , I_{so} , must be equal to $\frac{1}{2}I_o$ from consideration of symmetry. By analogy with eqn. 5.17 we can write for the fast and slow currents at x

$$(I_{fx})_{t+T_{fx}} = \tfrac{1}{2}I_o/\{1 + (T_{fx}/2V)(dV/dt)_t\} \qquad (5.23)$$

$$(I_{sx})_{t+T_{sx}} = \tfrac{1}{2}I_o/\{1 + (T_{sx}/2V)(dV/dt)_t\} \qquad (5.24)$$

Integrating eqn. 5.21

$$T_{fx} = (m/2eV)^{\frac{1}{2}}\int_o^x (1 - 97.8I_x^{\frac{1}{2}}/V^{\frac{3}{4}})dx \qquad (5.25)$$

Similarly

$$T_{sx} = (m/2eV)^{\frac{1}{2}}\int_o^x (1 + 97.8I_x^{\frac{1}{2}}/V^{\frac{3}{4}})dx \qquad (5.26)$$

Eqns. 5.22 - 5.26 define I_x , T_{fx} , T_{sx} . However there is a difficulty in obtaining numerical solutions inasmuch as eqn. 5.23 refers to I_{fx} at time $t + T_{fx}$ whereas eqn.

5.24 refers to I_{sx} at time $t + T_{sx}$ and we cannot obtain I_x simply by the addition of these two. Eqn. 5.23 gives I_{fx} at time $t + T_{fx}$. In order to obtain I_{sx} at this same time we should have to know T_{sx} and T_{fx} but this requires knowledge of I_{sx} which is what we are trying to find.

One method of solution would be to postulate I_x as a function of x, T and t and to correct this by successive approximation until the function was consistent with all eqns. 5.22 - 5.26. As this method is lengthy we shall here adopt a simple single approximation for I_x so that these equations may be solved analytically. The second term of the integral in eqns. 5.25, 5.26 is a small perturbation; thus quite substantial errors in I_x will produce only small errors in T_{fx}, T_{sx}. We can then use these approximate values of T_{fx}, T_{sx} in eqns. 5.23, 5.24 to obtain I_{fx}, I_{sx} to a fair degree of accuracy. We assume that I_x is given by the same expression as holds in the case of very small currents (cf. eqn. 5.17).

$$I_x \simeq I'_x = I_o/\{1 + (T_x/2V)(dV/dT)_t\} \qquad (5.27)$$

where T_x is the transit time to the point x for an electron which enters the drift tube at time t and is given by

$$T_x = (m/2eV)^{\frac{1}{2}}x \qquad (5.28)$$

(cf. eqn. 5.3)
Substituting I'_x for I_x in eqns. 5.25, 5.26 gives

$$T_{fx} \simeq (m/2eV)^{\frac{1}{2}}\int_o^x (1 - 97.8I'^{\frac{1}{2}}/V^{\frac{3}{4}})dx \qquad (5.29)$$

$$T_{sx} \simeq (m/2eV)^{\frac{1}{2}}\int_o^x (1 + 97.8I'^{\frac{1}{2}}/V^{\frac{3}{4}})dx \qquad (5.30)$$

For typical operating conditions (V_d = 100V, I_o = 1mA) these expressions for T_{fx}, T_{sx} are correct to about 2% for a stretching factor of 2. The error increases with

the stretching factor.

In the following Section results derived from this theory will be compared with experiment.

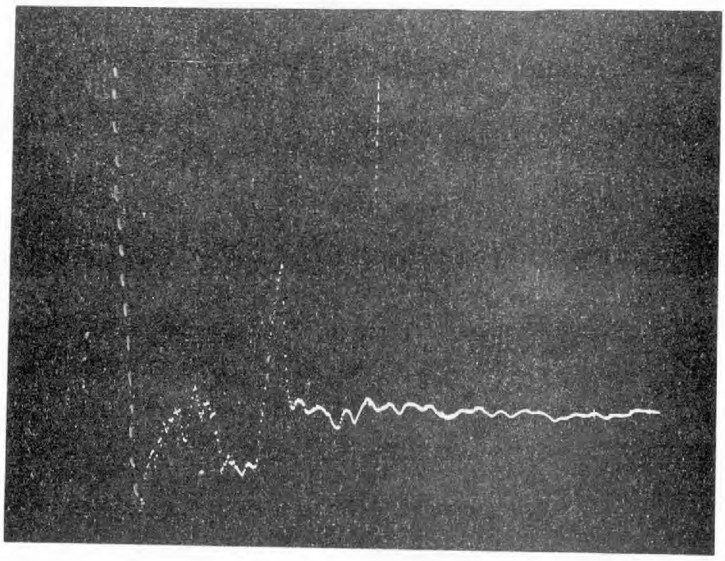
5.2.1. Experimental results.

Fig. 5.9a shows an example of a typical trace obtained when the dispersion pulse alone is applied to the tube. The negative current pulse corresponding with the dispersion of electrons can be clearly seen. This negative pulse is followed by a positive spike due to the rising edge of the dispersion pulse which occurs as the transistor is recovering from the initial avalanche process. (See Fig. 5.10). By allowing the transistor to recover more slowly this positive spike can be considerably attenuated. (Fig. 5.9b). In principle, a suitable rising voltage pulse applied to the drift section could be used to produce time contraction of electrical signals.

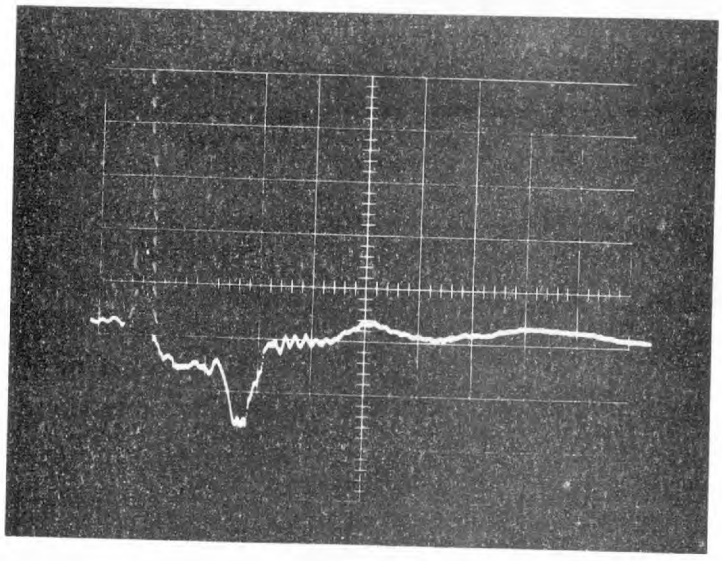
The large positive signal which can just be seen at the extreme left of Fig. 5.9 is direct feed-through from the dispersion pulse itself. It proved very difficult to eliminate this since the dispersion pulse amplitude is about 1000 times greater than that of the output signal. Most of the spurious ringing which occurs for about 100 nsec after the beginning of the dispersion pulse is also due to this cause; it is not due to oscillations of the beam electrons.

Fig. 5.10 shows the dispersion pulse detected at the tube. The slight irregularities in the trace are due to stray reactances in the cathode grid circuit which prevent perfect termination of the signal cable. From this figure dV/dt can be determined and together with eqns. 5.29, 5.30 used in eqns. 5.23, 5.24 to construct plots of I_{ss}, I_{ss} at the anode, where $x = s$. The result is shown in Fig. 5.12.

In Fig. 5.13 the total current I_x has been calculated by taking the sum of I_{ss} and I_{ss} . The maximum stretching factor $M = I_o/I_x$ can be seen to be about 2. The thick line is taken from a photograph of the trace obtained under the conditions for which the previous calculation was made.



(a)



(b)

Fig. 5.9 Examples of velocity modulation.
50 ns/cm, 10 mV/cm.
(a) V_d = 76 V (b) V_d = 105 V

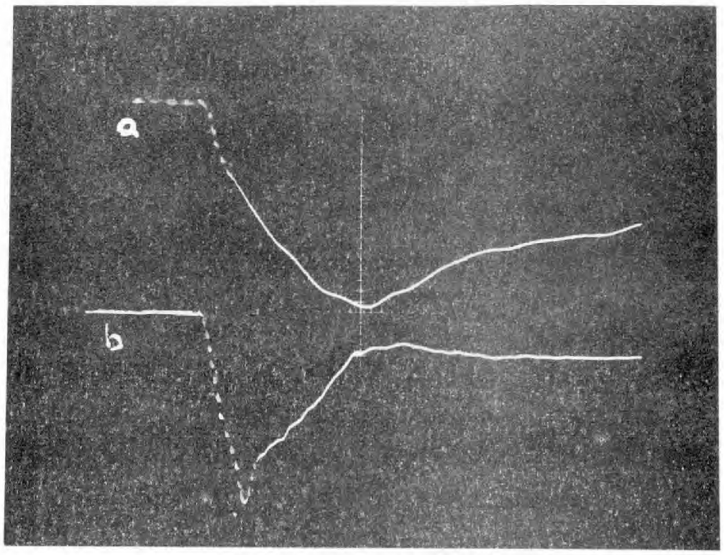


Fig. 5.10 Dispersion pulse on tube.
(a) 2ns/cm, 10V/cm. (b) 10ns/cm, 10V/cm

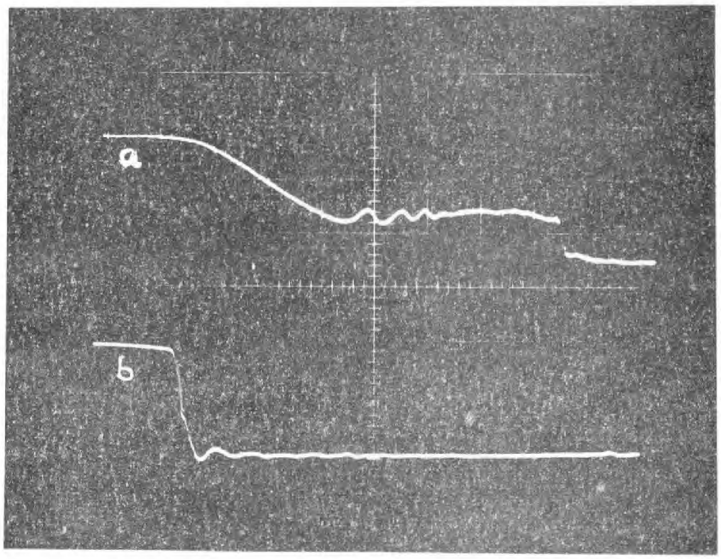


Fig. 5.11 Response to step pulse.
(a) output pulse, V_d = 50V. 5ns/cm, 5mV/cm.
(b) input pulse. 5ns/cm, 100mV/cm.

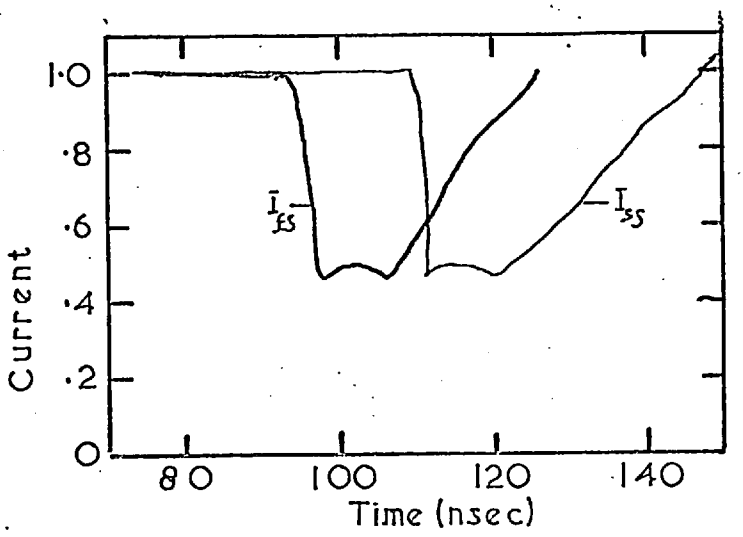


Fig.5.12 Current profiles I_{fs}, I_{ss}.

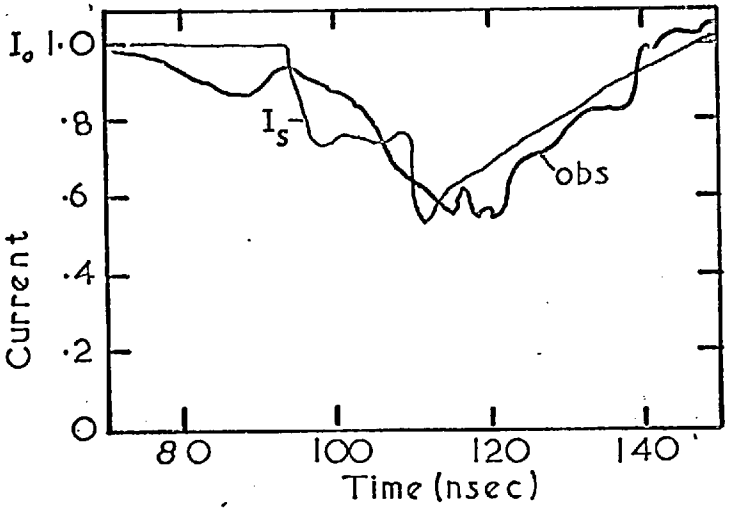


Fig. 5.13 Current profiles $I_s = I_{fs} + I_{ss}$ — and observed profile —

(V_d = 100V, I_a = 0.4 mA). The position and amplitude of the current depression agree fairly well with the calculated values but it is clear that the sharply falling edges shown in Fig. 5.12 do not occur in practice.

This is because at the beginning and end of the pulse the approximation of eqn. 5.27 is least appropriate since at the beginning the fast pulse will not overlap at all with the slow pulse but will travel down the tube accompanied by an unstretched part of the slow wave. A better approximation for the total current at the beginning of the pulse would therefore be

$$I' \simeq \tfrac{1}{2}I_o + I_{fx} \qquad (5.31)$$

Careful consideration of the manner in which I_x will depart from the value assumed in eqn. 5.27 leads to the conclusion that the beginning of the current depression for the fast and slow waves will not be sharp but gradual. We shall not be concerned with further quantitative discussion of this effect since it is already clear that the current profile resulting from the dispersion pulse is not related to it in any simple way when there is significant separation of the fast and slow waves. It will be shown in the following chapter how this fact restricts the use of the device for the time expansion of signals, for which purpose it must be operated in a mode in which this separation does not occur.

6. DISPERSIVE OPERATION

In the previous chapter the behaviour of the electron beam has been studied when either current or velocity modulations were independently initiated. In this chapter we consider the case where current and velocity modulations are synchronously applied and examine the extent to which this may result in dispersion of the current modulation to provide output signals which have been lengthened in time.

6.1. Ballistic theory of dispersive operation.

We commence the theory of dispersive operation by considering the case in which the beam current is so low that space charge can be disregarded.

Let $t = 0$ correspond with the beginning of the dispersion pulse. At time t_1 the modulation pulse commences and continues for a time τ. Consider an element of this pulse which enters the drift section at time t and after a further time T, the transit time, is detected at the anode. (See Fig. 6.1). At the anode it is convenient to define a new time t' such that $t' = 0$ corresponds with the beginning of the "output window", i.e. the current depression due to the dispersion pulse. If the transit time is T_o for electrons entering the drift section at $t = 0$ then we can write

$$t + T = T_o + t' \qquad (6.1)$$

In order that the input and output signals should be linearly related we require that an electron which enters the system at time t should appear at the output after the fixed time T_o plus Mt where M is the time stretching factor or magnifying constant for the system. Thus

$$t + T = T_o + Mt \qquad (6.2)$$

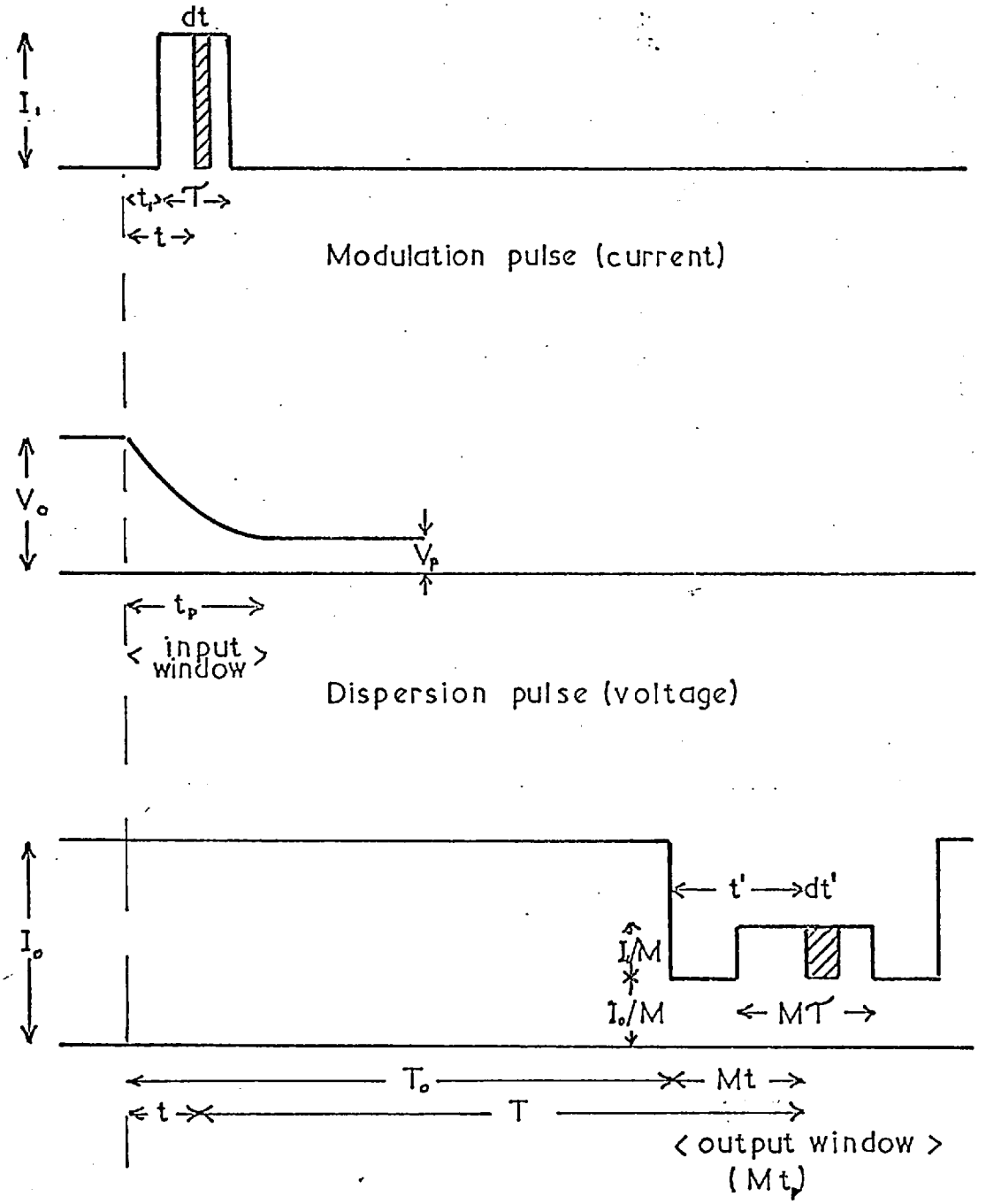


Fig. 6.1 Input and output waveforms.

and hence $t' = Mt$ (6.3)

If dT is the increase in the transit time T during the time dt that the element is entering the drift section then differentiation of eqn. 6.2 yields eqn. 5.15a which has already been used in the discussion of velocity modulation.

The form of the dispersion pulse required for linear operation can be obtained from eqns. 5.3 and 6.2. These give

$$V = V_o/\{1 + (M - 1)t/T_o\}^2 \qquad (6.4)$$

This expression is well approximated by the exponential function so long as V is not less than $V_o/4$, so that a suitable pulse may be derived from a simple resistive-inductive circuit.

If the dispersion pulse has the form given by eqn. 6.4 and lasts for a time t_p after which the potential on the drift section has fallen to V_p then eqn. 6.4 gives the expression for M namely

$$M = 1 + \{T_o/t_p\}\{(V_o/V_p)^{\frac{1}{2}} - 1\} \qquad (6.5)$$

It is useful to obtain an expression for the duration t'_p of the output window in terms of T_o and the initial and final potentials, V_o , V_p , of the dispersion pulse. On account of the linear relationship between t and t' we have

$$t'_p = Mt_p = t_p + T_o\{(V_o/V_p)^{\frac{1}{2}} - 1\} \qquad (6.6)$$

Both the expressions for M and t'_p contain the factor $(V_o/V_p)^{\frac{1}{2}} - 1$ which should be as large as possible for maximum stretching. However V_p cannot be made less than about 5 volts since below this value distortions due to the spread in energy of the electrons leaving the cathode will be significant. On the other hand the 2N708 avalanche transistor will give only about 30 volts in 75Ω so that the voltage difference $V_o - V_p$ cannot be greater than this. Thus the maximum value V_o/V_p is about 7 which corresponds

with a maximum value of t'_p of $1.45T_o$. In practice it is better to keep V_o/V_p to about 4 since this facilitates appropriate shaping of the dispersion pulse. In this case, since T_o is normally much greater than t_p eqns. 6.5 and 6.6 can be approximated by the simple relations

$$M \simeq T_o/t_p \tag{6.7}$$

$$t'_p \simeq T_o \tag{6.8}$$

which are convenient rules of thumb for design purposes.

The total number of electrons admitted to the drift section during the period of the input window must of course be equal to the number which emerge during the period of the output window. Thus if the modulation current pulse is lengthened in time at the output it must also be diminished in amplitude. If I_1' is the amplitude of the current pulse in the output window and I_o' is the corresponding standing current, then for linear operation

$$I_1' = I_1/M \tag{6.9}$$

$$I_o' = I_o/M \tag{6.10}$$

6.1.1. Pulse separation in dispersive mode.

In Section 5.1 the separation of the fast and slow pulses was calculated for the case of a fixed standing current. However in the dispersive case the standing current is continuously diminished as the dispersing electrons progress through the drift section. It is to be expected therefore that the pulse separation will be less

than if the standing current had remained constant. The separation $\bar{T}$ for constant current is given by eqn. 5.12 which with the aid of eqns. 1.5, 5.3, 5.4 and the assymptotic value of dF/dw can be written in the form

$$T_f - T_s = \bar{T}_{const} = 3.30\times10^{-4} I_0^{\frac{1}{2}} s/V^{\frac{5}{4}} \qquad (6.11)$$

It follows that at a distance x from the drift tube entrance the incremental increase in $\bar{T}$ as the electrons travel a further distance dx is given by

$$d\bar{T} = 3.30\times10^{-4} (I_x^{\frac{1}{2}}/V^{\frac{5}{4}})dx \qquad (6.12)$$

where I_x is the current at x and V was the potential seen by the electrons at x on entering the drift tube. Assuming that the dispersion is linear $1/I_x$ is proportional to x and we can write

$$I_x = I_0/\{1 + (M - 1)x/s\} \qquad (6.13)$$

Substituting this expression in eqn. 6.12 and integrating along the length s of the drift section gives

$$\bar{T}_{disp} = 3.30\times10^{-4} \{2(M^{\frac{1}{2}} - 1)/(M-1)\} I_0^{\frac{1}{2}} s/V^{\frac{5}{4}} \qquad (6.14)$$

which is the same as eqn. 6.11 except for the factor $2(M^{\frac{1}{2}} - 1)/(M - 1)$. Thus in the dispersive case, with M = 10, we should expect a standing current about twice that for the constant current case, for the same pulse separation.

The above analysis is valid only when the pulse separation is small compared with the duration of the output window, since linear magnification has been assumed.

6.2. First attempts at pulse stretching.

The existence of a current depression as a result of the action of the dispersion pulse shows that some dispersion

of the beam has occurred. It should therefore be possible to observe some form of time expansion in any modulation which has previously been applied to the current in this region. As a first attempt at pulse stretching it was decided to examine the output wave form when modulation and dispersion pulses were suitably synchronized, and to minimize the pulse separation effects as far as possible by using a high drift voltage and a low standing current. The modulation and dispersion pulses are shown in Fig. 6.2. The standing current was 0.25 mA, the drift voltage 50.

Fig. 6.3 shows the output obtained with and without the modulation pulse. The low standing current and consequent low output result in a rather poor signal to noise ratio. However it can be seen in the trace showing the modulation pulse that this pulse has been extended by about 3:1. From Fig. 6.2 it can be seen that the dispersion pulse is effectively 20 nsec long and 20 volts in amplitude. At a drift voltage of 50 eqn. 6.5 yields a value of M equal to 2.3, so that the stretching seems to be greater than expected. In fact much of this stretching is spurious and is due to the effects of frequency dispersive distortion discussed in Section 5.1.3. Fig. 6.4 shows that the pulse is extended as a result of transmission along the beam even when no dispersion pulse is applied. Nevertheless when the dispersion pulse is applied the modulation becomes further extended and its amplitude decreases thus showing that the device is operating, at least partially, in accordance with the dispersive principle.

The output pulses shown in Figs. 6.3, 6.4, are very far from ideal. The space-charge effects which result in pulse separation and frequency dispersion are far too great for the tube to be used in its present form for processing signals. In fact this is to be expected from Fig. 5.8 which shows that under the conditions used the pulse separation would be 10 - 20 nsec, i.e. of the same order as the output pulse duration. All that can be said at the present stage of the work is that some stretching of some kind has been produced. In the

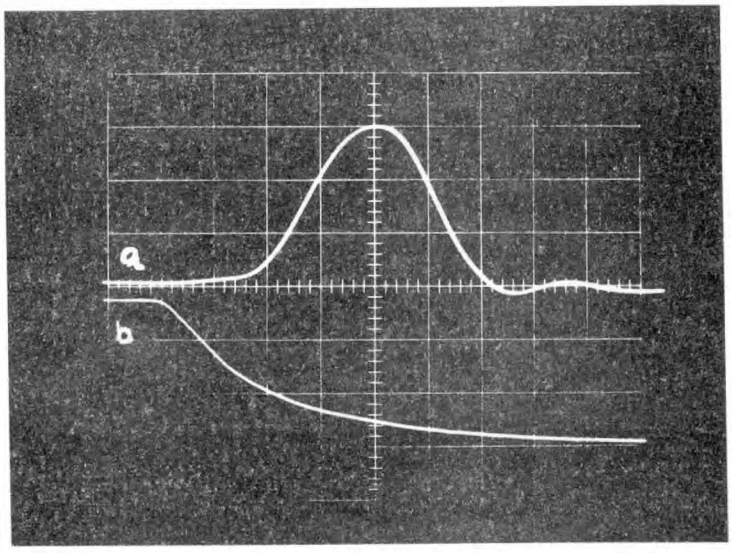


Fig. 6.2
(a) modulation pulse. 2ns/cm, 200mV/cm.
(b) dispersion pulse. 5ns/cm, 10V/cm.

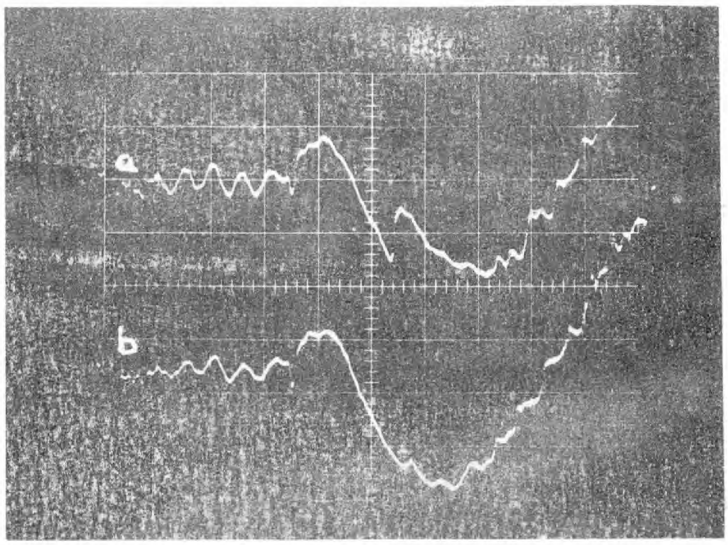


Fig. 6.3. Output with disp. pulse.
20 ns/cm, 4mV/cm. V_d=50V.
(a) with mod. pulse. (b) without mod. pulse.

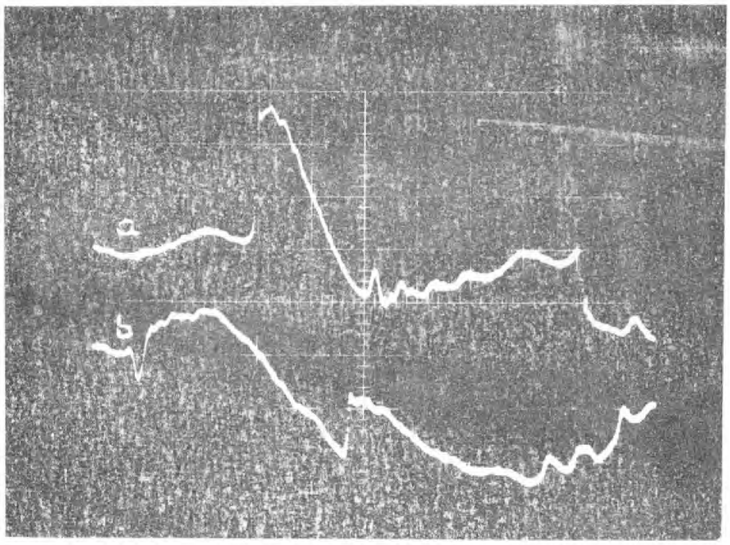


Fig. 6.4 Output with mod. pulse
10 ns/cm, 4mV/cm. V_d =50V
(a) without disp. pulse. (b) with disp. pulse.

next Section we consider changes that might be made in the tube design to produce an acceptable performance.

6.3. Designing for linearity.

The fundamental problem with the original design is that although the output wave form is related to the input wave form in a definite manner which can be understood on the basis of space-charge waves, this relationship is not a linear one. In a practical device linearity between output and input signals is essential.

In considering how the tube might be improved for practical use two modes of operation were analysed. In the first, two pulses are produced but these are so far apart in time that mutual interference does not occur. In the second mode, conditions are chosen in such a way that the pulse separation is so slight that it can be neglected.

Operation in the two pulse mode was eventually rejected as a practical possibility. One reason was that there would have been considerable difficulties in avoiding frequency dispersion in this mode. More significantly the time at which an element of the input pulse appears at the output is dependent on the integral of the current density along its path and there would thus be a tendency for the transit time of the element to be dependent on the shape of the modulation pulse. Such a situation must be avoided since the principle of dispersive operation is that the transit time of any current element depends only upon the time at which it enters the drift section. Furthermore operation with large pulse separation entails the use of high beam currents, yet the result of the electron dispersion is to reduce the effective beam current by the magnification factor, (see eqn. 5.16), so that large magnification is not compatible with large pulse separation.

Attention was therefore directed to the second mode in which the pulse separation is made as small as possible. It is interesting that in an unbounded beam the group velocities of the two waves are identical, even

though their phase velocities are not. (See Beck (10)). Since electron density variations are transmitted with the group velocity there should be no pulse separation in this case. It is the enclosure of the beam in a conducting cylinder which induces the separation. One design considered included an enclosed beam of very large diameter since it was thought that this might approximate an unbounded beam. It is necessary that dF/dw should be zero for the frequency range concerned. It can be shown that this condition is effectively fulfilled provided that

$$wb/u_0 > 10 \qquad (6.15)$$

where b is the beam diameter and u_0 is the beam velocity. (See Fig. 9.2). The lowest value of w likely to be required at the output is about 3MHz. For practical beam velocities this requires that b should be of the order of metres and so this system would be impracticable at least for frequencies acceptable by a conventional oscilloscope.

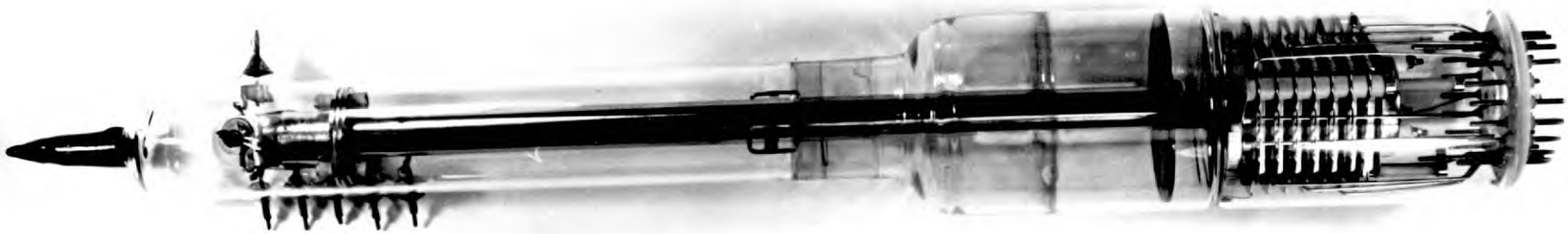
A system comprising a beam enclosed by a cylinder of resistive material was also examined since in the limiting case of infinite resistivity this is equivalent to an unbounded beam. It turns out however that for the range of frequencies required the tube resistivity has to be so high that the walls of the tube would charge up before the pulse separation was sufficiently reduced. A further difficulty with this idea is that the tube would not completely screen the enclosed electrons from electric fields and dispersion would have to be effected by means other than pulsing the drift tube. Drift tubes with resistive walls are nevertheless of considerable interest on their own account since under certain circumstances it is possible for one wave to be amplified at the expense of the other which is attenuated. A resistive wall amplifier based on this principle has in fact been constructed by Birdsall, Brewer and Haeff (27).

Another investigation concerned the effect of an inductive wall on the beam. An inductive wall can be formed by a conducting helix surrounding the beam. This was the most promising of the designs so far described

and it seems probable that a time dispersion tube could be constructed on this basis. The analysis suggests that as with the resistive wall some amplification of the signal could be achieved. However the idea was not followed for several reasons. Firstly there would have been difficulty in constructing a helix of sufficiently fine pitch within the tube envelope. Secondly the device would have been frequency dependent to some extent and it was not known how serious this effect might have been. Thirdly the mathematical account of waves in such a beam-helix combination can become very unwieldy so that it is difficult to predict the performance of any particular design.

Finally an investigation was made of the possibility of maintaining the essential features of the original design but using substantially smaller beam current. At currents of the order of 1μA the electron density is small enough for the pulse separation to be about 1 nsec when the transit time is 100 nsec and can thus be neglected. The small current has the disadvantage that an electron multiplier must be used to amplify the current emerging from the drift tube and this adds to the cost and length of the tube. On the other hand the physical operation is very simple and can be adequately described by the ballistic model. Moreover the tube is easier to construct than, for example, an inductive wall tube. For these reasons it was decided to use a low current design as the basis for a practical device which is described in the following chapter.

Some details of other devices employing long electron beams and a guide to the mathematical analysis used in their description are to be found in the review by Trotman (11).



Practical time dispersion tube

7. A PRACTICAL DEVICE.

Having found that a low current dispersion tube offered the best prospects of acceptable performance a design was prepared with the aim of achieving a time magnification of 30 and an input bandwith of 1000 MHz. In this chapter the details of this design and the resulting performance will be described.

7.1. The tube design, construction, and processing.

A diagram of the complete tube is shown in Fig. 7.1. A drift section of 20 cm was chosen so that the tube would be of a convenient overall length. Eqn. 6.6 shows that if the drift potential varies between 20 and 5 volts then the output window duration will be about 70 nsec. The pulse separation should be not more than 2 nsec at the lower drift potential if the output pulse is not to be significantly distorted. Application of eqn. 6.11 shows that the beam standing current, I_o , must then be less than 0.05 μA. Taking account of the reduction in pulse separation due to dispersion, (Section 6.1.1), it follows that the tube should be operated with a standing current of 0.1 μA or less.

The modulation structure incorporated a vidicon gun assembly supplied by E.M.I. Ltd. This provided a rigid structure in which the cathode-grid spacing, set to 0.006", could be accurately controlled. Furthermore the cathode-grid capacitance of 1.5 pF was not large enough to produce appreciable distortion of high frequency input signals, although it was found that the connection leads and heater coil increased the effective capacitance to 3 pF when the modulator was in the tube. In Chapter 2 it was shown that the conflicting aims of minimum transit angle and maximum mutual conductance at low current require that the cathode current is not less than 1/10th of the saturation current. At saturation the

X 1/2

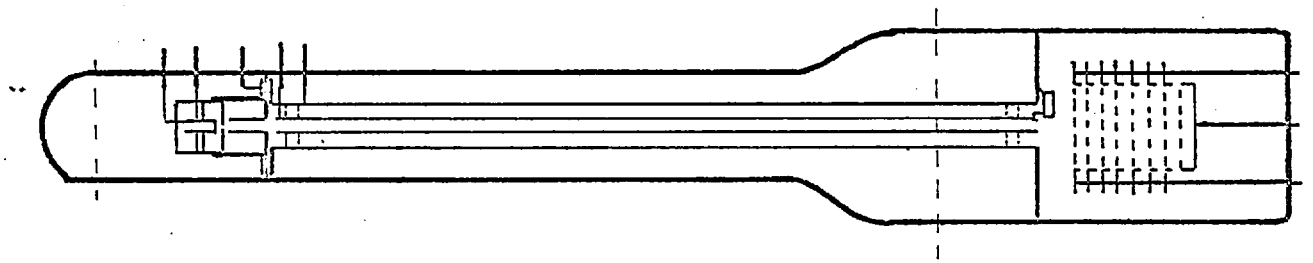


Fig. 7.1 Practical time dispersion tube.

current entering the drift tube should be about 1μA therefore. The current was limited by a small aperture, 0.007" in diameter, drilled in the front of the modulator. A mesh having 750 t.p.i. was welded across the cathode side of this aperture to prevent field penetration effects and consequent reduction in the mutual conductance.

An enlarged view of the cathode end of the tube is shown in Fig. 7.2. A grounded grid arrangement has been used, mainly on account of structural convenience but also because it results in an output signal of the same sense as the input signal. A disadvantage of the grounded grid is that the modulation signal imparts some velocity modulation to the beam, and this is superimposed on the velocity modulation due to the dispersion pulse. For example, if a 0.2 volt negative pulse is used to modulate the beam and the drift potential is 5 volts then the potential of the electrons corresponding with the peak of the pulse will be 5.2 volts. The transit time for the 5 volt electrons is 151 nsec whereas it is 148 nsec for the 5.2 volt electrons so there will be a tendency for the peak electrons to travel faster than the electrons in the rest of the pulse, and some distortion will result. However as long as the modulation pulse is not more than 0.2 volts in amplitude the distortion will not be serious and is in any case likely to be masked by the inherent spread in energy of the electrons leaving the cathode.

The screen section was machined from a single piece of metal and was insulated from the modulation and drift section by washers cut from 0.002" mica sheet. Contact to the screen was made via one of the 10 B.A. bolts holding the modulator, screen and drift sections together. These bolts were insulated by ceramic beads. The drift section comprised two stainless steel coaxial cylinders, the inner cylinder being located by pyrophilite annuli. These annuli were secured by inconel collars welded onto each cylinder. The outer cylinder was welded to a stainless steel annulus at the modulator end and this was secured by the bolts mentioned above. Some care was

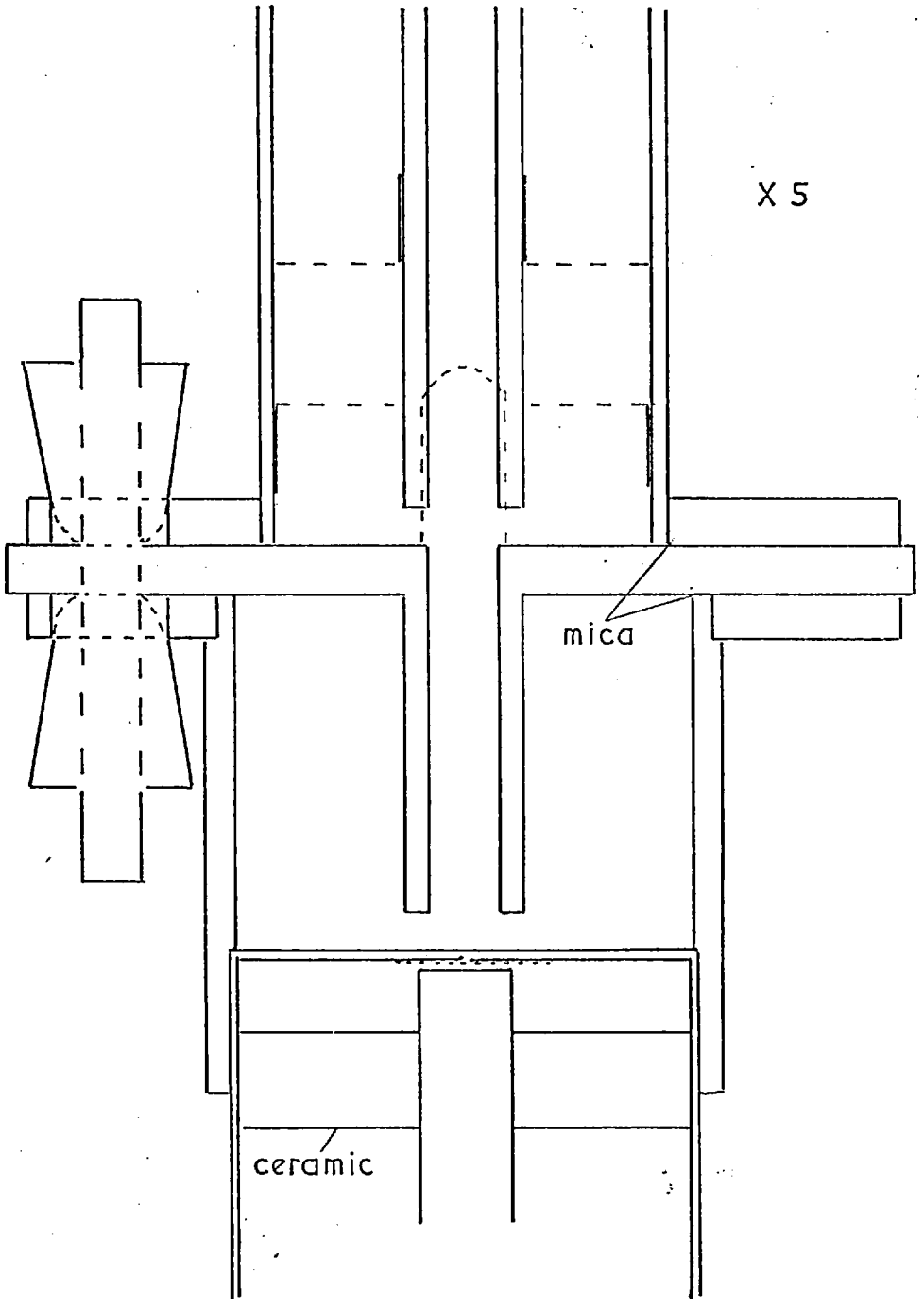


Fig. 7.2 Modulator assembly

required in making the weld to ensure that the annular plane was perpendicular to the cylinder's axis and that the axes of the modulator, screen and drift section were colinear. It was desired to make the diameters of the drift cylinders as small as possible but it was considered that if the inner diameter of the inner cylinder was less than 2 mm it would be difficult to align the beam within it. The ratio of the radii of the two cylinders was chosen in accordance with eqn. 2,4 so that the characteristic impedance of the transmission line so formed was 75 ohms, and a resistance of this value, prepared as described in Chapter 3 was connected between the cylinders at the multiplier end. At this end the outer cylinder was welded to an annulus of mild steel, 0.040" thick, which served to screen the multiplier from the axial magnetic field.

The design of the multiplier was chiefly influenced by two considerations. In the first place its gain should be sufficient to provide an output signal which can be readily detected by an oscilloscope without further amplification. With a standing current of 10^{-7} amps and a magnification of 30 the current entering the multiplier during the output window will be about 3×10^{-6} amps. A gain of 3×10^{4} will thus produce an anode current of 10^{-4} amps which should be directly detectable by an oscilloscope. The maximum rated output current for the multiplier used is 10^{-3} amps. Secondly, the multiplier risetime must be small enough not to introduce appreciable distortion in the output signal. With a time gain of 30 the output risetime of a 1000 MHz input signal will be 10 nsec so that ideally the multiplier risetime should be not more than 5 nsec. The multiplier has a finite risetime because the lengths of the paths traversed by individual electrons between dynodes are not the same and consequently the anode response is never instantaneous. The risetime is approximately proportional to the number of dynode stages and inversely proportional to the square root of the interdynode voltage (28). For minimum risetime it is desirable to use as few stages as possible and a high interdynode potential.

It was decided to operate each stage with an interdynode voltage such that near-maximum secondary emission

was achieved, since this ensures that for a given dynode material a minimum number of stages is used and the interdynode voltage is then also as high as practicable. Berylium-copper (BeCu) was chosen as the dynode material since, although this has a maximum secondary yield of 4.5 which is only half of that which can be obtained with caesiated dynodes, it has the advantage that it does not require further processing after it has been sealed onto the main tube structure. Furthermore since the dynodes can be exposed to air at atmopshere pressure for short periods the same multiplier can be used in successive experimental models. BeCu dynodes have a secondary yield of 4 at a primary electron energy of 370 volts. An 8 stage multiplier should thus provide a gain of the order of 10^4 at an overall voltage of 3 kV and can be expected to have a risetime around 6 nsec, this being the figure quoted for a 10 stage venetian blind photomultiplier (29). An 8 stage electron multiplier with BeCu dynodes was supplied by E.M.I. Ltd. It was essentially of the same design as their standard 9603 multiplier but with a smaller number of dynodes.

Multiplier phototubes are not usually operated with interdynode voltages as high as 370 volts since for a given supply voltage a greater overall gain can be obtained by using more dynodes and a lower interdynode voltage, usually about 200 volts. However no difficulties were found in using the higher voltage. Faster risetimes can be attained either by using caesiated dynodes, which achieve the same gain with fewer stages, or otherwise by using a focused dynode structure of the Rajchman type. An advantage of the venetian blind structure is that it will operate quite well in the presence of stray magnetic fields of 10 - 20 oerstead whereas the focused structure requires careful screening. Since a magnetic field is required for control of the electrons in the drift section a venetian blind multiplier is particularly suitable.

The multiplier was supplied with a kodial glass envelope. An appropriate seal was provided between the multiplier and the rest of the tube body which was of pyrex.

Contact to the electrodes was made through the glass by 1 mm diameter tungsten pins which were gripped inside the tube by inconel clips. These clips were connected to the appropriate electrodes by inconel strip or wire.

The general preparation of all the glass and metal parts prior to assembling and processing the tube followed the routine referred to in Chapter 2. The multiplier was supplied in an evacuated envelope and the modulator could not be vacuum stoved on account of the cathode coating so these parts were not given any further treatment. The glass envelope was made up in three parts indicated by the dotted lines in Fig. 7.1. The metal parts comprising the modulator, screen and drift sections were welded and bolted together and getters were attached to the drift section. The inconel clips and leads were attached to this main metal structure in such a way that it could be inserted into the central section of the glass envelope and a subsequent rotation of a few degrees allowed the clips to grip their respective pins. When reliable contact had been established the multiplier was cut open and sealed onto the central envelope section in an atmosphere of forming gas taking care not to heat the dynodes. The remaining section of the envlope including the pumping stem was joined to the other end of the tube and the whole was placed on the pump immediately.

The tube was baked at 350°C for 24 hours after which time the pressure was 4×10^{-7} T and fell to less than 10^{-7} T on cooling to room temperature. The cathode was activated by gradually increasing the heater voltage to 9.5 volts and ensuring that the pressure did not exceed 10^{-6} T. This took about 4 hours. Little gas evolved after the heater voltage had reached 4.5 volts. Half a volt was applied to the grid and 0.1 mA drawn from the cathode. After a few minutes this had increased to a steady value of 0.2 mA. The voltage was increased so that the current drawn was about 0.24 mA, and following an initial decrease, the current again stabilized at a

higher value. Proceeding in this way the cathode current was increased to 3 mA, after which no further increase could be obtained. If the voltage increment is too large the cathode current falls and does not regain its initial value. The heater voltage was reduced to its rated figure of 6.3 volts and a small current of about 1μA was drawn through the modulating aperture and collected on the screen to ensure that the vital part of the cathode surface behind the aperture was properly activated. Finally the getters were fired and the tube was sealed off the pump.

7.2. Electrical circuitry.

The electrical circuitry used to provide the electrode bias voltages and the modulation and dispersion pulse circuits was basically the same as described in Chapter 3. The circuit associated with the multiplier is shown in Fig. 7.3. With a supply voltage of 3 kV the divider chain provides 360 volts between each of the dynodes and 100 volts between the last dynode and the anode. A high voltage is not necessary at the anode as secondary emission is not involved and it leads to increased heat dissipation; 100 volts is sufficient to collect electrons from the last dynode. The divider current of 5 mA was sufficient to ensure that the variations of about 0.1 mA in the multiplier current did not significantly affect the interdynode potential.

The anode output circuit must be correctly designed if the minimum risetime of the multiplier, due to electron path length differences, is to be attained. Since the risetime of the output signal will be about 10 nsec the risetime of the anode circuit should not be more than 5 nsec which implies a time constant of 1.7 nsec. For a given anode current the output voltage will be proportional to the anode load resistance which should thus be as large as

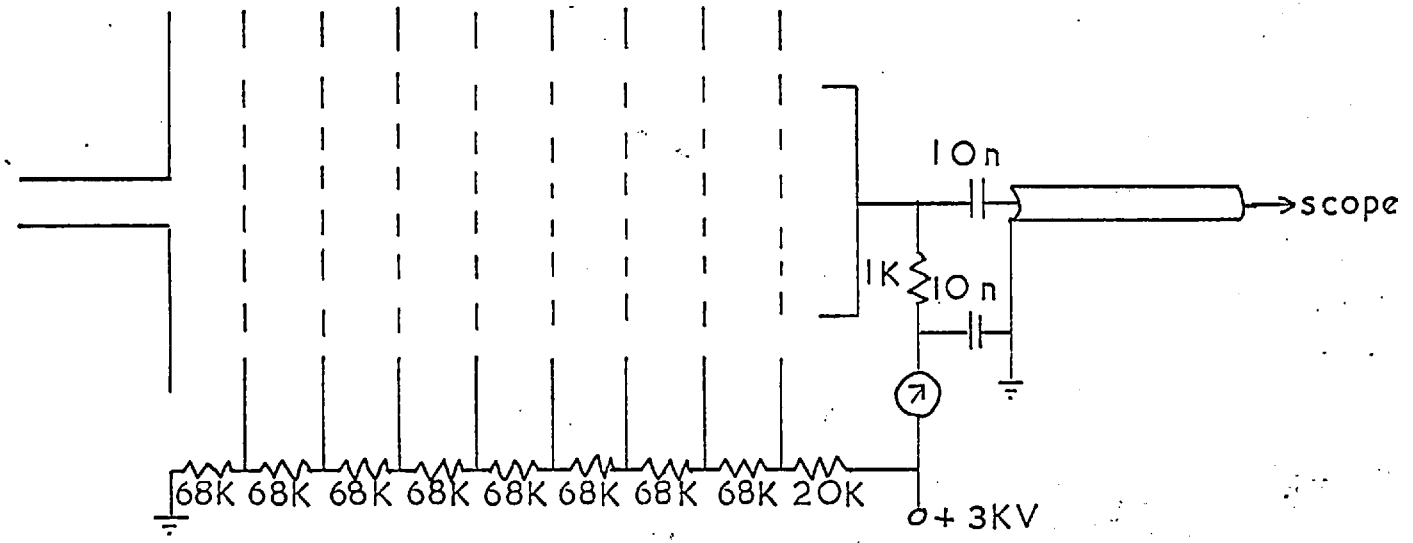


Fig.7.3 Multiplier circuit.

as possible. On the other hand the risetime consideration requires that the CR product should not exceed 1.7×10^{-9}. The anode capacitance to earth is 8 pF in the multiplier used. This capacitance alone would permit an anode load of 200 ohms which would result in output voltage of about 20 mV. However owing to the 50 ohm impedance of the 4SI sampling unit used with the 661 oscilloscope an effective load of 200 ohms was not practicable. The situation is not improved by the use of a high input impedance real time oscilloscope since these have an input capacitance of typically 20 pF which appears in parallel with the multiplier anode capacitance and the load can be only 60 ohms if the risetime requirement is to be met.

The 661 oscilloscope was the most suitable instrument available for detecting the output signal. The multiplier anode was connected to the EHT supply via a 1 kilohm resistor. This was in parallel with the 50 ohm load provided by the 661 but was large enough not to cause a significant reduction in the effective load and on the other hand small enough that the anode potential was not significantly affected by changes in the multiplier standing current. A meter was provided in the anode circuit so that the safe current of 0.1 mA should not be exceeded.

In view of the high anode potential and the lower frequency of the output signals the oscilloscope was not connected directly to the output circuit as in the earlier tube. There was some difficulty in obtaining isolating capacitors of adequate frequency response capable of withstanding the multiplier supply voltage. It was found that Radiospares ceramic disc capacitors were satisfactory although these were rated at only 750 volts.

The magnetic field of approximately 100 oerstead was provided by a solenoid of 8 coils having an inner diameter of 4". In order that the field should not affect its operation, the multiplier was allowed to protrude from one end of the solenoid to as great an extent as was possible

without the beam electrons landing on the drift tube wall. A magnetic screen in the form of a cast iron cylinder with a $\frac{1}{4}$" wall was prepared to surround the multiplier but was found to be unnecessary.

7.3. Experimental results.

7.3.1. Steady state operation.

The diode characteristic discussed in Section 4.6 was obtained for the new modulation assembly and is plotted in Fig. 7.4, together with the current transmitted by the modulator aperture. The diode characteristic has the usual form, with a slope of 1.5, and is similar to that obtained with the earlier tube. The area of the cathode coating is approximately 1 mm^2. Use of the ideal diode equation (eqn. 4.3) shows that the effective cathode-grid spacing is .008", .002" greater than it was designed to be. The saturated emission was 1.4 mA, corresponding to a cathode current density of 0.14 A/cm^2. The current density could be increased to about 1 A/cm^2 by running the heater at 10 volts.

The modulator aperture area was .024mm^2. Assuming that the electrons travel in straight lines parallel to the axis the current arriving at the aperture will be 2.4% of the total current. About half of this will be absorbed by the mesh across the aperture and the transmitted current should therefore be about 1% of the total current. Examination of Fig. 7.4 shows that actually this is not the case, the transmitted current being only about 0.25% of the total current. Moreover the transmitted current is not a constant fraction of the total current. The reason for these anomalies was not definitely established but is probably partly due to the transverse velocities of the electrons and partly because the modulator aperture has the form of a tunnel. In fact the .007"aperture was drilled in .005" thick metal so that not all of the electrons which arrive at the mouth of this tunnel will emerge from

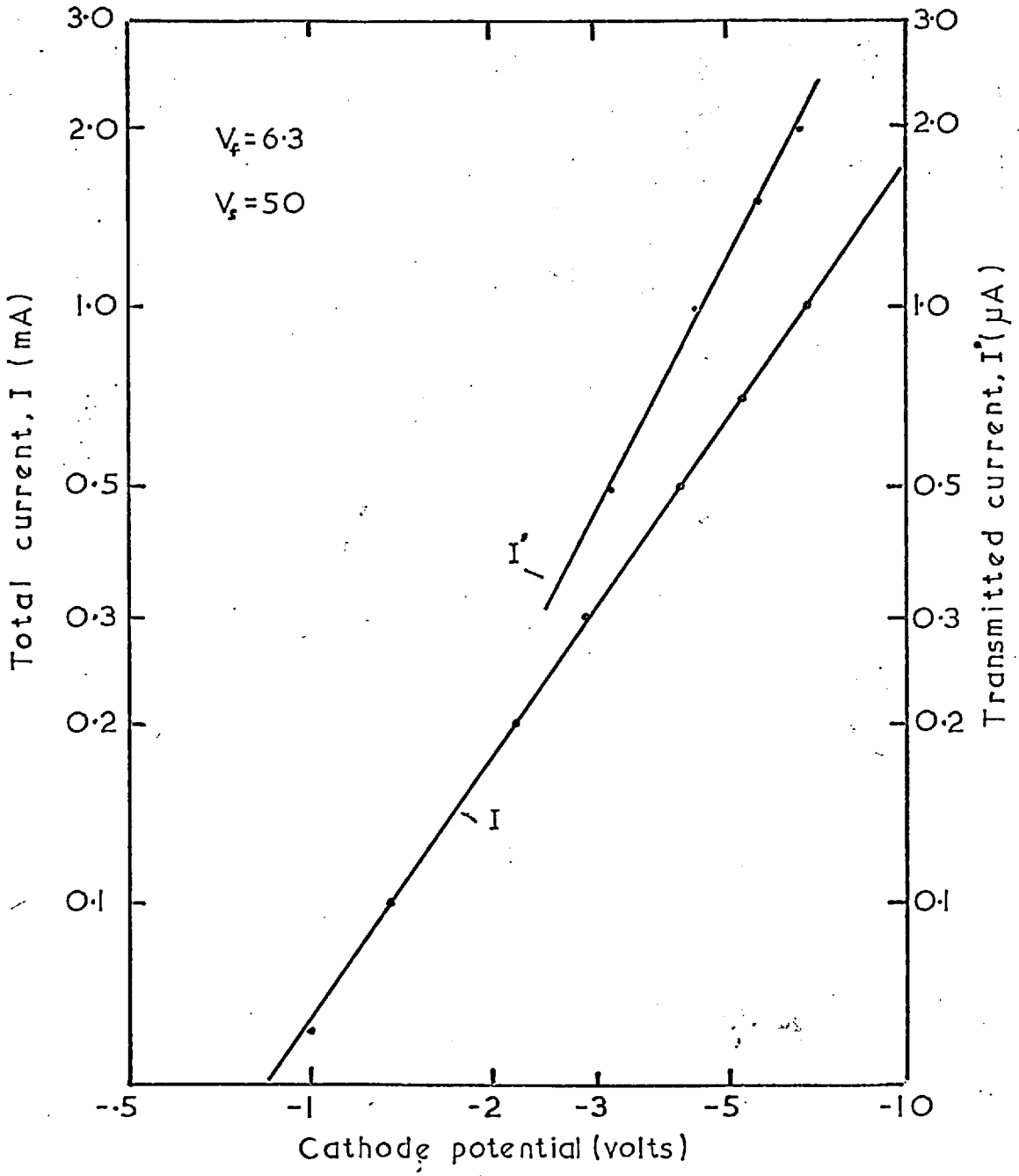


Fig. 7.4 Modulator characteristics

the other end but will be collected by the walls.

There were no meshes between the modulator and first multiplier dynode in this design so that in principle all of the current leaving the modulator could be collected by the multiplier. In practice it was found that there was some loss of current to the drift section and that about 75% of the current was collected. The multiplier gain characteristic is shown in Fig. 7.5.

Satisfactory focusing of the electron beam could not usually be obtained with fields less than 100 oerstead. The spreading of the beam cannot be due to space charge in this case, since this is too small to have a significant effect, but is due to transverse electron velocities. Assuming that the thermal transverse velocities may be as great as 0.5 volt we can put $V_a - V_b$ in eqn. 4.13 equal to this value. The resulting figure for H_{lim} is then 25 oerstead. A larger value is required in practice because the electrons acquire additional transverse velocities on account of the bulging of the electric field at the ends of the drift and screen sections.

7.3.2. Modulated operation.

The risetime of the circuit formed by the modulator was examined using the fast pulse available from the 661 oscilloscope. This voltage step, which had a risetime less than 350 psec, was fed to the modulation pulse cable and detected by the oscilloscope as it emerged from the bias cable. The risetime of the pulse at this point was 1.2 nsec. This showed that the modulator was not able to respond to fast signals as rapidly as was originally intended. The total length of unmatched pins and leads between the cable and the modulator was about 5 cm, and this coupled with the modulator capacitance is sufficient to account for the degradation of risetime in the applied pulse. It seems therefore, that in order to obtain

Fig. 7.5 Multiplier gain characteristic

satisfactory performance with input signals of up to 1000 MHz, the unmatched glass-metal seals of the present design should be replaced by a coaxial seal in which proper matching could be continued right up to the emitting surface of the cathode. Nevertheless the modulator risetime was fast enough to permit an investigation of the modulation of the beam in the new low current mode.

The modulation signal seen at the cathode, shown in Fig. 7.6, was derived directly from an FJH 101 integrated circuit as this generated signals of adequate risetime and of greater amplitude than those available from the tunnel diode in Fig. 3.2. The output signal obtained with a beam standing current of 0.1 μA is shown in Fig. 7.7 for various values of drift voltage. The drift transit time varies in accordance with eqn. 5.3 when due allowance has been made for the effect of the grid potential of + 1 volt relative to the cathode. The duration of the observed pulse is about 20 nsec, considerably longer than the pulse applied at the grid, but this is due to the risetime of the multiplier. There is no sign of the double pulse, characteristic of the earlier tube. The shape of the pulse is well preserved as the delay increases. It is only in the lowest trace when the effective drift potential is 4.8 volts that distortion begins. This is mainly due to the separation of the fast and slow pulses, although distinct pulses cannot be seen on account of the relatively slow multiplier risetime. Eqn. 6.11 shows that for the conditions corresponding with the lowest trace the pulse separation should be 3 nsec and it can be seen that the pulse duration has been increased by roughly this amount. Reduction of the beam current to .02 μA restored the same pulse shape as in the other traces. There does not appear to be any evidence of distortion attributable to spread in energy of the emitted electrons, although in view of the multiplier risetime this would be difficult to detect.

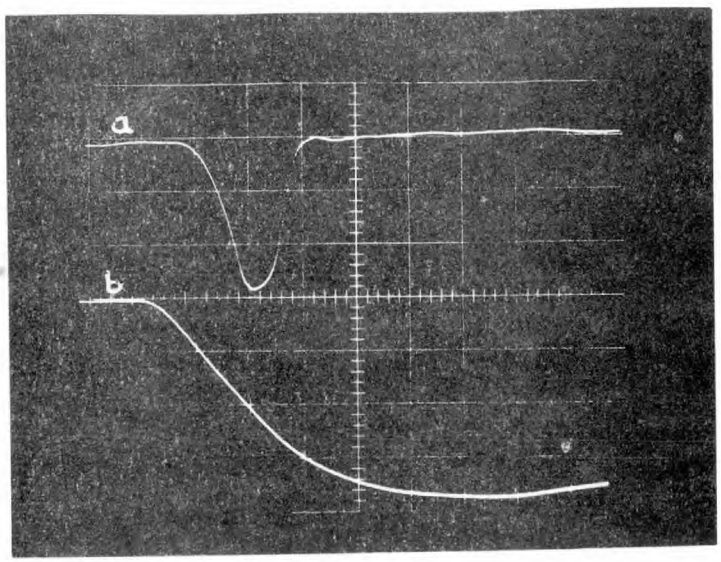


Fig. 7.6 Input waveforms.
(a) modulation pulse, 5ns/cm, 100mV/cm.
(b) dispersion pulse, 5ns/cm, 5V/cm.

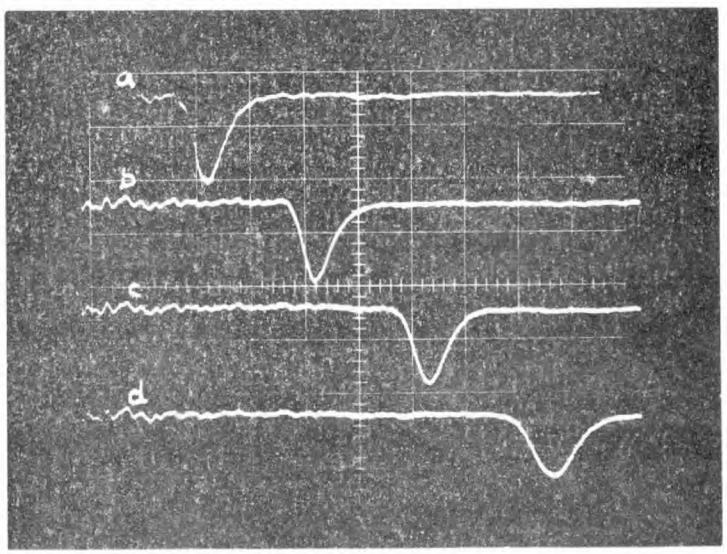


Fig. 7.7 Response to modulation pulse
20ns/cm, 5mV/cm. (a) V_d = 76V,
(b) V_d = 19V, (c) V_d = 7.6V, (d) V_d = 3.75V

7.3.3. Dispersive operation.

Initial measurements were taken with a drift bias of 20 volts and a beam standing current of .01 μA. Taking into account the cathode bias the effective drift potential was 21.8 volts. The dispersion pulse is shown in Fig. 7.6. In Fig. 7.8 the actual dispersion pulse is compared with ideal waveform required for linear operation as defined by eqn. 6.4, with $T_o/(M - 1)$ equal to 18 nsec. The two curves agree to within 10%. Since T_o is equal to 72 nsec at the specified drift potential the magnification factor M to be expected under these conditions is 5.0. Fig. 7.9 shows the output pulse on a horizontal scale of 25 nsec/division compared with the input pulse on a scale of 5 nsec/division and confirms that the expected magnification has been obtained. The secondary pulse visible in the output trace marks the end of the output window (cf. Section 5.2.1.).

In Fig. 7.10 the effect of the dispersion pulse is clearly demonstrated. Trace (a) shows the output waveform obtained with the dispersion pulse alone. The output window can be seen although it is not very pronounced on account of the low beam standing current. Trace (b) shows the result when the modulation pulse is also applied, and trace (c) was obtained with the modulation pulse alone. Comparison of (b) and (c) shows that the effect of the dispersion pulse is that the output pulse is increased in width and diminished in amplitude, and this is the characteristic feature of the dispersive effect.

A horizontal magnification factor of ten was achieved by reducing the drift bias potential and optimising the synchronization of the modulation and dispersion pulses. The result is shown in Fig. 7.11 together with the modulation pulse. Further reduction of the drift bias potential produced increasing distortion. Moreover the multiplier gain could not be increased sufficiently to offset

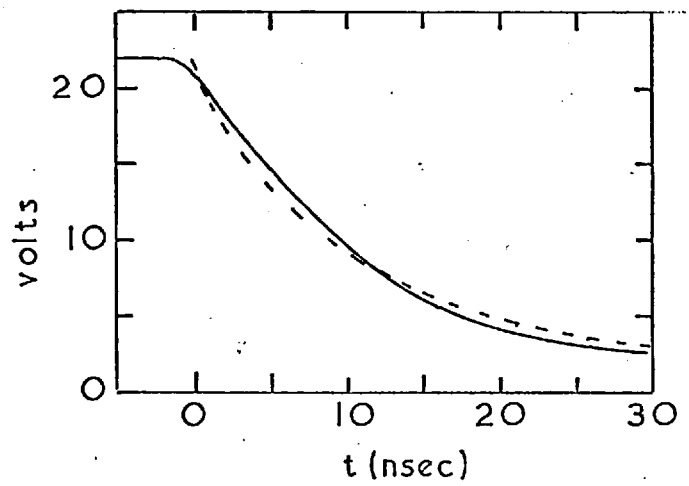


Fig. 7.8 Actual dispersion pulse waveform(—) compared with ideal waveform(---) for linear operation

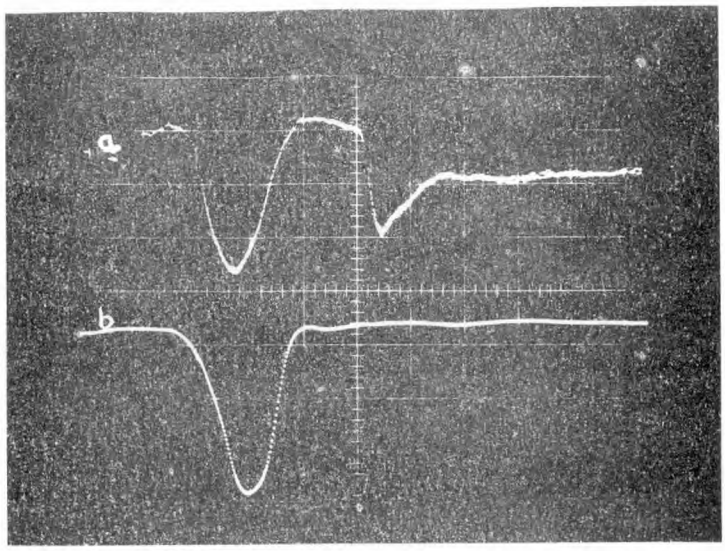


Fig. 7.9 Output waveform at 2.5 ns/cm (a), compared with input waveform at 5 ns/cm (b). Vertical sensitivity: (a) 5 mV/cm, (b) 100 mV/cm

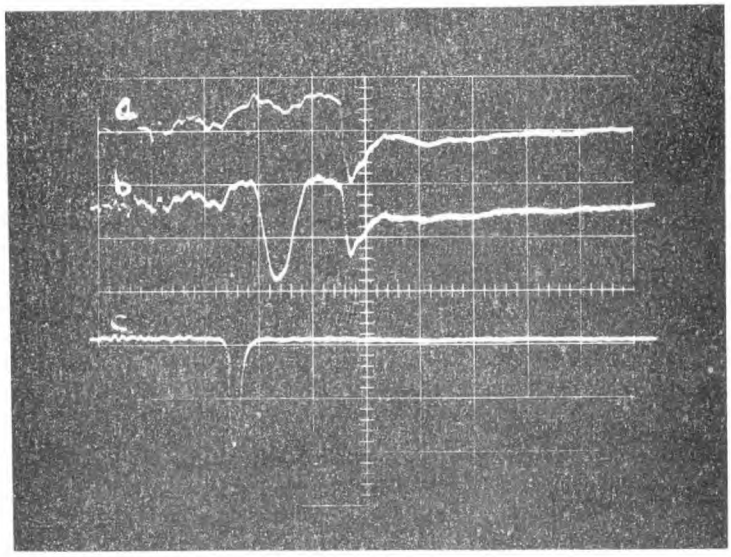


Fig. 7.10 Output waveforms showing effect of dispersion pulse. V_d = 20 V
(a) dispersion pulse only, 50 ns/cm, 5 mV/cm
(b) disp. and mod. pulses, 50 ns/cm, 5 mV/cm
(c) modulation pulse only, 50 ns/cm, 10 mV/cm.

the loss of amplitude. It can be seen in Fig. 7.11 that the output window duration is about 150 nsec, and this is the maximum which can be expected with a 20 cm drift section. As the modulation pulse duration exceeds 10 nsec, it is the duration of the output window which restricts the magnification which can be obtained. Higher magnification should be obtainable using shorter modulation and dispersion pulses, but a modulation pulse of sufficient amplitude could not be obtained from the electronic circuit used.

7.3.4. Operation with a real-time oscilloscope.

As a final demonstration of the practical utility of the device the tube bias potentials were adjusted to give an output pulse of 100 nsec and this was fed to a real-time Tektronix 551 oscilloscope which has a risetime of 13 nsec. In order to minimise the capactive load on the multiplier the x 10 attenuator probe with a capacitance of 10.5 pF was used. The result is shown in the top trace in Fig. 7.12. This output signal was obtained with a 500 ohm resistive load in the multiplier anode circuit. The middle trace shows the signal obtained with no modulation and demonstrates the output window. The lower trace shows the response obtained when the modulation signal was applied directly to the oscilloscope. As the oscilloscope cannot respond sufficiently rapidly, a pulse of 100 mV amplitude and 20 nsec duration is recorded which may be compared with Fig. 7.6.

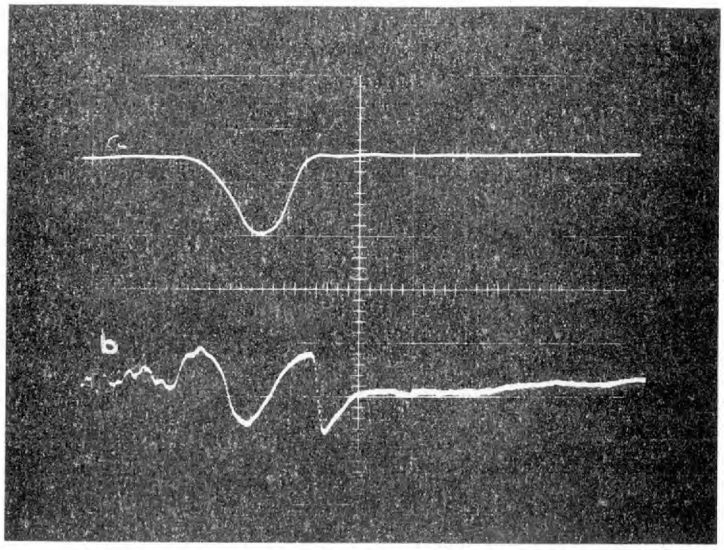


Fig. 7.11 Output waveform at 50ns/cm (b), compared with input waveform at 5ns/cm (a). Vertical sensitivity: (a) 200mV/cm, (b) 5mV/cm

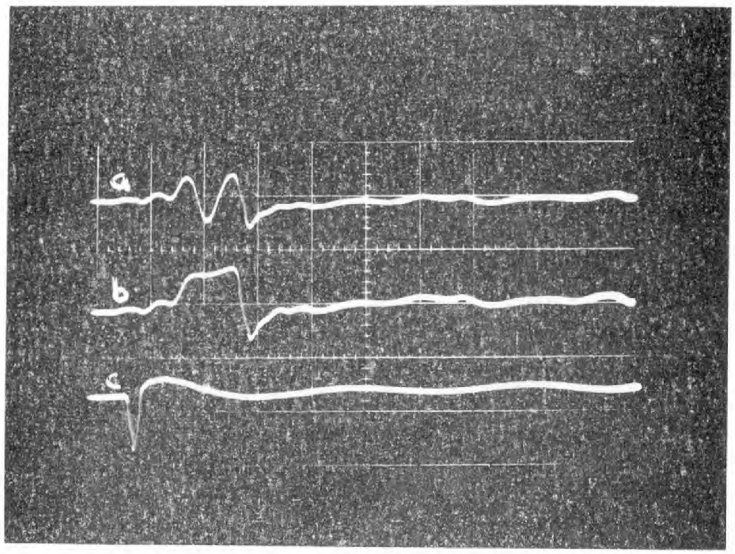


Fig. 7.12 Waveforms obtained with real time oscilloscope (Tektronix 551) 100ns/cm, 100 mV/cm.
(a) output with mod. and disp. pulses
(b) output with disp. pulse only.
(c) mod. pulse fed directly to scope.

8. CONCLUSIONS AND SUGGESTIONS FOR FURTHER DEVELOPMENT.

The work described in this thesis has shown how the dispersion of a modulated beam in a field free space may be understood in terms of two concepts. The first is relevant to the case when the electron density is sufficiently low that mutual interaction is negligible. Here the electron may be regarded as a classical particle; it proceeds without change in its motion until it is absorbed or reflected by an electrode or until it leaves the field free space and becomes subject to a force. Secondly, as the electron density increases, their mutual interaction becomes increasingly important and this situation can be understood by considering the electrons as a continuous plasma. In the steady state, i.e. in the absence of modulation, the plasma is adequately described by Poisson's equation. As a result of density or velocity modulation, space-charge waves are induced in the plasma, a slow and a fast wave generally being propagated. By making suitable physical assumptions an idealized model of this situation can be set up which may be treated by analytical mathematical methods and it has been found that the predictions of the theory of space-charge waves are in good agreement with experimental facts.

This investigation was stimulated by the possibility of using the principle of time dispersion to facilitate the display of high speed transient signals. In the preceeding chapter it has been shown how this may be accomplished and effective time dispersion has been demonstrated.

Further development should include the improvement of practical devices. The device described was limited in performance chiefly by the response of the input circuit which requires redesign in a coaxial form. The sensitivity was also adversely affected by the relatively large grid-cathode spacing which was designed to be 0.006" but in fact was probably closer to 0.008". Since for a given voltage change the change in cathode current is inversely proportional

to the square of the grid cathode spacing a reduction of this distance to 0.002" should increase the input sensitivity by a factor of 16, as well as improving the transit angle. From a practical point of view it is undesirable to operate the tube with a large external solenoid. Adequate confinement of the beam in the drift section could be provided by magnetising the inner or outer drift cylinders. The screen section should be dispensable since with a small modulation aperture there is little field penetration. In fact a change of 60 volts in the screen potential was found to produce a change of 4% in the transmitted current when the cathode was at -1 volt relative to the grid. A multiplier with smaller caesiated dynodes would produce a more compact instrument. Moreover a smaller anode with a smaller capacitance to earth would enable the response of the output circuit to be improved. The maximum output current available from the present multiplier is not really sufficient to drive most oscilloscopes and could be increased, either by an improved design, or, since a continuous current is not required, by the use of pulsed operation.

In addition to improvements in tube design there is the question of the ultimate performance which can be expected. In this respect a study of the intrinsic noise associated with the various parts of the tube is required. This is a complex problem. A description of some relevant work on the noise performance of u.h.f. triodes and electron beams may be found in the reviews by Beck (9, 10) and Trotman (11). The maximum input frequency will be limited by the speed with which it is possible to modulate an electron beam. The triode structure of the present design would restrict modulation to frequencies up to a few GHz on account of the transit angle. It should be possible to produce modulation at a point remote from the cathode by varying the potential of an electrode in the vicinity of zero volts. This would have the advantage that the electrons could be previously accelerated to a high potential and the transit angle thus considerably reduced.

In some initial experiments it was found that modulation could be produced by this means but that the effect was complicated by oscillations of the space charge in front of the cathode caused by the returning electrons. However it should not be difficult to eliminate this problem.

Once a tube has been made which will work satisfactorily with an input frequency of 1 GHz it would be possible to feed this from the output of another tube designed to operate with input frequencies in the 1 - 10 GHz range. Dispersion tubes for this frequency range would be an attractive proposition as they require a drift length of a few centimetres only, and as the electron beam is not dispersive in this region a multiplier should not be necessary.

A further possible development is to replace the thermionic cathode with a photocathode and thus use the dispersive principle to obtain time resolved in formation from incident light signals. There would be no modulation problem in this case.

There remains therefore much to be done in this field and it offers new means to the knowledge of events which occur so rapidly as to be beyond the present reach of science.

9. APPENDIX

This Appendix contains an abbreviated account of that part of the theory of space-charge waves which is particularly relevant to this thesis. For a complete account reference should be made to the work of Beck (10) Ramo (25), and Trotman (11). Also included is some relevant work of Llewellyn and Peterson (30)

9.1 Derivation of the space-charge wave equation

Consider an infinitely wide beam between two planes at potential V_o immersed in an infinitely strong z-directed d.c. magnetic field. The average electron charge density is compensated by an equal density of positive ions so that the d.c. potential is uniform throughout the beam. Because of their greater mass the ions may be considered stationary. Under these ideal conditions all electrons travel in straight lines parallel to the z axis, and the d.c. potential is everywhere V_o. The electron charge is taken as -e and a current flowing to the right is designated -I

Maxwell's equations are:

$$\nabla.\underline{E} = \rho/\varepsilon_o \tag{9.1}$$

$$\nabla.\underline{H} = 0 \tag{9.2}$$

$$\nabla\times\underline{E} = -\mu(\delta H/\delta t) \tag{9.3}$$

$$\nabla\times\underline{H} = \varepsilon_o(\delta E/\delta t) + J \tag{9.4}$$

From eqns. 9.3, 9.4,

$$\text{grad}\nabla.\underline{E} - \nabla^2\underline{E} = -\mu_o\varepsilon_o(\delta^2 E/\delta t^2) + \mu_o(\delta J/\delta t) \tag{9.5}$$

We also require the equation of continuity:

$$\nabla.\underline{J} = -(\delta\rho/\delta t) \tag{9.6}$$

the force equation:

$$(du_1/dt) = (e/m)E_z \tag{9.7}$$

and the definition of convection current:

$$J_o + J_1 = (\rho_o + \rho_1)(u_o + u_1) \qquad (9.8)$$

In eqns. 9.7, 9.8, J_1, ρ_1, u_1, refer respectively to the alternating components of current density, charge density, and velocity. If we assume that ρ_1, u_1, are small in comparison with ρ_o, u_o, i.e. that we are concerned only with small modulations, we can neglect the product $\rho_1 u_1$ and write

$$J_1 = \rho_o u_1 + u_o \rho_1 \qquad (9.8a)$$

It is assumed that ρ_1, u_1, J_1, all have wave functions of the form $\exp j(wt - \beta z)$. Considering only the z component of $\underline{E}$ and manipulating eqns. 9.6, 9.7, 9.8a, we obtain

$$u_1 = j(e/m)E_z/(w - \beta u_o) \qquad (9.9)$$

$$J_1 = -jw\varepsilon_o w_p^2 E / (w - \beta u_o) \qquad (9.10)$$

where w_p, the electron plasma frequency is given by

$$w_p^2 = (e/m)\rho_o/\varepsilon_o \qquad (9.11)$$

or for a beam of area Σ

$$w_p^2 = (e/m)I_o/(\varepsilon_o u_o \Sigma) \qquad (9.11a)$$

Substituting for u_1, J_1, in eqn. 9.5 gives

$$\frac{\delta^2 E}{\delta x^2} + \frac{\delta^2 E}{\delta y^2} + (\beta^2 - k^2)\left[\frac{w_p^2}{(w - \beta u_o)^2} - 1\right]E = 0 \qquad (9.12)$$

which is the space-charge wave equation.

For a rectilinear system

$$\frac{\delta^2 E}{\delta x^2} = \frac{\delta^2 E}{\delta y^2} = 0$$

and thus

$$(\beta^2 - k^2)\left[\frac{w_p^2}{(w - \beta u_o)^2} - 1\right]E = 0 \qquad (9.13)$$

There are four roots:

$$\beta_{1,2} = \pm jk \tag{9.14}$$

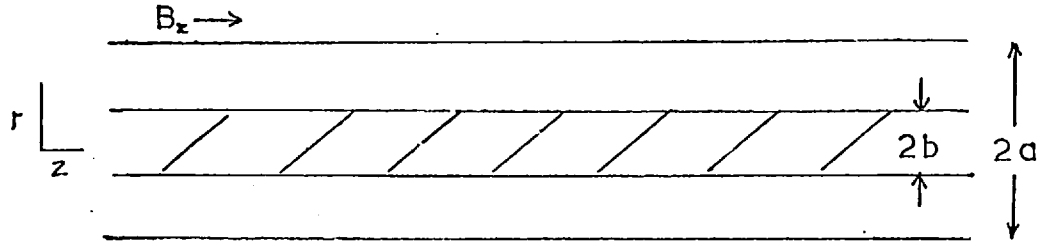
$$\beta_{3,4} = (w \pm w_p)/u_0 \tag{9.15}$$

The first two waves propagate with the velocity of light. The remaining two have phase velocities just above and just below the beam velocity, namely

$$u = u_0/(1 \pm w_p/w) \tag{9.16}$$

In subsequent equations where $\pm$, $\mp$, signs are used it is to be understood that the upper sign refers to the slow wave.

9.2 Application to a cylindrical system.



In the case of a beam confined within a conducting cylinder of radius a (see above figure) we require a solution of the wave equation in which E_z is finite on the axis of the system and zero on the walls.

The space-charge wave equation expressed in cylindrical coordinates is

$$\frac{1}{r}\frac{\delta}{\delta r}\left[r\frac{\delta E_z}{\delta r}\right] + \gamma_r^2 E_z = 0 \tag{9.17}$$

where

$$\gamma_r^2 = (\beta^2 - k^2)\left[\frac{w_p^2}{(w - \beta u_0)^2} - 1\right] \tag{9.18}$$

Eqn. 9.17 is Bessel's equation. The solutions will be different inside and outside the beam. Inside,

$$E_{z1} = AJ_0(\gamma_r r) \tag{9.19}$$

Outside,

$$E_{z2} = CI_0(\gamma_0 r) + BK_0(\gamma_0 r) \tag{9.20}$$

I_0, J_0, K_0, here express the usual notation for Bessel functions. A, B, C, are constants.

We now utilize the boundary conditions to eliminate the constants. The conditions are

$$\begin{aligned} E_{z2} &= 0 \text{ at } r = a \\ E_{z1} &= E_{z2} \text{ at } r = b \\ \delta E_{z1}/\delta r &= \delta E_{z2}/\delta r \text{ at } r = b \end{aligned} \tag{9.21}$$

and give

$$-\frac{(\gamma_r b)J_1(\gamma_r b)}{J_0(\gamma_r b)} = \gamma_0 b \, \frac{I_1(\gamma_0 b)K_0(\gamma_0 a)+I_0(\gamma_0 a)K_1(\gamma_0 b)}{I_0(\gamma_0 b)K_0(\gamma_0 a)-I_0(\gamma_0 a)K_0(\gamma_0 b)} \tag{9.22}$$

This equation expresses γ_r as a function of γ_o and is most easily solved graphically. Fig. 9.1 shows a plot of the RHS and LHS as a function of $\gamma_1 b$ for a/b = 1.5. There are an infinite number of values of $\gamma_1 b$ corresponding to one value of $\gamma_0 b$. These correspond to various modes of wave propagation in the beam. (Only the first three modes are represented in Fig. 9.1). For the moment we consider only the fundamental mode.

Outside the beam $w_p = 0$ so we can write

$$\gamma_0^2 = \beta^2 - k^2 \tag{9.23}$$

The wave phase velocity can be expected to be nearly equal to the electron velocity u_0, so $\beta \approx w/u_0$. β is thus much larger than k (= w/c) and therefore

$$\gamma_0 \approx w/u_0 \tag{9.24}$$

Still neglecting k we put

$$\beta = (w \pm Fw_p)/u_0 \tag{9.25}$$

by analogy witheqn. 9.15 and substitute in eqn. 9.18 to

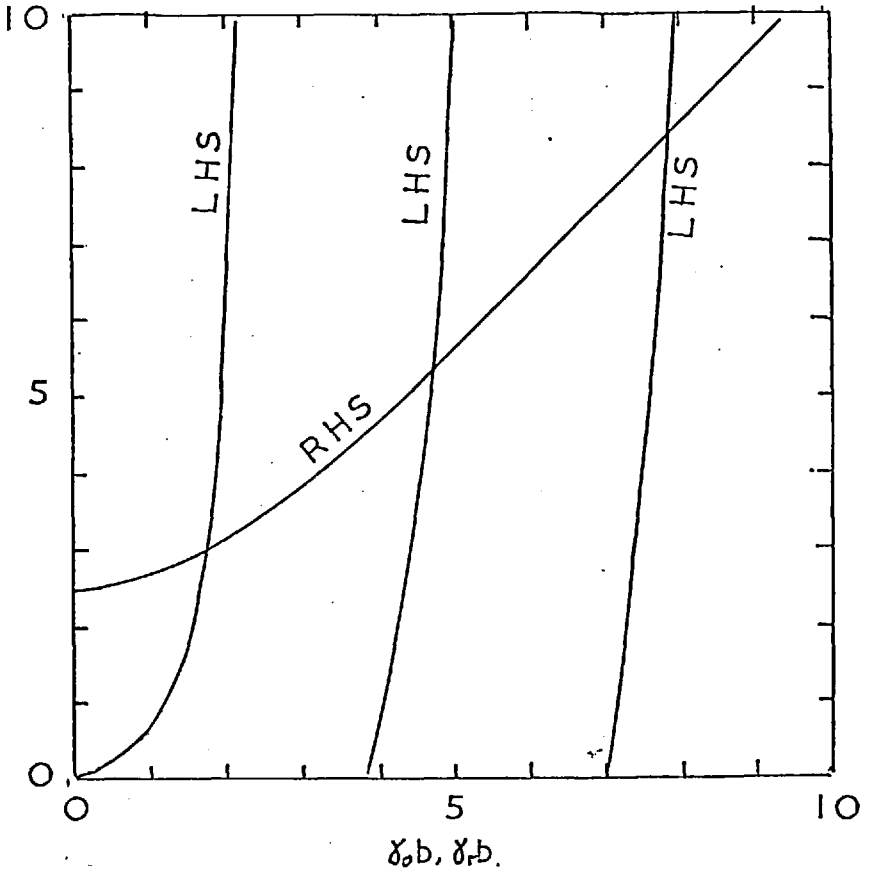
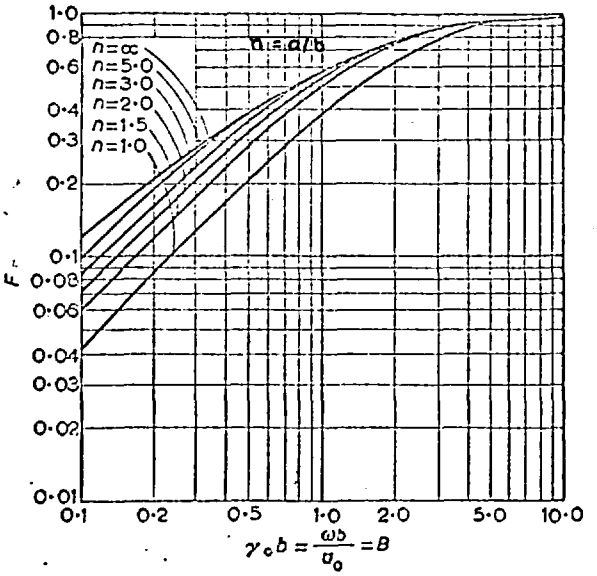


Fig. 9.1 Plot of eqn. 9.22. a/b =1.5.



Space-charge reduction factors for cylindrical beams in cylindrical tunnels.

Fig. 9.2
(after Beck)

obtain

$$\gamma_r^2 = \left[\frac{(w \pm Fw_p)}{u_o}\right]^2 \left[\frac{1}{F^2} - 1\right] \qquad (9.26)$$

γ_r can be obtained from eqn. 9.23 to give F. F is called the space-charge reduction factor.

In the particular case of the experimental tube where a/b = 1.5, b = .0025, it follows from Fig. 9.1 that as w varies between 0 and 2 x10^9, b varies only between 1.78 and 2.0 (for the first mode). We take the former value which applies to low frequencies with which we are specifically concerned in Chapter 5. Substituting in eqn. 9.26 we obtain

$$\{(1/F)^2 - 1\}^{\frac{1}{2}}(w \pm Fw_p) = 712u_o \qquad (9.27)$$

which is eqn. 5.5

Fig 9.2 shows values of F which have been calculated for ratios of a/b other than 1.5.

The velocities of the slow and fast waves can be obtained from eqns. 9.23, 9.24,

$$u_g = \delta w/\delta\beta = u_o/\{1 \pm w_p(dF/dw)\} \qquad (9.28)$$

The transit times through the drift section, of length s are s/u_g and are thus expressed by eqns. 5.1, 5.2.

So far we have considered only th e propagation of a continuous wave of frequency w. Transient pulses can be considered as the sum of an infinite number cf such waves as expressed by the Fourier Integral Transform.

9.3 Higher order modes

As mentioned in the previous Section it is possible for other space-charge modes to propagate on the beam. In general the boundary conditions in the tube have to be satisfied by an infinite series of such waves. However these higher modes have increasingly smaller F values and their group velocity lies increasingly close to the electron velocity. In practical devices we are likely to be concerned with operating conditions in which the

difference between the fast and slow wave velocities is negligible. If this is so for the fundamental mode it must also be true for the other modes. Accordingly, we need not be concerned further with these modes.

9.4 Convectional impedance of space-charge limited diode.

The application of Llewellyn's analysis to a space- charge limited diode has been studied by Birdsall and Bridges (18). We follow their notation here. They have shown that the convection current I_b, the total current density J, and the anode voltage V_b, are related by the equations

$$\begin{aligned} V_b &= A^* J \\ I_b &= D^* J \end{aligned} \tag{9.29}$$

where A*, D*, are the Llewellyn-Peterson coefficients (30). The convection impedance, Z_v, is defined by

$$Z_v = V_b / I_b = A^*/D^* \tag{9.30}$$

and substituting the expressions for A*,D*, (not given here), one obtains

$$Z_v = \frac{\tau^2 u_b}{6\varepsilon_o} \frac{\beta^3 + 6S}{P\beta^2} \tag{9.31}$$

Here τ is the cathode-anode transit time, u_b is the electron velocity in the grid plane, and $\beta = \omega t$. u_b is given by

$$u_b = \sqrt{(2eV_b/m)} \tag{9.32}$$

S and P are given by

$$\begin{aligned} S &= 2P - \beta(1 - e^{-\beta}) \\ P &= 1 - e^{-\beta} - e^{-\beta} \end{aligned} \tag{9.33}$$

In a space-charge limited diode the transit time T is related to the spacing d by the equation

$$T = 3d/\sqrt{(2eV_b/m)} \tag{9.34}$$

Substituting eqns. 9.34, 9.32 in 9.31 gives

$$Z_v = \frac{3d^2}{2\varepsilon_0\sqrt{(2eV_b/m)}} \frac{\beta^3 + 6S}{P\beta^2} \tag{9.35}$$

Now the current density J and the anode voltage V_b are related by the diode equation

$$J = (4\varepsilon_0/9)\sqrt{(2e/m)}V_b^{\frac{3}{2}}/d^2 \tag{9.36}$$

Hence the steady state or low frequency plate impedance is given by

$$r_p = \frac{\delta V_b}{\delta J} = \frac{3d^2}{2\varepsilon_0\sqrt{(2eV_b/m)}} \tag{9.37}$$

Comparing this result with eqn. 9.35, it is evident that

$$Z_v = r_p \frac{\beta^3 + 6S}{P\beta^2} \tag{9.38}$$

Since P and S are complex it is convenient to express Z_v as a sum of real and imaginary parts. We write first

$$Z_v = r_p \frac{a_1 + jb_1}{a_2 + jb_2} = r_v + jx_v \tag{9.39}$$

Using this relation together with eqns. 9.33, 9.38 and writing $\beta = j\theta$ we find

$$\begin{aligned} a_1 &= 6\{2(1 - \cos\theta) - \theta\sin\theta\} \\ a_2 &= -\theta^2\{1 - \cos\theta - \theta\sin\theta\} \\ b_1 &= 6\{2\sin\theta - \theta(1+\cos\theta) - \theta^3/6\} \\ b_2 &= \theta^2\{\theta\cos\theta - \sin\theta\} \end{aligned} \tag{9.40}$$

Separating eqn. 9.39 into real and imaginary parts gives

$$\begin{aligned} \frac{r_v}{r_p} &= \frac{a_1a_2 + b_1b_2}{a_2^2 + b_2^2} \\ \frac{x_v}{r_p} &= \frac{a_2b_1 - a_1b_2}{a_2^2 + b_2^2} \end{aligned} \tag{9.41}$$

These relations are plotted as funtions of θ in Fig. 2.2.

10. ACKNOWLEDGEMENTS.

I am particularly indebted to Professor J.D.McGee for his help and encouragement in this study. My thanks are also due to many colleagues in the Applied Physics Department at Imperial College who have assisted me in diverse ways and especially to Messrs. Barr, Beckwith, Beisiegal and Thurley, for providing much of the technical expertise essential to the work. I am most grateful to members of E.M.I. Valve Division for their cooperation in supplying the cathode assemblies and electron multipliers for the later tubes. Finally I wish to acknowledge the financial support given by the Paul Instrument Fund of the Royal Society.

11. REFERENCES

1. I.A.D. Lewis, F.H. Wells, "Millimicrosecond Pulse Techniques" (Second Edition), Pergamon Press (1959).
2. B. Gilbert, Mullard Tech. Comn. 5, 317 (1960).
3. A. Gersho, Proc. I.E.E.E. 54, 1574 (1966).
4. D.H. Cooper, Proc. I.E.E.E. 55; 712 (1967).
5. A.G.J. Holt, C. Nightingale, Electronics Letters 4, 319 (1968).
6. W.J. Caputi, J.I.E.R.E. 29, 135 (1965).
7. C.E. Fay, A.L. Samuel, W. Shockley, Bell Syst.. Tech. J. 17, 49 (1938).
8. L.P. Smith, P.L. Hartman, J. Appl. Phys. 11, 220 (1940).
9. A.H.W. Beck, "Thermionic Valves", C.U.P. (1953).
10. A.H.W. Beck, "Space-Charge Waves", Pergamon Press (1958).
11. R.E. Trotman, "Longitudinal Space-Charge Waves", Chapman and Hall (1966).
12. Edgerton, Germeshausen and Grier Inc., Boston, Mass., U.S.A. Cathode ray oscilloscope No. 2236.
13. B. Jackson, D.R. Hardy, R. Feinberg, Nature 172, 1056 (1953).
14. F.B. Llewellyn, "Electron-Inertia Effects", C.U.P. (1941).
15. C.K. Birdsall, W.B. Bridges "Electron Dynamics of Diode Regions", Academic Press (1966).
16. I. Langmuir, Phys. Rev. 21, 419 (1923).

17. C. Snow, "Formulas for computing Capacitance and Inductance", N.B.S. Circular 544 (1954).

18. F. Rosebury, "Handbook of Electron Tube and Vacuum Techniques", Addison-Wesley (1965).

19. J. Hillman, H. Taub, "Pulse, Digital and Switching Waveforms", McGraw Hill (1965).

20. G.B.B. Chaplin, A.R. Owens, Proc. I.E.E. 106, (Part B Supplement), 806 (1959).

21. H. Boersch, Z. Phys. 139, 118 (1954).

22. D. Hartwig, K. Ulmer, Z. Phys. 173, 294 (1963).

23. H. Bruining, "Physics and Applications of Secondary Electron Emission", Pergamon Press (1962).

24. K.G. McKay, Advances in Electron Physics 1, 65 (1948).

25. S. Ramo, Phys. Rev. 56, 276 (1939).

26. E. J. Sternglass, Phys. Rev. 95, 345 (1954).

27. C. K. Birdsall, G.R. Brewer, A.V. Haeff, Proc. I.E.E.E. 41, 865 (1953).

28. "R.C.A. Phototubes and Photocells", Technical Manual PT - 60. Radio Corporation of America (1963).

29. "E.M.I. Photomultiplier Tubes", Brochure 30 M/6 - 67. Electrical and Musical Industries Ltd. (1967).

30. F. B. Llewellyn, L.C. Peterson, Proc. I.E.E.E. 32, 144 (1944).